About the Cover: Dysregulated translation drives key hallmarks of cancer and is controlled by Phase 2 candidate eFT508 binding to the MNK protein, exploiting stereoelectronic interactions, critical to the compound's selectivity and potency. (Reich, S. H.; et al. *J. Med. Chem.* **2018**, *61*, DOI: 10.1021/acs.jmedchem.7b01795)

Journal of Medicinal Chemistry

Article

Cite This: J. Med. Chem. 2018, 61, 3516−3540

pubs.acs.org/jmc

Structure-based Design of Pyridone−Aminal eFT508 Targeting Dysregulated Translation by Selective Mitogen-activated Protein Kinase Interacting Kinases 1 and 2 (MNK1/2) Inhibition

Siegfried H. Reich,*[,†] Paul A. Sprengeler,[†] Gary G. Chiang,[†] James R. Appleman,[‡] Joan Chen,[†] Jeff Clarine,[†] Boreth Eam,[†] Justin T. Ernst,[†] Qing Han,[§] Vikas K. Goel,[†] Edward Z. R. Han,[§] Vera Huang,[∥] Ivy N. J. Hung,[†] Adrianna Jemison,[⊥] Katti A. Jessen,[#] Jolene Molter,[†] Douglas Murphy,[∇] Melissa Neal,[†] Gregory S. Parker,[†] Michael Shaghafi,[○] Samuel Sperry,[†] Jocelyn Staunton,[†] Craig R. Stumpf,[†] Peggy A. Thompson,[†] Chinh Tran,[†] Stephen E. Webber,[△] Christopher J. Wegerski,[†] Hong Zheng,[§] and Kevin R. Webster[†]

[†]eFFECTOR Therapeutics, 11180 Roselle Street, San Diego, California 92121, United States

[‡]Primmune Therapeutics, Inc., 3210 Merryfield Row, San Diego, California 92121, United States

[§]Structure-Based Design, Inc., 6048 Cornerstone Court West #D, San Diego, California 92121, United States

[∥]Molecular Stethoscope, 10835 Road to the Cure #100, San Diego, California 92121, United States

[⊥]Department of Chemistry, University of Pennsylvania, 231 South 34th Street, Philadelphia, Pennsylvania 19104, United States

[#]Oncternal Therapeutics, 3525 Del Mar Heights Road #821, San Diego, California 92130, United States

[∇]Molcentrics, Inc., 11835 Carmel Mountain Road #1304-110, San Diego, California 92128, United States

[○]Abide Therapeutics, 10835 Road to the Cure, Suite 250, San Diego, California 92121, United States

[△]Polaris Pharmaceuticals, 9373 Towne Centre Drive #150, San Diego, California 92121, United States

Supporting Information

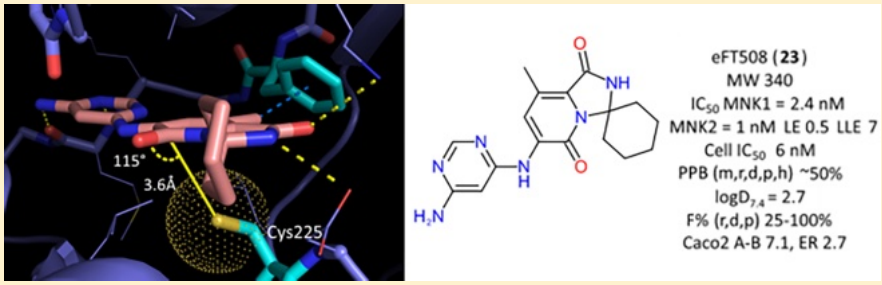

ABSTRACT: Dysregulated translation of mRNA plays a major role in tumorigenesis. Mitogen-activated protein kinase interacting kinases (MNK)1/2 are key regulators of mRNA translation integrating signals from oncogenic and immune signaling pathways through phosphorylation of eIF4E and other mRNA binding proteins. Modulation of these key effector proteins regulates mRNA, which controls tumor/stromal cell signaling. Compound **23** (eFT508), an exquisitely selective, potent dual MNK1/2 inhibitor, was designed to assess the potential for control of oncogene signaling at the level of mRNA translation. The crystal structure-guided design leverages stereoelectronic interactions unique to MNK culminating in a novel pyridone−aminal structure described for the first time in the kinase literature. Compound **23** has potent *in vivo* antitumor activity in models of diffuse large cell B-cell lymphoma and solid tumors, suggesting that controlling dysregulated translation has real therapeutic potential. Compound **23** is currently being evaluated in Phase 2 clinical trials in solid tumors and lymphoma. Compound **23** is the first highly selective dual MNK inhibitor targeting dysregulated translation being assessed clinically.

■ INTRODUCTION

Translation, the most energy consuming process in the cell, plays a significant role in gene regulation and ultimately the control of protein levels. The precept that there is a direct correspondence between the abundance of mRNA and that of its corresponding protein product is an oversimplification. Translation is a tightly controlled process for a select set of mRNAs, and dysregulation of this process drives aberrant proliferation, angiogenesis, survival, and alterations in immune function, all hallmarks of cancer (Figure 1).[1−5] The key step of cap-dependent translation initiation relies upon the availability

Received: December 5, 2017
Published: March 10, 2018

DOI: 10.1021/acs.jmedchem.7b01795
J. Med. Chem. 2018, 61, 3516−3540

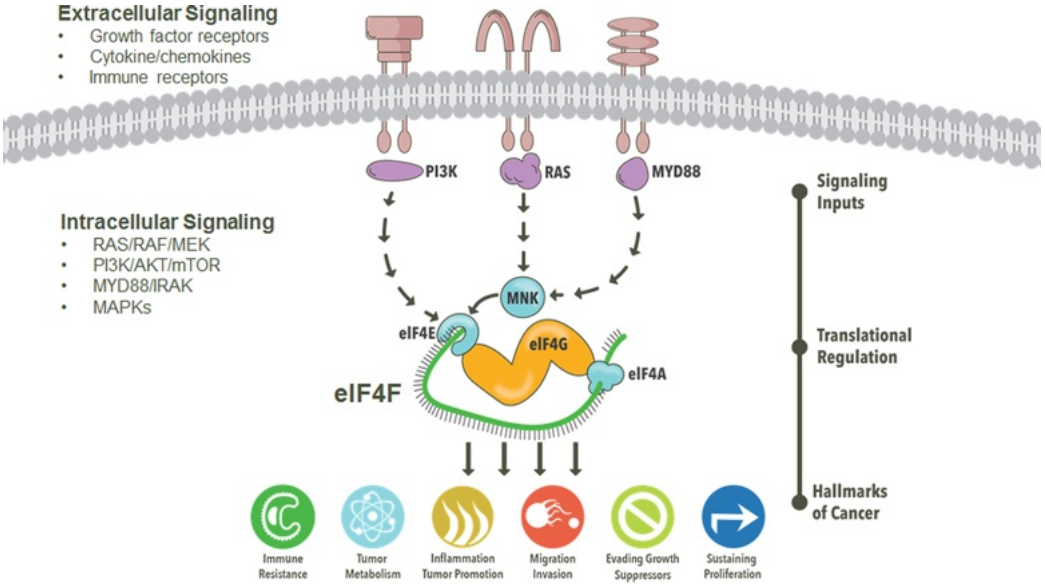

Figure 1. Translation is a tightly controlled process for a select set of mRNAs and dysregulation of this process drives aberrant proliferation, angiogenesis, survival, and alterations in immune function, all hallmarks of cancer. The key step of cap-dependent translation initiation by the eIF4F complex relies upon the availability of eukaryotic initiation factor eIF4E, which is in turn regulated by the mitogen-activated protein kinase interacting kinases MNK1/2. The MNKs are key regulators of mRNA translation integrating signals from oncogenic and immune signaling pathways (Ras, p38, TCR, and TLRs).

and activity of eukaryotic initiation factor eIF4E, which is in turn regulated by the mitogen-activated protein kinase interacting kinases (MNK)1/2.[6−11] The MNKs are activated by upstream Ras/Raf/Erk and MyD88/p38 signaling pathways, resulting in regulation of RNA translation through eIF4E and other key effector proteins such as heterogeneous nuclear ribonucleoprotein A1 (hnRNPA1) and protein-associated splicing factor (PSF).[1,2,4,12−16] Phosphorylation of these mRNA binding proteins selectively regulates the translation and stability of a subset of cellular mRNA that control both tumor and stromal cell signaling. MNK, a Ser/Thr kinase, is the only kinase known to phosphorylate eIF4E at serine 209. This modification has been shown to be essential for eIF4E's role in tumorigenesis but not for normal development and cell homeostasis. MNK1/2 double knockout studies in mice further demonstrated that these kinases are not required for normal growth and development.[17−19] Thus, the underlying genetics of MNK lead to an expectation that a potent and selective MNK inhibitor would not necessarily have a strong antiproliferative phenotype but would limit cellular processes necessary for oncogene driven signaling and survival, sparing normal tissues and offering the potential for a good therapeutic window. This distinction between transformed versus normal cells makes the MNKs particularly exciting as a therapeutic opportunity. Interestingly, the literature has examples of less selective MNK inhibitors that do have a broad antiproliferative phenotype, which may be a result of off-target effects unrelated to MNK.[20−24] Other MNK inhibitors have demonstrated improved selectivity.[25−28] While the biology of MNK and its effects on tumorigenesis have been the subject of many studies, the breadth of these effects, particularly through pharmacological intervention, has not been demonstrated for a potent, selective dual MNK inhibitor to date. As a consequence, the full potential for control of mRNA translation via MNK in cancer therapy has not been revealed.[11]

As a result, we sought to identify a dual MNK1/2 inhibitor with both exceptional kinome selectivity and cellular potency so that the pharmacologic phenotype of MNK1/2 inhibition could be fully explored. We have designed a highly selective and potent MNK1/2 inhibitor, compound **23** (eFT508), leveraging the unique active site of this kinase in an iterative structure-based approach.[29] The pyridone-aminal chemotype has not been reported in kinase inhibitors to date.[30,31] Compound **23** activity in models of diffuse large cell B-cell lymphoma (DLBCL) is associated with potent p-eIF4E knockdown and selective destabilization of pro-inflammatory cytokine mRNA. Pro-inflammatory cytokines, including interleukin-6 (IL-6), interleukin-8 (IL-8), and TNFα, are drivers of many hallmarks of cancer, e.g., tumor cell survival, migration and invasion, angiogenesis, immune evasion, and stress response, while affecting drug resistance.[32,33] Importantly, this p-eIF4E and cytokine knockdown translates into potent *in vivo* antitumor activity in DLBCL models harboring activating MyD88 mutations, consistent with the MNKs being activated by TLR signaling.[13,32] In addition, efficacy has been demonstrated in solid tumor settings, which may reflect the MNKs' impact on mRNA translation that controls tumor and stromal cell signaling. This breadth of antitumor activity highlights the significant potential for control of dysregulated translation by a small molecule inhibitor.[33] Compound **23** is currently in Phase 2 clinical trials for the treatment of both solid and hematologic cancers and has been granted Orphan Drug status by the FDA for the treatment of DLBCL.

■ RESULTS

Molecular Design Strategy Leading to the Pyridone–Aminal Chemotype. A common approach to selective kinase inhibition is to begin with a molecule that contains a potent hinge binding motif and whose shape complements the targeted kinase. Additional groups are then added that are tolerated by the kinase of interest but make negative interactions with the antitargets.[34] Our approach to MNK inhibitor design focused on incorporating *favorable* stereo-electronic interactions with the MNK active site residues that

DOI: 10.1021/acs.jmedchem.7b01795
J. Med. Chem. 2018, 61, 3516−3540

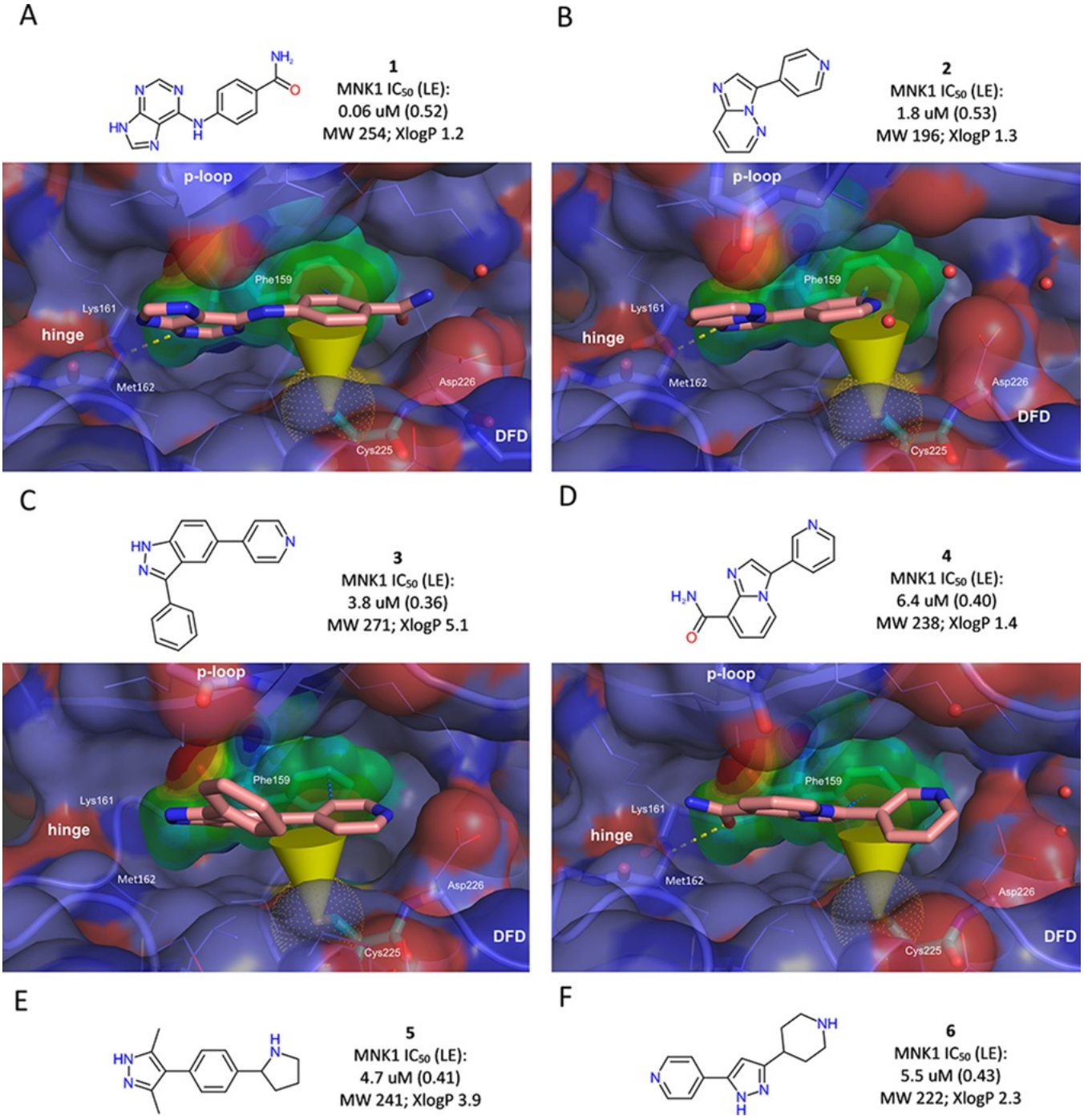

Figure 2. Crystal structures were obtained with MNK2 mutated to the canonical DFG from DFD to facilitate cocrystallization experiments.[38] (A) Cocrystal structure showing the MNK2 active site with carboxamide **1** bound along with its binding data (PDB code: 6CJE). The surface representation of the electrostatic potential of Phe159 was calculated by DFT using the B3LYP method employing the 6-31G* basis set with Spartan (Wavefunction). (B) MNK2 crystal structure and binding data of compound **2** (PDB code: 6CJW). (C) Compound **3** structure and data (PDB code: 6CJH). (D) One conformation of the compound **4** cocrystal structure along with its binding data (PDB code: 6CJ5). (E,F) Two-dimensional structures and data for the compounds for which a cocrystal structure with MNK2 was not obtained, **5** and **6**.

differentiate it from other kinases. Stereoelectronic interactions are highly sensitive to distance and orientation, which can improve selectivity.[35−37] These interactions are often less affected by solvation, which can enhance potency and permeability. There are several atypical residues in the ATP binding site of MNK1/2, two of which offered the greatest opportunity for stereoelectronic interactions, the gatekeeper, Phe159, and the pre-DFG residue, Cys225, and these were the focus of our design.[38] Across the kinome, only Flt3 and 4, cyclin-dependent kinase-like (CDKL)1−5, PRP4 (serine/threonine-protein kinase-PRP4), a dual specificity tyrosine-phosphorylation-regulated kinase family kinase, mitogen-activated protein kinase-7, and MNK have this combination suggesting that interacting with these residues in a ligand efficient manner could facilitate the design of MNK-selective inhibitors (Figure 2A). A unique sequence element in the

DOI: 10.1021/acs.jmedchem.7b01795
J. Med. Chem. 2018, 61, 3516−3540

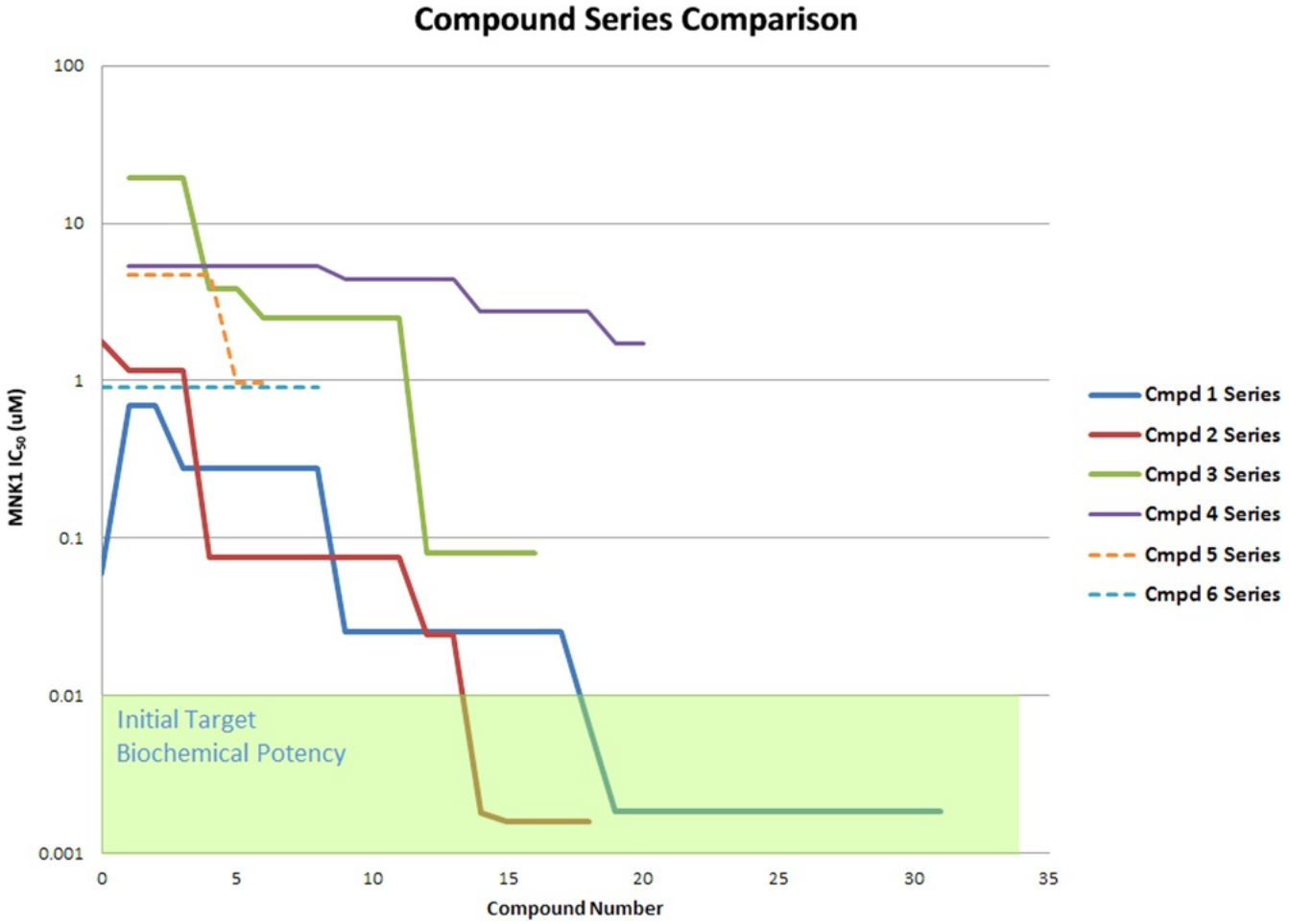

Figure 3. Trajectory of the series based on each of the starting molecules. Plot generated by only showing data for compounds that improve potency over the proceeding compounds, otherwise the previous molecules data was plotted (an exception was made for the Cmpd 1 Series where the first loss in potency from deconstruction is plotted).

MNK1/2 kinases is a DFD motif in place of the canonical DFG; however, these residues are more distant from the hinge.[39] The active sites of MNK1 and MNK2 are nearly identical (90%), so there was an expectation that achieving similar affinity for both isoforms should be feasible.[25] Dual inhibition was thought to be necessary as the isoforms can compensate for one another in the phosphorylation of eIF4E.[4]

Our early strategy was to identify a chemical starting point with high ligand efficiency. Time spent on identifying the best starting scaffold and then maintaining its attributes can greatly facilitate medicinal chemistry success later; this is the underlying principle of fragment-based drug discovery wherein a priority is placed on ligand efficiency and physicochemical properties at the outset of design. We identified six initial fragments or fragment-like scaffolds (15−20 heavy atoms, Figure 2A−F). Compounds **1**, **2**, **3**, and **6** were in the public domain, and **4** and **5** were designed using common kinase inhibitor hinge binding motifs modeled into the MNK2 crystal structure. We utilized a mutated MNK protein for crystallization as it has been shown that mutation of the WT MNK from DFD to the more canonical DFG results in a more readily crystallized protein.[38] All had good affinity for MNK as measured by their MNK1 IC_{50} and ligand efficiency. We attempted to obtain crystal structures of each compound in complex with mutated MNK2 to understand their potential for making protein interactions and facilitate the design of a cohort of initial follow-on molecules; structures were obtained for four of the six. Figure 2A shows the cocrystal structure of carboxamide **1** in the MNK2 active site and highlights the electrostatic potential of the gatekeeper residue Phe159 and the cone representing the nucleophilic directionality of the sulfur of the pre-DFG Cys225. The negative potential of the Phe159 face suggested that ligand moieties having positive potential (i.e., the edge of an aromatic ring, a methyl group, a polarizable atom, etc.) would be complementary. This structure indicated potential interactions were possible with both key residues, Phe159 and Cys225, for compound **1** optimization. It also revealed that the N-9 nitrogen of the imidazole ring was engaged with the hinge through a 3.5 Å hydrogen bond to the Met162 carbonyl oxygen, a weak interaction. The binding mode of compound **2** (Figure 2B) also showed good potential for interactions with Phe159 and Cys225 (compound **2** shares the imidazo[1,2-*b*]pyridazine core of BAY1143269).[27] Compound **3**, however, did not make intimate interactions with either the gatekeeper or the hinge, and its suitability for engaging Cys225 was deemed low. Compound **4** crystallized in two conformations (only the pose most representative of the series shown), and similar to **3**, the ability of compound **4** to interact with the gatekeeper and Cys225 was considered to be marginal. The crystal structures for **5** and **6** could not be determined; nevertheless, a small cohort of compounds was designed using all six fragments as starting points, and the

DOI: 10.1021/acs.jmedchem.7b01795
J. Med. Chem. 2018, 61, 3516−3540

Table 1. Biochemical and Cellular Potency and Associated Physicochemical Properties of Key Compounds in the Primary Series[a]

Structure	ID	R1	R2	MNK1 IC_{50} (nM) (LE, LLE)	MNK2 IC_{50} (nM) (LE, LLE)	HCT-116 Cell peIF4E IC_{50} (nM) (LE, LLE)	MW	XlogP
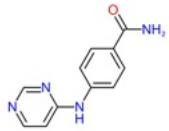	7	-	-	690 (0.53, 5.3)	-	-	214	0.87
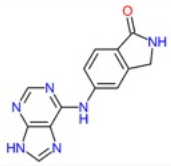	8	-	-	23 (0.53, 6.4)	-	-	266	1.3
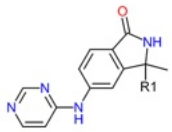	9	H	-	28 (0.58, 6.1)	45 (0.56, 5.9)	28000 (0.35, 3.1)	240	1.4
	10	Me	-	100 (0.51, 5.2)	61 (0.52, 5.4)	4400 (0.39, 3.5)	254	1.8
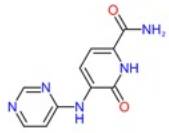	11	-	-	3000 (0.45, 6.5)	-	-	231	-0.99
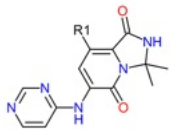	12	H	-	60 (0.50, 6.4)	57 (0.50, 6.5)	3800 (0.37, 4.6)	271	0.79
	13	F	-	6.5 (0.54, 7.3)	2.6 (0.56, 7.7)	580 (0.41, 5.3)	289	0.89
	14	Me	-	10 (0.53, 6.8)	19 (0.51, 6.5)	160 (0.45, 5.6)	285	1.2
	15	Cl	-	3.3 (0.56, 7.1)	1.2 (0.59, 7.5)	73 (0.47, 5.7)	306	1.4
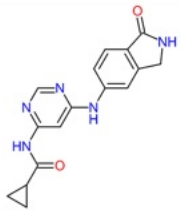	16	-	-	1.9 (0.52, 7.4)	5.7 (0.49, 6.9)	430 (0.38, 5.0)	309	1.3
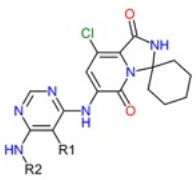	20	H		0.51 (0.43, 6.5)	1.8 (0.40, 5.9)	0.31 (0.44, 6.7)	429	2.8
	21	H	H	0.65 (0.51, 7.1)	0.68 (0.51, 7.1)	0.79 (0.5, 7.0)	361	2.1
	22	Cl	H	-	0.36 (0.52, 5.7)	0.084 (0.53, 7.4)	395	2.7

[a]LE = 1.36 × pIC_{50}/HAC (HAC = heavy atom count); LLE = pIC_{50} − clogP; XlogP = calculated using Dotmatics (IPCPU).

potency trajectory of each scaffold was assessed (Figure 3). The carboxamide scaffold **1** emerged as the preferred structure, having one of the highest ligand efficiencies and good vectors allowing rapid optimization to low nanomolar binding to MNK with less than 20 compounds. The purine was deconstructed to pyrimidine **7** resulting in a 10-fold loss in potency; however, the molecular weight and logP were reduced, and ligand efficiency was maintained (Table 1). A loss of potency in exchange for improved physicochemical properties is an often overlooked yet powerful optimization strategy in medicinal chemistry. Lactam compound **8** was designed through analysis of the cocrystal structure of compound **1** and was 2.5-fold more active. This lactam was expected to have improved permeability due to the loss of one hydrogen bond donor. Furthermore, introduction of the lactam sp^3 carbon afforded vectors out of the aryl plane. We thought substitution of this buried methylene might force the bicyclic ring system to flip 180° accommodating the increased size of this substitution and accessing the p-loop, a rich source

DOI: 10.1021/acs.jmedchem.7b01795
J. Med. Chem. 2018, 61, 3516−3540

of kinase binding affinity. Compound **9** was 25-fold more potent than the original carboxamide **7**, and the cocrystal structure showed that the ring flip had indeed occurred relative to its unsubstituted counterpart compound **8** (Figure 4).

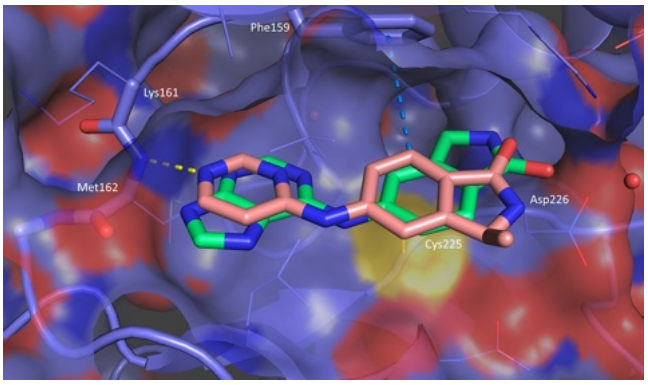

Figure 4. Comparison of the binding modes from cocrystal structures of compounds **8** (green, PDB code: 6CJY) and **9** (salmon, PDB code: 6CK3) confirming the ring flip and orientation of the sp^3 substituent toward the p-loop of MNK (p-loop located above the plane and not shown for clarity). The distance to the hinge Met226 NH for compound **9** was 3 Å vs 3.5 Å for compound **8** suggesting improved binding. The figure was generated by overlapping the protein C-alphas for each cocrystal structure of compounds **8** and **9**; only the protein for compound **9** is displayed.

Linkers between the pyrimidine and benzene rings other than nitrogen (i.e., C, O, or S) and replacement of the pyrimidine with pyridine consistently resulted in less active molecules likely due to reduced planarity.

As described previously, the sulfur of Cys225 can make favorable stereoelectronic interactions affording the potential to both increase potency and selectivity (Figure 2A).[37] Heterocycles in general can interact positively with cysteines, and several tested were effective binders. A single attempt at covalent interaction with Cys225 with a α,β-unsaturated amide was unsuccessful, suggesting that Cys225 is not particularly reactive. Stereoelectronic interactions of atoms having free lone pairs of electrons with carbonyl groups in a manner similar to the Dunitz attack for amide hydrolysis are observed quite often in crystal structures both in the PDB and CSD databases.[40,41] Highly polarizable chlorine and sulfur atoms are especially capable of engaging in this type of interaction, but it is also observed for fluorine, oxygen, and nitrogen. The pyridone ring system of **11** was designed to provide a stereoelectronic (Dunitz) interaction with Cys225 (Figure 5A). While **11** was four-fold less active in terms of binding affinity, importantly, its clogP was almost two orders of magnitude lower (XlogP = −0.99, Dotmatics) than its benzene counterpart **7** as reflected in the 16-fold improvement in lipophilic ligand efficiency (LLE) (Table 1, 6.5 − 5.3 = 1.2, $10^{1.2}$ = 16).[42] This modest reduction in binding affinity commensurate with a 72-fold reduction in lipophilicity was a critical result in the overall optimization process. The *gem*-dimethyl pyridone, compound **12**, was equipotent with its benzene counterpart **10**, maintaining the 17-fold improvement in LLE. The cocrystal structure of **12** confirmed that atom distances and angles between the sulfur atom and carbonyl were consistent with a Dunitz interaction (Figure 5B). Comparison of the kinome profiles of **10** and **12** (>400 kinases) showed that the pyridone imparts selectivity over the benzene ring (Figure 5C). This trend for greater selectivity was observed across additional pyridone−benzene pairs.

Another advantage of the pyridone scaffold was its considerably more facile synthesis and exceptional chemical stability. The pyridone aminal could be readily substituted by simply heating the pyridone carboxamide with a ketone in strong acid (Figure 6A and Scheme 5), a big improvement over the generally low yielding alkylation strategy required for the benzolactam. As a consequence of this simple condensation, greater diversity could now be incorporated at the aminal carbon as outlined in Figure 6A, facilitating the exploration of potential interactions with the p-loop.

Pyridone Cellular eIF4E-Ser209 Phosphorylation Potency. A focused protein structure-guided library was pursued, and the properties of this library are depicted in Figure 6B. The compounds are segregated by potency and substitution pattern and cover a spectrum of both clogP (XlogP) and MW.[42] Potential substituents off of the aminal carbon with MW < 200 were modeled into the MNK crystal structure, taking into account that the p-loop is quite flexible. Compounds that were exceptionally potent fell into the area of unfavorably high logP and high molecular weight (shaded area, Figure 6B). Highly substituted spirocyclic compounds were preferred, with six-membered rings showing the best kinome selectivity. Chiral compounds at the aminal carbon had no advantage in terms of potency or selectivity over achiral molecules so the latter became the focus of further design. The potencies of the compounds were routinely at the lower limit of the ATP competitive biochemical assay (ca. 1.5 nM) so the inhibition of eIF4E phosphorylation in cells was used to track potency. Cellular potency was improved 30−300-fold (cf. **12** to **17**) by incorporation of a cyclopropylamide in the 4-position of the pyrimidine **16** (Tables 1 and 2). This moiety has led to improved potency in inhibitors targeting other kinases, e.g., JAK2, TYK2, bRAF, Abl, VEGFR2, etc.

Antiproliferative effects were correlated with lack of kinase selectivity. Compound **17**, having single digit nanomolar cell potency for eIF4E phosphorylation and good selectivity for MNK1/2, showed no antiproliferative effects in three solid tumor cell lines (PC3, HCT-116, SW-620). In contrast, compounds **18** and **19** with less MNK1/2 selectivity demonstrated antiproliferative effects across multiple cell lines (Table 2). Compound **18** is an example from the structure-guided library described above, which is potent; however, it is chiral, has higher MW, and has higher logP. Potent cellular inhibition of p-eIF4E along with the *absence* of an antiproliferative signal was used as a measure of on-target selectivity not usually possible in an oncology drug discovery program. Compound **17** demonstrated target engagement over the dosing period as measured by p-eIF4E reduction and, when dosed *in vivo*, showed antitumor activity.

As described earlier, the ring flip observed for substituted lactams and aminals created an unfilled pocket adjacent to gatekeeper residue Phe159, which was our second residue of focus in the initial analysis. We hypothesized that this space might accommodate a single heavy atom positioned in the 5-position of the pyridone ring. A greater than 50-fold improvement in potency was observed with a 5-chlorine followed closely by a 5-methyl, whereas a 5-fluorine had significantly less benefit (compounds **15**, **14**, and **13** vs **12**, Table 1 and Figure 8). The enhanced affinity of the chlorine and methyl group is consistent with their ability to interact with the negative potential of the Phe159 aryl face, as revealed by the

DOI: 10.1021/acs.jmedchem.7b01795
J. Med. Chem. 2018, 61, 3516−3540

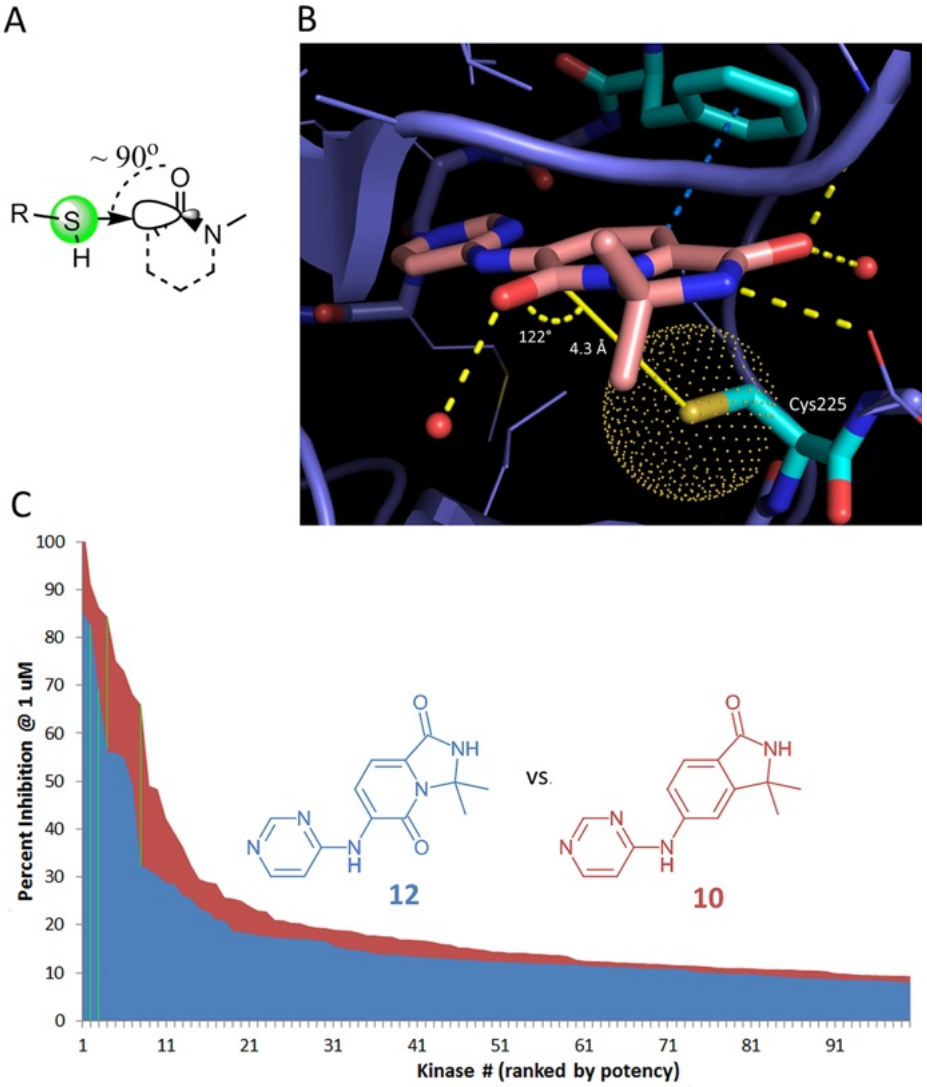

Figure 5. (A) Depiction of the Dunitz interaction between a sulfur atom and the LUMO of an amide bond as found in compound **11**. (B) Crystal structure of compound **12** bound to MNK2 showing the interaction of the Cys225 sulfur with the carbonyl carbon of the pyridone (PDB code: 6CKI). (C) Visual depiction of the kinome selectivity difference between compounds **10** and **12** (see data in Table S3). The plot shows the MNK2% inhibition of the first 100 kinases in a 419 kinase panel screen of compounds **10** and **12** at 1 μM. For each compound, the kinases were sorted by percent inhibition, numbered from 1 to 419, and the % inhibition for each is plotted by kinase number. Green vertical lines indicate MNK1 and MNK2 for each profile. The plot shows the first 100 kinases and reveals that area under the curve described by compound **12** is 20% less than that of compound **10**. In addition, compound **12** at 1 μM inhibited MNK1 and MNK2 at 83 and 68%, respectively, while inhibiting only five other kinases >40% and one at 86%. Conversely, compound **10** in the same experiment inhibited MNK1 and 2 at 84 and 66%, respectively, but inhibited nine other kinases >40% and two at 100 and 91%, respectively. A similar trend was observed for other pyridone/benzene pairs.

electrostatic potential analysis (Figure 2A). The methyl substituent provided the best balance of kinome selectivity and potency enhancement overall.

Final Optimization and Identification of Compound 23. It was found that an unsubstituted 4-amino pyrimidine was able to maintain the hydrogen bond to Met162 backbone carbonyl as was observed with the cyclopropyl amide (cf. compound **20** vs **21**), but importantly, the free amino group abrogated metabolism observed for molecules with spirocarbocycles off the pyridone aminal. While the cyclopropylamide improved potency, it was also slightly less selective, adding five additional heavy atoms with an increased logP; therefore, we focused on 4-aminopyrimidines. A chlorine in the 5-position of the pyrimidine provided up to a log of additional affinity likely through a favorable interaction with the carbonyl of Leu90 (compound **22**, 84 pM cell activity, Table 1).

Starting with and maintaining good overall physicochemical properties along with the above potency enhancements provided a cohort of optimized molecules having low nanomolar cellular p-eIF4E potency, *in vivo* efficacy, good metabolic stability, and kinome selectivity. These were narrowed further based on multispecies pharmacokinetics (mouse, rat, dog, and monkey; Table 3). Compound **23** had the best overall profile and was consistently the top performer in tumor growth inhibition (TGI) and pharmacokinetic/pharmacodynamic (PK/PD) studies and was therefore selected as the development candidate (Figure 9). The crystal structure of compound **23** is shown in Figure 7A and confirms the pyridone's involvement in a Dunitz interaction with the Cys225 sulfur.

Compound 23 Is a Potent Inhibitor of MNK1 and MNK2 Signaling and Tumor Growth. We examined the

DOI: 10.1021/acs.jmedchem.7b01795
J. Med. Chem. 2018, 61, 3516−3540

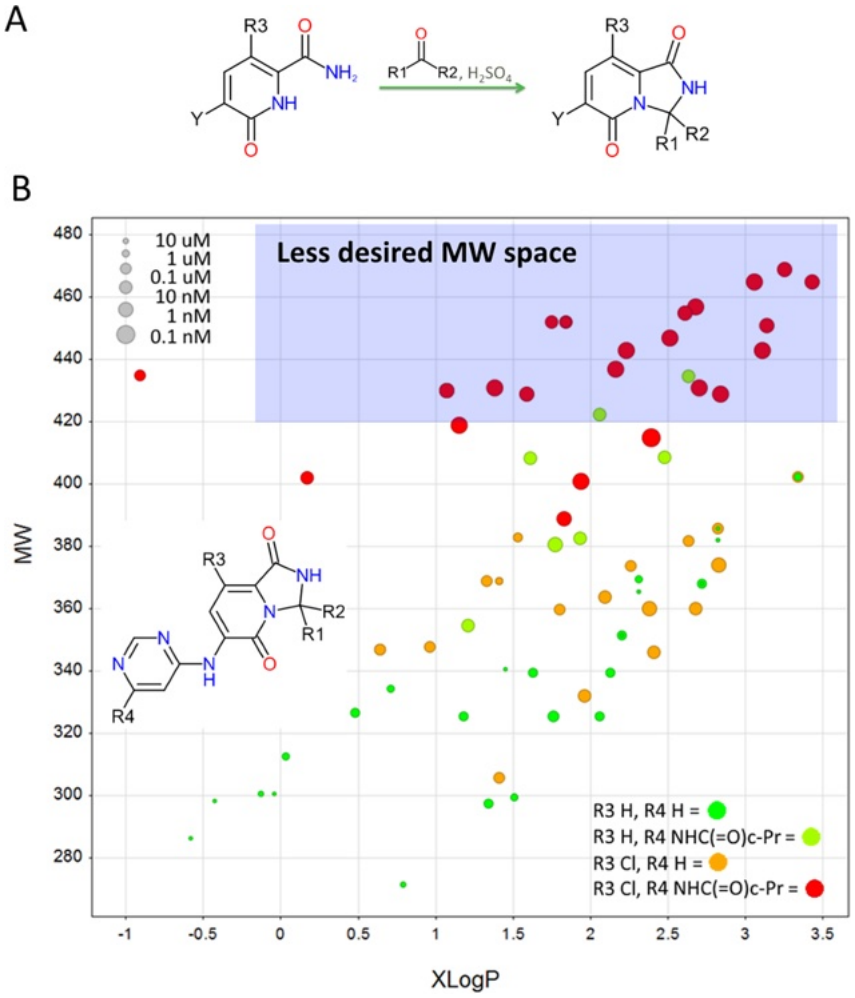

Figure 6. (A) Facile formation of stable pyridone−aminal via acid-catalyzed ketone condensation. (B) Properties of the structure-guided focused pyridone library (80 compounds). Note that the compounds that are exceptionally potent fall in the area of higher logP and molecular weight noted in light blue.

Table 2. Comparison of Biochemical, Cellular Potency (p-eIF4E), and Proliferation Data for Compounds 17, 18, and 19

Structure	ID	R1	R2	MNK1 enzyme IC_{50} (nM)	MNK2 enzyme IC_{50} (nM)	Cell Proliferation EC_{50} (nM)			HCT-116 peIF4E$_{(s209)}$ EC_{50} (nM)	Off-target kinases with >80% inhibition[a]
						PC3	HCT-116	SW-620		
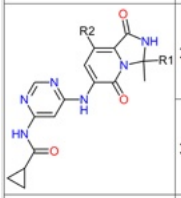	17	Me	H	2.7	2.3	>30,000	>30,000	>30,000	12.3	4[b]
	18		Cl	1.6	1.2	NA	2,700	2,800	1.8	10[c]
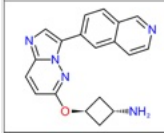	19	-	-	1.5	7.8	590	210	310	120	17[d]

[a]Fifty kinases tested at 1 μM compound. [b]KDR, Abl1, RET, Flt3. [c]Flt3, KDR, RET, YES1, ABL1, DYRK1A, PDGFRB, LCK, Aurora A, PDGFRA. [d]DYRK1A, Flt3, CDK2, CLK1, PDGFRB, PDGFRA, PlM1, CAMK2A, ROCK1, IRAK1, AMPK A1/B1/G1, LCK, TRKA, KDR, BRAF, MEK2, RSK1.

effect of compound **23** on eIF4E phosphorylation in an expanded set of tumor cell lines using the p-eIF4E Ser209 homogeneous time-resolved fluorescence (HTRF) assay. In all cell lines tested, compound **23** inhibited Ser209 phosphorylation of eIF4E with IC_{50} values ranging from 1.4 to 22 nM (Table S1). The effect of compound **23** on eIF4E Ser209 phosphorylation is specific to MNK1/2 inhibition, as overexpression of wild-type or a **23**-resistant allele of MNK2 (C225L) is sufficient to increase the **23** IC_{50} 100- to 860-fold, respectively (Figure S2A). Consistent with the HTRF results,

DOI: 10.1021/acs.jmedchem.7b01795
J. Med. Chem. 2018, 61, 3516−3540

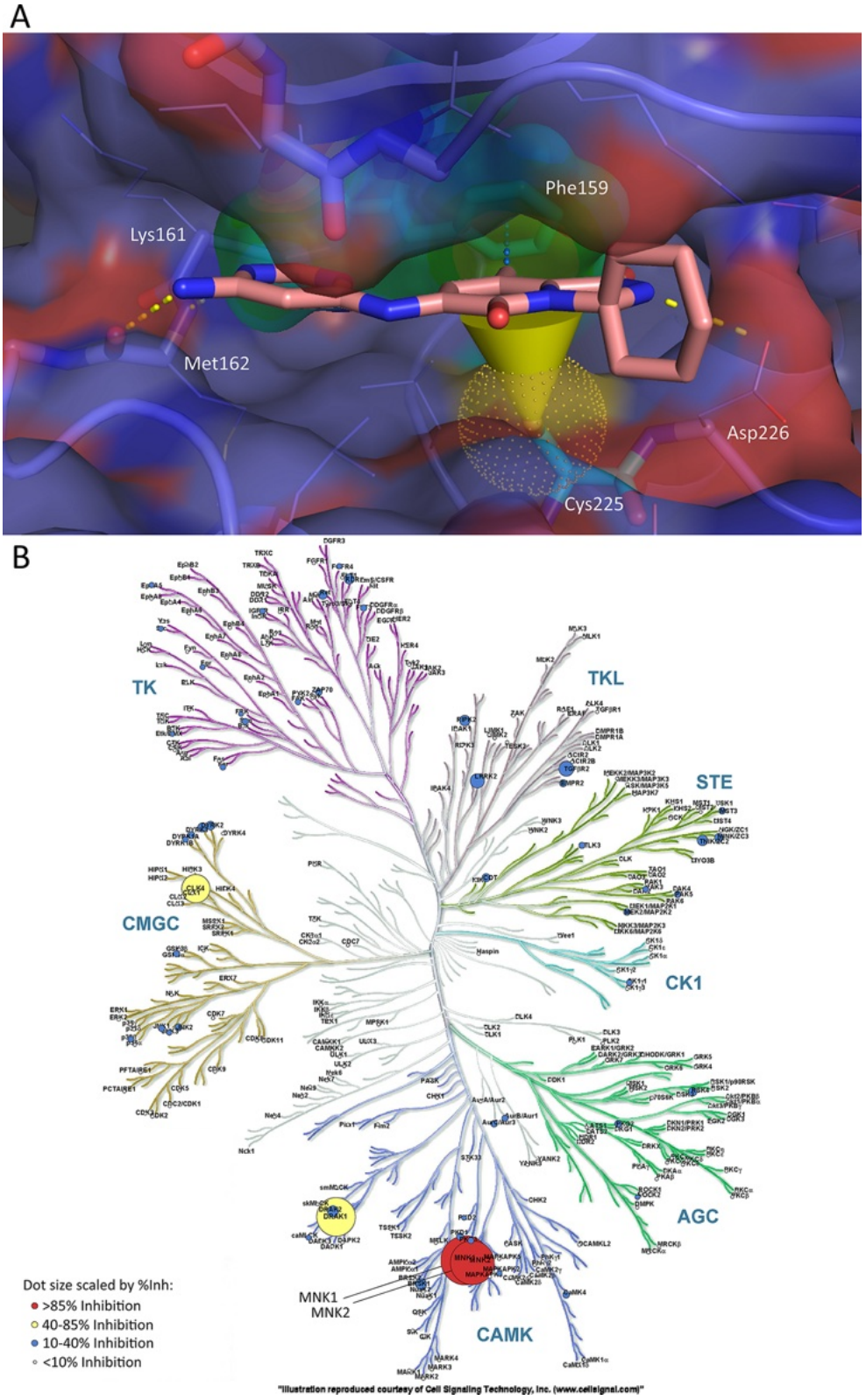

Figure 7. (A) Cocrystal structure of **23** bound to MNK2 (PDB code 6CK6). Compound **23** makes H-bond interactions with both hinge residues, Lys161 and Met162. The pyridone methyl interacts with the face of Phe159, and the Cys225 sulfur makes a similar Dunitz interaction as seen for compound **12** (Figure 5B). In addition, the five-membered ring amide nitrogen interacts with Asp226. (B) Kinome plot depicting the selectivity of **23** across >400 kinases.

potent dose-dependent inhibition of eIF4E Ser209 phosphorylation was observed by immunoblot analysis (Figures 10A and S2B). In addition, compound **23** did not affect expression of 4E-BP1 or its phosphorylation at Thr37 or Thr46. Importantly, phosphorylation of MAPK at Thr202/Tyr204 was also unaffected by compound **23**, demonstrating that **23** did not

DOI: 10.1021/acs.jmedchem.7b01795
J. Med. Chem. 2018, 61, 3516−3540

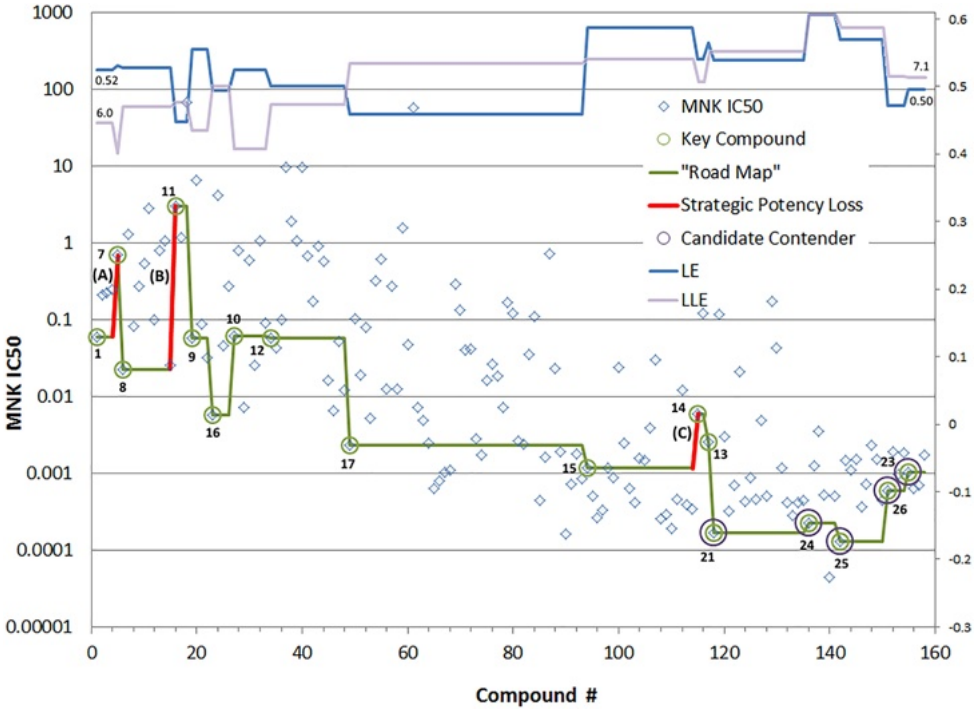

Figure 8. Plot showing the biochemical MNK IC_{50} for compounds in the diarylamine series (including both pyridones and nonpyridones) leading up to **23**. The roadmap for the key molecules discussed in the text (circled in green) highlighting strategic potency loss (red vertical lines) and the key contenders for the candidate selection (circled in purple). Strategic potency losses: (A) Deconstruction of the hinge binder (increase in novelty); (B) incorporation of the pyridone (shift to lower logP); and (C) replacement of the 5-chloro on the pyridone ring with methyl (selectivity improvement). Note that for all of these key changes, the corresponding LE and LLE were largely maintained throughout the optimization.

Table 3. Key Data for Compounds 21 and 23−26

ID	Structure	R1	MNK1 IC_{50} (nM) (LE, LLE)	MNK2 IC_{50} (nM) (LE, LLE)	peIF4E IC_{50} (nM) (LE, LLE)	Calc MW	XlogP	$LogP_{(exp)}$	HAC	Caco2 A to B (10^{-6}cm/s)	Caco2 Efflux Ratio	Liver Microsomes (%)[a] Mouse	Liver Microsomes (%)[a] Rat	Liver Microsomes (%)[a] Human	PK[b] (F%)	Off-Target Kinase Profile >50% inh @ 1 uM (Protein:% inh)
21	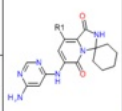	Cl	0.65 (0.51, 7.1)	0.68 (0.51, 7.1)	0.79 (0.5, 7.0)	361	2.1	3.2	25	4.2	6	73	69	89	58 (mouse)[c] 28 (rat)[c] >100 (dog)[d] 50 (monkey)[d]	DRAK1:96, DRAK2:82, CLK4:75, KDR:71, LRRK2:59, RIPK2:59, TGFBR2:57, DYRK3:56, BRSK1:55, RET:55
23		Me	2.4 (0.48, 6.7)	1.0 (0.50, 7.1)	6 (0.45, 6.3)	340	1.9	2.7	25	7.1[f] (19)	2.7[f] (2.8)	90	93	87	79 (mouse)[c] 85 (rat)[c] >100 (dog)[e] 24 (monkey)[e]	Drak1:82 (IC_{50}:131 nM), CLK4:60 (IC_{50}:787 nM)
24	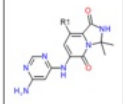	Cl	2.2 (0.54, 7.6)	0.14 (0.62, 8.8)	12 (0.5, 6.9)	321	1.1	1.8	22	0.9	27	95	100	100	79 (mouse)[c] 50 (rat)[c] >100 (dog)[e] 54 (monkey)[e]	DRAK1:88, KDR:74, DYRK2:67, BRSK1:52
25	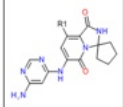	Cl	0.88 (0.52, 7.4)	0.13 (0.57, 8.3)	0.62 (0.53, 7.6)	347	1.6	2.4	24	1.2	18	71	73	85	80 (mouse)[c] 69 (rat)[c] >100 (dog)[e] 51 (monkey)[e]	KDR:96, DRAK1:95, FLT4:89, RET:87, DRAK2:82, DYRK2:81, CLK4:75, TGFBR2:74, DYRK3:67, FGR:60, BRSK1:58, RSK4:58, PDGFRA:55, FLT3:55, MAPKAPK3:54, LRRK2:52
26	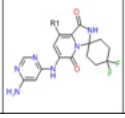	Me	1.4 (0.48, 6.7)	1.0 (0.50, 7.1)	24 (0.39, 5.5)	376	2.1	2.4	27	1.1	20	99	100	97	85 (mouse)[c] 56 (rat)[c] >100 (dog)[e] 58 (primate)[e]	DRAK1:68

[a]Percent compound remaining after 30 min incubation. [b]From solution formulations using a 1 mg/kg IV dose. [c]10 mg/kg oral dose. [d]5 mg/kg oral dose. [e]3 mg/kg oral dose. [f]Determined at Absorbtion System, LLC.

impact the activation status of signaling pathways that lie upstream of MNK1/2. We next expanded our analysis to growth factor and cytokine signaling pathways following compound **23** treatment. Treatment of TMD8 cells with **23** led to a dose-dependent reduction in secreted IL-6, IL-8, and TNFα (Figure 10B−D). Mechanistically, the decreased cytokine production arising from **23** treatment of TMD8 cells corresponded with reduced mRNA stability (Figure 10E), which is consistent with previous reports implicating MNK kinases in regulating the phosphorylation of RNA binding proteins.[12−14]

Other small molecule inhibitors possessing activity against MNK1/2, such as cercosporamide, CGP57380, merestinib, and cabozatinib, show antiproliferative activity in cell-based assays,

DOI: 10.1021/acs.jmedchem.7b01795
J. Med. Chem. 2018, 61, 3516−3540

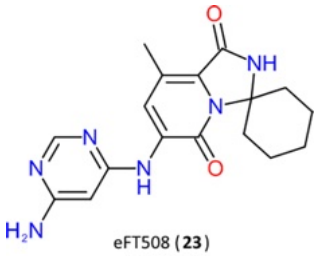

eFT508 (**23**)
MW 340
IC_{50} MNK1 = 2.4 nM
MNK2 = 1 nM LE 0.5 LLE 7
Cell IC_{50} 6 nM
PPB (m,r,d,p,h) ~50%
$logD_{7.4}$ = 2.7
F% (r,d,p) 25-100%
Caco2 A-B 7.1, ER 2.7

Figure 9. Compound **23** and some of its key properties.

which could potentially be attributed to their broader kinome activity as we also observed similar effects with our less-selective MNK1/2 compounds.[20,21,23,24] In contrast, compound **23** did not show antiproliferative activity in a panel of solid and hematological tumor cell lines (IC_{50} > 30 μM), although modest sensitivity (IC_{50} < 10 μM) was observed in a subset of DLBCL and a multiple myeloma cell line (Figure S3). This finding is not surprising given that genetic studies demonstrate that MNK1/2 is dispensable for normal growth but required for oncogene-induced transformation as assessed by anchorage-independent growth *in vitro* or tumorigenesis *in vivo*. The sensitivity observed in the DLBCL cell lines is consistent with previous studies demonstrating a role for MNK kinases in integrating signals from TLRs to regulate pro-inflammatory cytokines.[43,44] In particular, TMD8 cells harbor activating mutations in myeloid differentiation primary response gene 88 and CD79 and exhibit constitutive TLR pathway signaling, consistent with their sensitivity to **23**. In addition, elevated levels of eIF4E have been observed in DLBCL patient samples.[45]

Compound **23** potently inhibited eIF4E phosphorylation, select mRNA stability, and pro-inflammatory cytokine production in DLBCL cells; we therefore examined the efficacy of **23** in a TMD8 xenograft model. Compound **23** was well-tolerated at doses of 1 and 10 mg/kg QD as measured by lack of body weight loss (Figure S4), which corresponds to a minimal therapeutic index of ≥10 in this model. Furthermore, **23** treatment produced significant TGI over a 10-fold dose

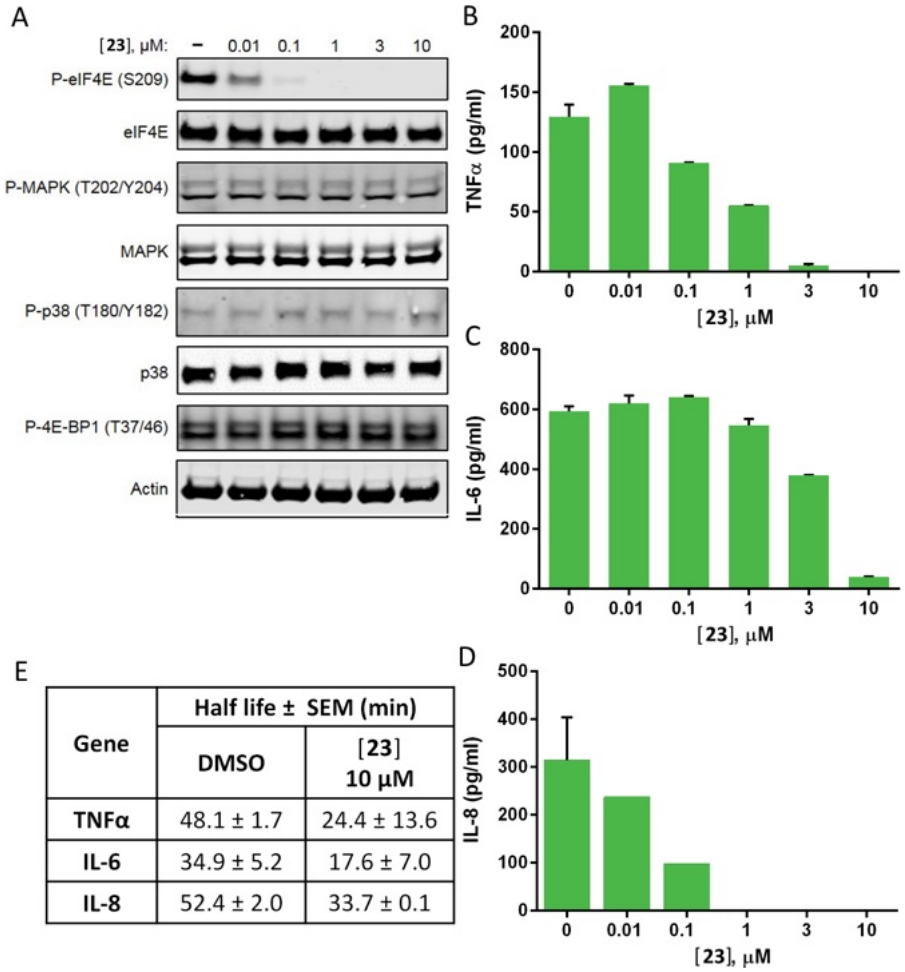

Gene	Half life ± SEM (min)	
	DMSO	[23] 10 μM
TNFα	48.1 ± 1.7	24.4 ± 13.6
IL-6	34.9 ± 5.2	17.6 ± 7.0
IL-8	52.4 ± 2.0	33.7 ± 0.1

Figure 10. Compound **23** inhibits MNK signaling and the production of pro-inflammatory cytokines important for tumorigenesis. (A) TMD8 cells were treated with the indicated concentrations of **23** for 2 h. Cell lysates were analyzed by immunoblotting with the indicated antibodies. (B−D) TMD8 cells were treated with the indicated concentrations of **23** for 48 h. Cell supernatants were collected, and the indicated cytokines were quantitated by ELISA. (E) TMD8 cells were treated with 10 μM **23** for 24 h. Actinomycin D was added, and RNA was harvested from the cells at various time points (0−360 min). Quantitation of RNA was performed by TaqMan assay, and calculated mRNA half-lives are shown.

DOI: 10.1021/acs.jmedchem.7b01795
J. Med. Chem. 2018, 61, 3516−3540

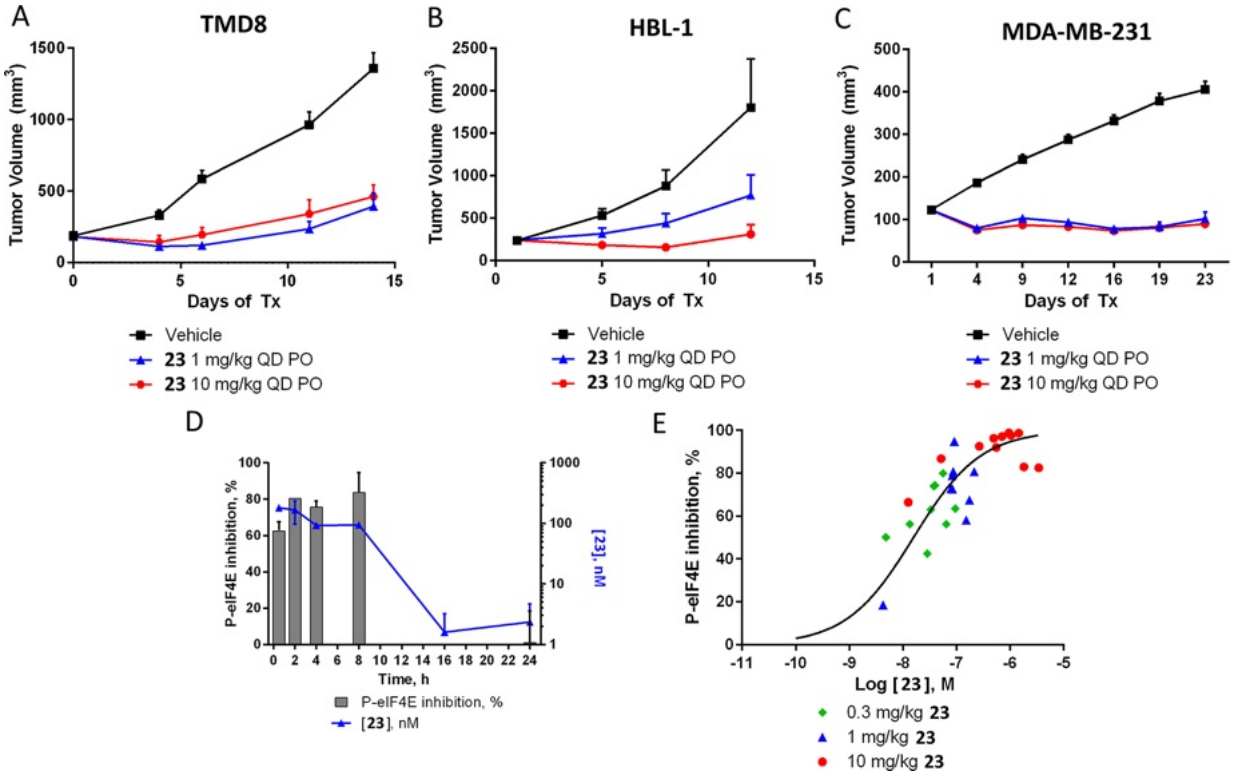

Figure 11. Compound **23** is efficacious in tumor xenografts. (A) TMD8 xenografts (10 mice/group) were treated with the indicated dose/schedule/route of **23** for 14 days. (B) HBL-1 xenografts (10 mice/group) were treated with indicated dose/schedule/route of **23** for 12 days. (C) MDA-MB-231 xenografts (10 mice/group) were treated with indicated dose/schedule/route of **23** for 23 days. Error bars are SEM. (D) TMD8 xenograft-bearing animals were treated with 1 mg/kg of **23**, and tumor and plasma samples were harvested at time points (0.5–24 h) postdose. Phosphorylation of eIF4E in the tumor was measured by immunoblot (% inhibition, left axis), and **23** levels were measured in plasma (nM, right axis). (E) Exposure–response plot of all time points and dosing groups of the TMD8 PK/PD study plotted as a function of the corresponding **23** exposure in plasma.

Scheme 1. Synthesis of Imidazopyridine 4[a]

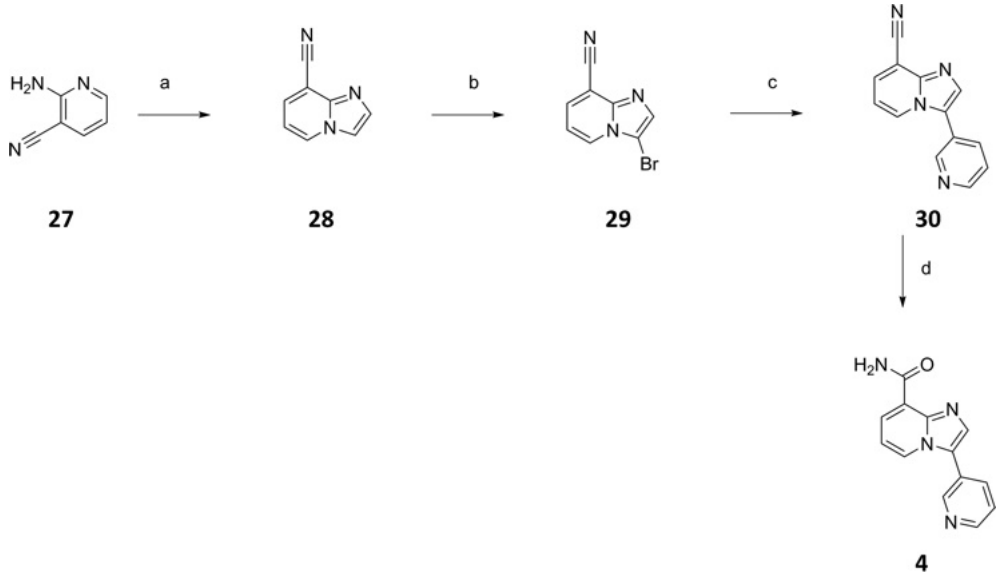

[a]Reagents and conditions: (a) 2-chloroacetaldehyde, ethanol, reflux, 86%; (b) NBS, DMF, 25 °C, 77%, (c) pyridine-3-ylboronic acid, Pd(dppf)Cl_2, K_2CO_3, 1,4-dioxane-H_2O, 100 °C, 40%; (d) 30% H_2O_2, K_2CO_3, 0 to 25 °C, 28%.

range, achieving an average TGI of 71% and 75% when dosed orally at 1 and 10 mg/kg QD, respectively (Figure 11A). We also observed similar activity in HBL-1 xenografts, an additional model of MyD88/CD79 mutant DLBCL (Figure 11B). Again, compound **23** was well-tolerated in the animals, and treatment resulted in an average TGI of 66% and 96%, when dosed at 1 or 10 mg/kg QD, respectively. This activity is consistent with the hypothesis that MNK plays a significant role in mediating TLR-

DOI: 10.1021/acs.jmedchem.7b01795
J. Med. Chem. 2018, 61, 3516–3540

MyD88 signaling in DLBCL. Finally, we tested compound **23** in the MDA-MB-231 breast cancer xenograft model. Increased phosphorylation of eIF4E has been shown in breast cancer patients and has been linked to poorer clinical outcome.[46] The growth of MDA-MB-231 xenografts *in vivo* was significantly inhibited (TGI > 100%) when animals were dosed with 1 or 10 mg/kg **23** QD (Figure 11C). Consistent with the MNK phenotype previously observed with compound **23**, MDA-MB-231 cells did not show growth inhibition *in vitro*, underscoring the fact that tumor cell/tumor microenvironment (TME) interactions important for tumorigenesis may be regulated by MNK.

In conjunction with the efficacy experiments, we assessed MNK inhibition through PK/PD measurement of p-eIF4E (Ser209) in the TMD8 xenografts at three dose levels (0.3, 1, and 10 mg/kg). In general, an oral dose of 1 mg/kg of **23** QD produced maximal efficacy and exhibited over 80% reduction in p-eIF4E for 8 h (Figure 11D). Plotting of the aggregated data from the three dose groups to generate an exposure−response curve resulted in calculated IC_{50} and IC_{90} values of 15.8 and 376 nM, respectively, which are consistent with the p-eIF4E inhibition values obtained *in vitro* (Figure 11E, Table S1). Importantly, these results demonstrate that p-eIF4E can be used as a PD marker for MNK inhibition *in vivo* and that ≥80% inhibition is associated with efficacy.

Synthetic Chemistry. All compounds described herein were prepared as outlined in Schemes 1−6. Compound **4** was obtained in the following manner (Scheme 1). Heating of 2-aminonicotinonitrile **27** with aqueous 2-chloroacetaldehyde afforded imidazocarbonitrile **28**. Subsequent bromination followed by Suzuki coupling with pyridinyl-3-ylboronic acid yielded compound **30**, which was hydrolyzed with basic hydrogen peroxide to give final compound **4**. Final compound **5** was obtained in three steps by Boc protection of pyrrolidine **31**, followed by Suzuki coupling with a Boc-protected pyrazole boronic ester to form the protected pyrazole, which was bis-deprotected to afford final compound **5** (Scheme 2).

Scheme 2. Synthesis of Pyrazole 5[a]

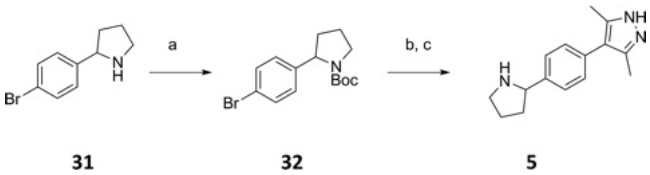

[a]Reagents and conditions: (a) di-*t*-butyl pyrocarbonate, 10% NaOH·H_2O, 0 °C, 86%; (b) *t*-butyl-3,5-dimethyl-4-(4,4,5,5-tetramethyl-1,3,2-dioxaborolan-2-yl)-1*H*-pyrazole-1-carboxylate, tetrakis-(triphenylphosphine)palladium(0), Na_2CO_3, 1,4-dioxane, 100 °C, 24%. (c) HCl-1,4-dioxane, 0−25 °C, 42%.

Pyrimidines **7** and **8** were prepared using conventional acid-catalyzed SNAr chemistry, from 4,6-dichloropyrimidine and 6-chloro-9*H*-purine **35**, respectively (Scheme 3). Monochloro pyrimidine **34** was dehalogenated via hydrogenolysis to produce final compound **7**. Final isoindolinone compounds **9** and **10** were prepared as outlined from the same bromomethylbenzoate **37** (Scheme 4). Coupling of *p*-methoxybenzylamine with **37** followed by ring closure produced PMB protected lactam **38**. Bis-methylation of **38** by heating with excess MeI in the presence of NaH, followed by Buchwald coupling with 4-aminopyrimidine and PMB deprotection gave final lactam compound **10**. Monomethylation of **38** was affected by treating with 1.5 equiv of MeI at room temperature to give **39**, which was subjected to the same two-step sequence of Buchwald coupling/PMB deprotection to yield final lactam compound **9**. Pyridone **11** was prepared beginning with esterification of 5-chloro-2-pyridine carboxylic acid **40** followed by oxidation to the *N*-oxide **41**. *N*-Oxide **41** was converted to the pyridone with trifluoroacetic anhydride followed by benzylic protection to give compound **42**. Buchwald coupling of **42** with 4-aminopyrimidine yielded **43**, which was debenzylated with triflic acid followed by aminolysis to afford final compound **11**.

Scheme 3. Synthesis of Benzamide 7 and Lactam 8[a]

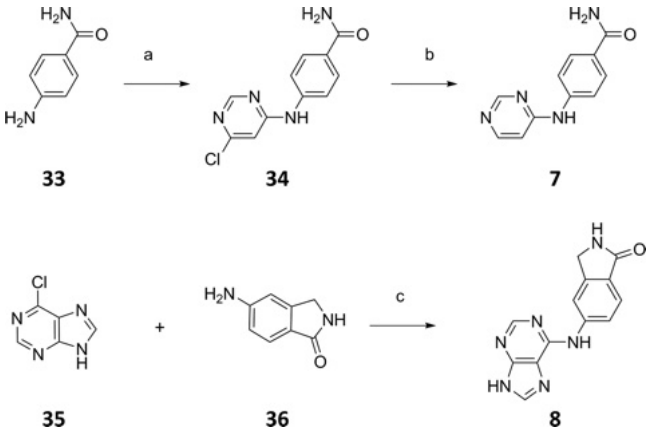

[a]Reagents and conditions: (a) 4,6-dichloropyrimidine, pTSA, toluene: 1,4-dioxane, 140 °C, 23%; (b) 10% Pd/C, H_2, 1,4-dioxane/CH_2Cl_2/MeOH, 15%; (c) camphorsulfonic acid, iPrOH, 100 °C, 58%.

Pyridones **12**−**15**, **17**, **18**, and **20**−**26** were all prepared using the general procedure outlined in Scheme 5. The suitably substituted pyridone **44**, prepared in a similar fashion outlined for **42**, was subjected to aminolysis to give the key intermediate carboxamide **45**. Formation of the lactam structure **46** was carried out by simply heating the respective carboxamide **45** with the desired ketone (R_1R_2CO) in H_2SO_4/1,4-dioxane to afford good yields of the desired cyclized material. Buchwald coupling of the corresponding halo-lactam **46** with the required substituted 4-amino pyrimidine (R4), yielded the final compounds in good yields after either basic or acidic deprotection.

The remaining two compounds **16** and **19** were prepared as outlined in Scheme 6. 6-Chloro-2-aminopyrimidine **47** was bis-protected with Boc-anhydride and then coupled with cyclopropanecarboxamide under palladium catalysis to give amide **48**. Boc deprotection with acid followed by Buchwald coupling with PMB protected lactam **38**, and final deprotection yielded the final cyclopropylamide **16**. Suzuki coupling of bromide **50** with isoquinolin-6-ylboronic acid gave compound **52**. SNAr coupling of *t*-butyl-(3-hydroxycyclobutyl)carbamate, **52**, and sodium hydride yielded intermediate ether **53**, which was deprotected with aqueous HCl to provide final compound **19**.

■ DISCUSSION AND CONCLUSIONS

Recruitment of mRNA to the ribosome is a fundamental component of mRNA translation and is regulated through translation initiation by eIF4E. Importantly, eIF4E has been shown to play a key role in the translation of proteins involved in driving tumorigenesis. While the MNKs are key modulators

DOI: 10.1021/acs.jmedchem.7b01795
J. Med. Chem. 2018, 61, 3516−3540

Scheme 4. Synthesis of Lactams 9−11[a]

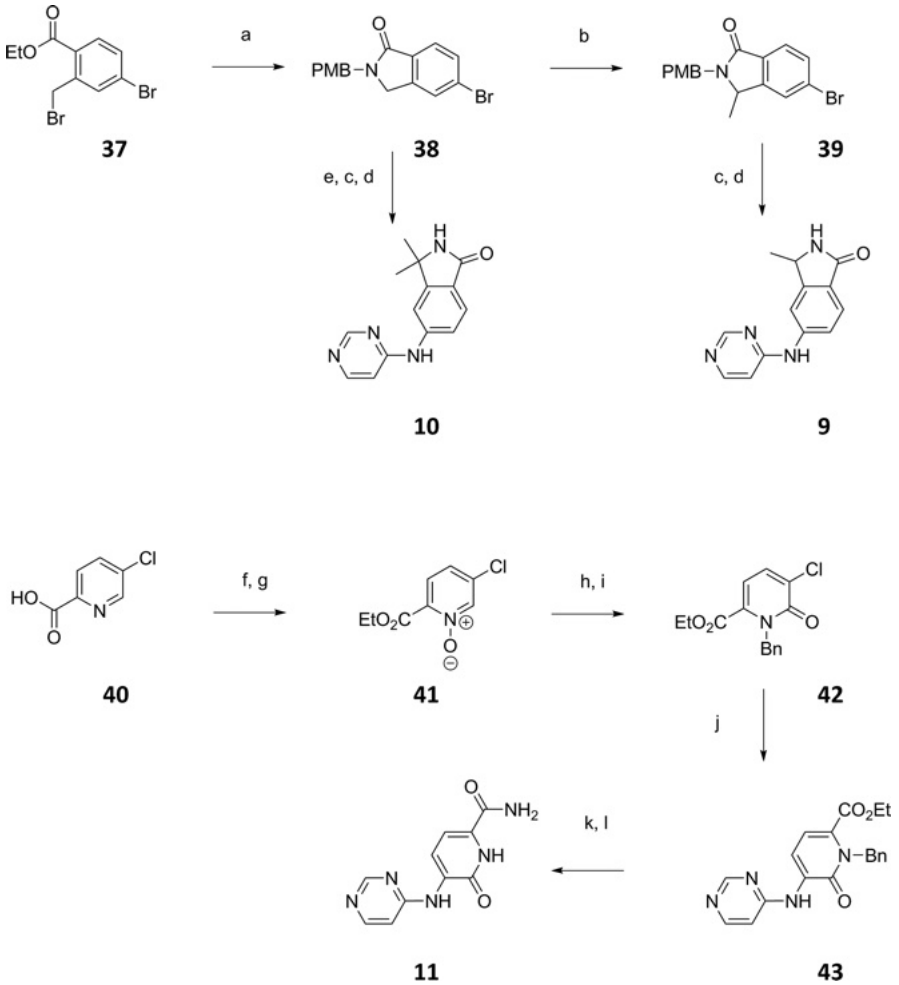

[a]Reagents and conditions: (a) *p*-MeOBnNH$_2$, DMF, Et$_3$N, 65 °C, 75%; (b) NaH, MeI, THF, 25 °C, 57%; (c) 4-aminopyrimidine, NaO-*t*-Bu, XPhos, Pd$_2$(dba)$_3$, toluene, 110 °C, 58−65%; (d) TFA, 100 °C, 19−22%; (e) NaH, MeI, THF, 70 °C, 37%; (f) EtOH, H$_2$SO$_4$, 80 °C, 86%; (g) urea, H$_2$O$_2$, TFAA, CHCl$_3$, 0−25 °C, 65%; (h) TFAA, DMF, 50 °C, 60%; (i) K$_2$CO$_3$, LiBr, Bu$_4$NBr, BnBr, toluene−water, 80 °C, 65%; (j) 4-aminopyrimidine, Cs$_2$CO$_3$, xantphos, Pd$_2$(dba)$_3$, dioxane, 90 °C, 61%; (k) TfOH, toluene, 140 °C, MW, 61%; (i) NH$_4$OH, 25 °C, 52%.

Scheme 5. General Synthesis of Lactams 12−15, 17, 18, 20−26[a]

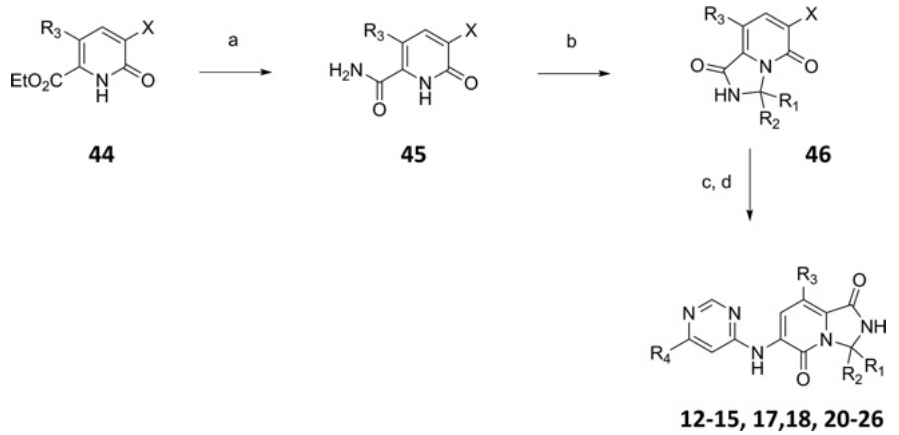

[a]Reagents and conditions: (a) 30% NH$_4$OH, 0−25 °C, 75%; (b) R$_1$R$_2$CO, 1,4-dioxane, H$_2$SO$_4$, 100 °C, 83%; (c) 4-amino-6-R$_4$-pyrimidine, Pd(OAc)$_2$, xantphos, Cs$_2$CO$_3$, 1,4-dioxane, 95 °C, 10−61%; (d) deprotection, KOH, EtOH, THF, H$_2$O, 25 °C or 4 M HCl, 1,4-dioxane, CH$_2$Cl$_2$, MeOH, 25 °C, 80%.

of eIF4E activity, the eIF4E protein has been targeted directly with an antisense oligonucleotide, ISIS 183750.[47] In addition, small molecule inhibitors such as EGI-1, briciclib, and 4E1R-cat that block the binding of eIF4E to eIF4G have been pursued,

DOI: 10.1021/acs.jmedchem.7b01795
J. Med. Chem. 2018, 61, 3516−3540

Scheme 6. Synthesis of Lactam 16 and Compound 19[a]

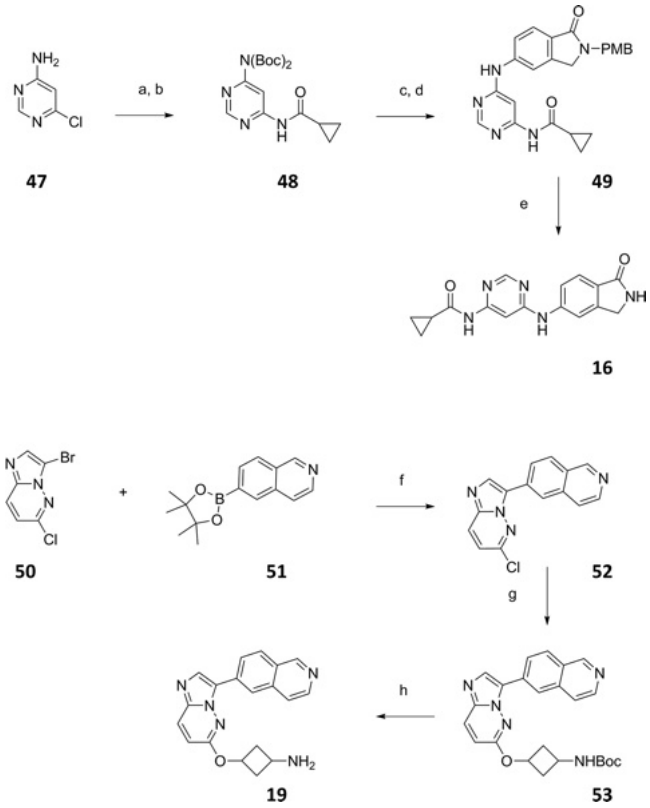

[a]Reagents and conditions: (a) $(Boc)_2O$, DMAP, THF, 25 °C, 51%; (b) cyclopropanecarboxamide, Cs_2CO_3, xantphos, $Pd_2(dba)_3$, 1,4-dioxane, 25 °C, 96%; (c) 4 N HCl, 1,4-dioxane, 25 °C; (d) **38**, Cs_2CO_3, Xphos, $Pd_2(dba)_3$, 1,4-dioxane, 90 °C, 42%, two steps; (e) TFA, reflux, 46%; (f) K_2CO_3, $Pd(PPh_3)_4$, monoglyme-H_2O, 85 °C, 62%; (g) *t*-butyl-(3-hydroxycyclobutyl)carbamate, NaH, THF, °C, 29%; (h) 4 N HCl, MeOH, 25 °C, 58%.

yet only modest antitumor activity has been observed with these agents and little progress has been made clinically.[48−51] In addition, a number of MNK small molecule inhibitors have been described that are either less potent or lack selectivity against MNK1/2.[20−23,25,26,52] BAY1143269, which is more selective for MNK1, entered the clinic, but enrollment is currently suspended.[27] There may be limitations with an MNK1 selective approach as MNK2 can function in a compensatory fashion. A dual MNK inhibitor has been reported to be in Phase 1 clinical trial in Singapore.[53] A selective and potent dual MNK1/2 inhibitor represents a new therapeutic opportunity; yet, to date, compounds to definitively assess this potential have remained elusive.

We have outlined the design of a very potent and selective dual MNK1/2 inhibitor, **23**, having a novel pyridone−aminal chemical structure described for the first time in the kinase literature, and the first dual MNK inhibitor to be tested clinically in the treatment of both solid and hematological malignancies. The design process leveraged specific stereo-electronic interactions with the unique active site of this kinase in an iterative structure-based approach employing 30 cocrystal structures. Potency was deliberately traded for drug-like properties (lower logP and MW) during optimization (Figure 8). Importantly, only 110 pyridone containing compounds were required to identify **23**, highlighting the efficient optimization approach employed and the value of beginning with and maintaining good physicochemical properties. A roadmap for the key molecules in the optimization process is outlined in Figure 8 highlighting strategic potency loss (1−3, red vertical lines) and key contenders for candidate selection. During the course of optimization, cell potency closely tracked enzyme potency, LE was maintained finishing slightly higher (0.6), and final LLEs improved to >8.

Compound **23** was designed to be equally effective against both MNK1 and MNK2 isoforms as they are generally coexpressed and can both serve to phosphorylate eIF4E at Ser209, implying that dual inhibition would be necessary to avoid compensatory signaling by either isoform. As such, inhibition of eIF4E phosphorylation was always commensurate with the activity against the less sensitive MNK isoform, suggesting that dual MNK1/2 engagement was critical for maximal reduction in p-eIF4E levels and robust efficacy. Importantly, **23** potently inhibits p-eIF4E in a range of solid and hematological tumor cell lines. In contrast to other small molecule inhibitors of MNK1/2, **23** does not cause inhibition of proliferation across a broad panel of tumor cell lines. This biology might have been masked by a less selective kinome profile and broad antiproliferative effects, and this understanding facilitated the design of **23**. Sufficient selectivity against the broader protein and lipid kinome is essential to understanding MNK pharmacology. Only two protein kinases outside of MNK were significantly inhibited by **23** in biochemical assays (Figure 7B): DRAK1/STK17A, a member of the death-associated protein family of serine/threonine kinases, has been shown to have a pro-apoptotic role in certain contexts, but a pro-tumorigenic effect in others;[54−57] and CLK4, a member of the cdc2/cdc28-like kinase family, plays a role in alternative mRNA splicing and in cytokinesis.[58,59] It is unclear whether **23** significantly inhibits DRAK1 and CLK4 in intact cells, and we do not see any cellular phenotypes consistent with inhibition of either kinase in tumor cells.

DLBCL is currently defined by three main subtypes: activated B-cell (ABC), germinal center B-cell, and primary mediastinal B-cell lymphoma.[60] Patients with ABC-DLBCL have the worst prognosis with <40% cure rate. ABC-DLBCL has been characterized by constitutive activation of NFkB signaling due to oncogenic mutations that activate B cell receptor signaling (e.g., CD79, CARD11, and A20).[61] In addition, activating mutations in MyD88 occur in ∼39% of ABC-DLBCL leading to NFkB activation that drives increased cytokine and chemokine production. MNK1/2 are recognized regulators of cytokine signaling and production. Pro-inflammatory cytokines are key survival factors for ABC-DLBCL tumors, and cytokine expression is associated with poor prognosis.[32,33] Compound **23** is effective at blocking pro-inflammatory cytokine production in MyD88 mutant models of ABC-DLBCL. Post-transcriptional regulation of cytokine production is known to be regulated at the level of mRNA stability through adenylate−uridylate-rich elements in the 3′-untranslated regions of their mRNA.[62] Compound **23** treatment results in a 1.5−2-fold decrease in cytokine mRNA half-life, consistent with the observed reduction in secreted cytokine proteins. Further testing of **23** *in vivo* demonstrated significant efficacy in multiple MyD88 mutant DLBCL tumor models illustrating its potential as a novel therapeutic strategy for this disease (Figure 11). Compound **23** is well tolerated at doses that deliver maximal efficacy and target engagement *in vivo* as measured by inhibition of p-eIF4E, consistent with normal viability and development of MNK1/2 double knockout mice.

DOI: 10.1021/acs.jmedchem.7b01795
J. Med. Chem. 2018, 61, 3516−3540

Tumor-promoting inflammation is recognized as an enabling characteristic of cancer.[63] Pro-inflammatory cytokines and chemokines are key mediators of this effect, impacting both tumor cell survival signaling and the composition and signaling of the TME. Compound **23** selectively regulates the production of pro-inflammatory cytokines and chemokines and has the potential to reshape the TME. This mechanism of action is likely contributing to the antitumor efficacy in both the DLBCL and MDA-MB-231 models and is the focus of continuing evaluation.

This work has highlighted the strong potential for agents that modulate dysregulated translation acting through eIF4E and also affecting mRNA stability. We have shown that potent MNK inhibition has significant effects on multiple pro-tumorigenic cytokines, such as TNFα, IL-6, and IL-8, which are, in turn, important mediators of oncogenesis and tumor progression.[64,65] These profound effects, both intrinsic and extrinsic to the tumor, are particularly interesting given that a potent and selective dual MNK inhibitor does not display broad antiproliferative activity *in vitro*, yet demonstrates potent antitumor activity *in vivo* against models utilizing the same cell lines. These data are consistent with the phenotype of the MNK1/2 double knockout mouse, which develops normally. This also highlights the potential limitation of screening for anticancer activity in an *in vitro* antiproliferative setting alone, particularly for agents that might act via mechanisms extrinsic to the tumor. Based on the preclinical profile of **23** and demonstrated *in vivo* activity in multiple tumor models, selective inhibition of MNK1 and MNK2 has potential in the treatment of cancer. Compound **23** is currently under evaluation in Phase 2 clinical trials in patients with advanced solid tumors and lymphoma.

■ EXPERIMENTAL SECTION

General. All reagents and solvents were used as purchased from commercial sources. Flash column chromatography was performed with a Teledyne ISCO CombiFlash Rf system using normal-phase silica columns (230−400 mesh). ^{1}H NMR spectra were recorded on a Bruker Advance-400 spectrometer at 400 MHz or a Bruker-Biospin AVANCE 500 MHz NMR spectrometer. Coupling constants (J) are expressed in hertz (Hz). Chemical shifts (δ) of NMR are reported in parts per million (ppm) units relative to an internal control (TMS). Microwave reactions were performed with a Biotage Initiator focused beam microwave reactor (300 W). HPLC purification was performed on a Waters automated purification system with 2767 sample controller and 2545 binary pump using Mass Lynx software and a Waters Sunfire C-18 (19 × 250 mm, 10 μm)/Waters X-Select Phenyl Hexyl (19 × 250 mm,5 μm) column. Analytical purity was assessed on a Waters Acquity Ultra Performance UPLC with 3100 SQD equipped with Acquity BEH C-18 (2.1 × 50 mm, 1.7 μm) column, and all compounds tested were determined to be >95% pure using this method. High resolution mass spectroscopy (HRMS) was performed using a Triple TOF 5600+ mass spectrometer (hybrid quadrupole time-of-flight platform; AB Sciex) connected to a 1290 UHPLC system (Agilent). The mass spectrometer was operated in electrospray positive ionization mode (ESI+). Acquisition was a full scan from m/z 100 to 1000 with a pulser frequency of 18.092 kHz and accumulation time of 75 ms. All animal studies were carried out in accordance with the guidelines established by the Institutional Animal Care and Use Committee at Explora BioLabs (San Diego, CA; Animal Care and Use Protocol (ACUP) #EB15−053).

*4-((7H-Purin-6-yl)amino)benzamide (**1**).* See Oyarzabal et al.[28] Purchased from Ryan Scientific, Inc. Purity >95%; ^{1}H NMR (400 MHz, DMSO-d_6) δ 13.30 (br s, 1 H), 10.07 (s, 1 H), 8.48 (s, 1 H), 8.36 (s, 1 H), 8.10 (d, J = 22 Hz, 1 H), 7.92−7.84 (m, 3 H), 7.30 (s, 1 H).

*3-(Pyridin-4-yl)imidazo[1,2-b]pyridazine (**2**).* See Oyarzabal et al.[28] HPLC Purity 95.7%; ^{1}H NMR (400 MHz, DMSO-d_6) δ 8.76 (dd, J = 8, 3 Hz, 1 H), 8.72 (d, J = 15 Hz, 2 H), 8.61 (s, 1 H), 8.34−8.26 (m, 3 H), 7.42 (dd, J = 23, 11 Hz, 1 H).

*3-Phenyl-5-(pyridin-4-yl)-1H-indazole (**3**).* See Reich et al.[66] HPLC Purity >99%; the spectral data of the compound matched those in the reference.

*3-(Pyridin-4-yl)imidazo[1,2-a]pyridine-8-carboxamide (**4**).* Synthesized via the methodology described in Yang et al. (Scheme 1).[67]

A mixture of 2-aminonicotinonitrile **27** (2.5 g, 21 mmol) and 40% aqueous 2-chloroacetaldehyde (18.8 mL, 94.88 mmol, 4.5 equiv) in ethanol (100 mL) was refluxed overnight. The volatiles were evaporated, and the residue was treated with ethyl acetate (20 mL). The solid was collected by filtration, washed with EtOAc (5 mL), and dried under vacuum to give the desired product as the HCl salt. The salt was treated with 2 N aqueous Na_2CO_3 solution (20 mL), and extracted with DCM (50 mL × 2). The combined DCM solution was washed with brine, dried (Na_2SO_4), and concentrated to give imidazo[1,2-a]pyridine-8-carbonitrile **28** as a light brown solid (2.6 g, yield 86%). ^{1}H NMR (400 MHz, DMSO-d_6) δ 8.88 (d, J = 16.9 Hz, 1H), 8.15 (s, 1H), 7.96 (d, J = 17.6 Hz, 1H), 7.73 (s, 1H), 7.06 (t, J = 17.3 Hz, 1H); MS (ESI) m/z 144.17 [M + H]$^+$. To a stirred solution of 2-methylimidazo[1,2-a]pyridine-8-carbonitrile **28** (1.5 g, 9.5 mmol) in DMF (15 mL) at rt was added NBS (1.8 g, 10 mmol). The resulting mixture was stirred for 5 min and was diluted with water (150 mL). The mixture was extracted with EtOAc (100 mL × 2). The combined extracts were washed with brine, dried (Na_2SO_4), and concentrated to give the title compound **29** as a white solid (1.73 g, yield 77%). The compound was pure enough for the next reaction. ^{1}H NMR (400 MHz, DMSO-d_6) δ 8.69 (d, J = 17.2 Hz, 1H), 8.09 (d, J = 17.7 Hz, 1H), 7.91 (s, 1H), 7.23 (t, J = 17.6 Hz, 1H); MS (ESI) m/z 223.90 [M + H]$^+$.

To a mixture of 3-bromoimidazo[1,2-a]pyridine-8-carbonitrile **29** (0.5 g, 1 equiv), pyridin-3-ylboronic acid (1.1 equiv), and K_2CO_3 (5 equiv) in 1,4-dioxane (10 mL) and water (2.5 mL) under nitrogen atmosphere was added Pd(dppf)Cl_2 (0.1 equiv). The resulting reaction mixture was heated at 100 °C overnight. The reaction was cooled to rt, diluted with water (30 mL), and extracted with EtOAc (30 mL × 2). The combined organic extracts were washed with brine, dried (Na_2SO_4), and evaporated to give the crude product, which was purified on a silica gel column to provide 3-(pyridin-3-yl)imidazo[1,2-a]pyridine-8-carbonitrile **30** in 40% yield. ^{1}H NMR (400 MHz, DMSO-d_6) δ 8.90 (d, J = 4.6 Hz, 1H), 8.88 (d, J = 17.4 Hz, 1H), 8.68 (dd, J = 11.7, 2.9 Hz, 1H), 8.16 (dt, J = 15.4, 4.2 Hz, 1H), 8.06 (d, J = 17.6 Hz, 1H), 8.04 (s, 1H), 7.60 (dd, J = 19.6, 12.1 Hz, 1H), 7.12 (t, J = 17.6 Hz, 1H); MS (ESI) m/z 221.06 [M + H]$^+$.

To a solution of 3-(pyridin-3-yl)imidazo[1,2-a]pyridine-8-carbonitrile **30** (0.15 g) in DMSO (3 mL) cooled with an ice water bath was added 30% H_2O_2 (1.2 mL) and anhydrous K_2CO_3 (0.2 g). The reaction mixture was allowed to warm to rt and stirred for 10 min. The reaction mixture was diluted with water (10 mL) and extracted with EtOAc. The ethyl acetate extracts were concentrated and the residue was purified on a silica gel column to provide 3-(pyridin-3-yl)imidazo[1,2-a]pyridine-8-carboxamide **4** as a light yellow solid in 28% yield. HPLC purity: 96.25%; ^{1}H NMR (400 MHz, DMSO-d_6), δ 9.54 (br, 1H), 8.91 (d, J = 1.6 Hz, 1H), 8.78 (dd, J = 6.8, 0.8 Hz, 1H), 8.68 (dd, J = 4.8, 1.2 Hz, 1H), 8.17 (dt, J = 8.0, 2.0 Hz, 1H), 8.11 (dd, J = 7.2, 1.2 Hz, 1H), 8.05 (br, 1H), 8.01 (s, 1H), 7.61 (dd, J = 7.6, 5.2 Hz, 1H), 7.17 (t, J = 7.2 Hz, 1H); ^{13}C NMR (125 MHz, DMSO-d_6) δ 163.6, 149.2, 148.7, 144.0, 135.3, 132.4, 128.2, 127.6, 124.6, 124.0, 123.0, 121.0, 112.8; mass spectrometry atmospheric pressure ionization: m/z 239 [M + H]$^+$. HRMS: measured m/z [M + H]$^+$ 239.0927 (calcd. for $C_{13}H_{11}N_4O$: 239.0928).

*3,5-Dimethyl-4-(4-(pyrrolidin-2-yl)phenyl)-1H-pyrazole (**5**).* To a solution of 2-(4-bromophenyl)pyrrolidine **31** (0.5 g, 2.20 mmol) in 1,4-dioxane (12.5 mL), 10% sodium hydroxide solution (2 mL) was added at 0 °C, and the mixture was stirred for 10 min (Scheme 2). Di-t-butyl pyrocarbonate (0.6 mL, 3.0 mmol) was added, and the reaction mixture was allowed to stir at rt for 3 h. The reaction mixture was diluted with water and extracted with ethyl acetate. The organic layer

DOI: 10.1021/acs.jmedchem.7b01795
J. Med. Chem. 2018, 61, 3516−3540

was separated, washed with brine, dried over Na_2SO_4, and concentrated under reduced pressure to obtain a residue, which was purified by silica gel column chromatography to afford *t*-butyl 2-(4-bromophenyl)pyrrolidine-1-carboxylate **32**. Yield: 0.62 g, 86%; ^{1}H NMR (400 MHz, chloroform-d_1) δ 7.41 (d, J = 7.92 Hz, 2H) 7.05 (d, J = 7.92 Hz, 2H) 4.67−4.79 (m, 1H) 3.60−3.62 (m, 2H) 2.29−2.32 (m, 1H) 1.83−1.91 (m, 2H) 1.75−1.78 (m, 1H) 1.22 (s, 9H); MS (ESI) m/z 333 [M + H]$^+$. A solution of *t*-butyl 2-(4-bromophenyl)-pyrrolidine-1-carboxylate **32** (0.3 g, 0.93 mmol), *t*-butyl-3,5-dimethyl-4-(4,4,5,5-tetramethyl-1,3,2-dioxaborolan-2-yl)-1H-pyrazole-1-carboxylate (0.303 g, 0.93 mmol), and 2 M sodium carbonate (0.3 g, 2.79 mmol) in 1,4-dioxane (12 mL) was degassed with argon for 30 min. Tetrakis(triphenylphosphine)palladium(0) (0.054 g, 0.046 mmol) was added, and the reaction mixture was further degassed for 15 min. The reaction mixture was heated at 100 °C for 16 h. The reaction mixture was filtered through Celite and washed with ethyl acetate. The filtrate was concentrated under reduced pressure, and the residue was purified by silica gel column chromatography to afford *t*-butyl 4-(4-(1-(*t*-butoxycarbonyl)pyrrolidin-2-yl)phenyl)-3,5-dimethyl-1*H*-pyrazole-1-carboxylate. Yield: 0.1 g, 24%. MS (ESI) m/z 442 [M + H]$^+$.

To a stirred solution of *t*-butyl 4-(4-(1-(*t*-butoxycarbonyl)-pyrrolidin-2-yl)phenyl)-3,5-dimethyl-1*H*-pyrazole-1-carboxylate (0.1 g, 0.22 mmol) in 1,4-dioxane (8 mL), 4 M 1,4-dioxane/HCl (8 mL) was added at 0 °C, and the reaction mixture was stirred at rt for 15 h. After complete consumption of starting material, the solvent was removed under reduced pressure, and the residue was neutralized with sodium carbonate resin. The reaction mixture was filtered and concentrated under reduced pressure and purified by repeated washing with ether and pentane to obtain 3,5-dimethyl-4-(4-(pyrrolidin-2-yl)phenyl)-1*H*-pyrazole **5**. Yield: 0.03 g, 42%. HPLC purity: 98.37%; ^{1}H NMR (400 MHz, methanol-d_4) δ 7.52 (d, J = 7.9 Hz, 2H), 7.39 (d, J = 7.9 Hz, 2H), 4.59 (dd, J = 9.5, 6.5 Hz, 1H), 3.49−3.29 (m, 2H), 2.56−2.41 (m, 1H), 2.32−2.12 (m, 9H); ^{13}C NMR (125 MHz, DMSO-d_6) δ 142.8, 131.9, 128.2, 128.1, 126.5, 125.5, 116.7, 61.5, 54.3, 46.3, 34.5, 25.2, 11.3. MS (ESI) m/z 242 [M + H]$^+$ HRMS: measured m/z [M + H]$^+$ 242.1651 (calcd. for $C_{15}H_{20}N_3$: 242.1654).

*4-(3-(Piperidin-4-yl)-1H-pyrazol-5-yl)pyridine (**6**).* Prepared as reported by Bilodeau et al.[28,68] HPLC Purity 83%; the spectral data of the compound matched those in the reference.

*4-(Pyrimidin-4-ylamino)benzamide (**7**).* To a stirred suspension of 4,6-dichloropyrimidine (2 g, 13.51 mmol) and 4-aminobenzamide **33** (1.83 g, 13.51 mmol) in toluene-1,4-dioxane (20 mL, 1:1), *p*-toluenesulfonic acid (pTSA) (2.82 g, 14.86 mmol) was added, and the reaction mixture was heated at 140 °C for 5 h in a sealed tube (Scheme 3). The reaction mixture was neutralized with saturated aqueous $NaHCO_3$ solution, and the compound was extracted with 10% methanol−DCM. The combined organic layer was dried over anhydrous Na_2SO_4, filtered, and concentrated under reduced pressure. The resulting solid was washed with ethyl acetate to afford 4-((6-chloropyrimidin-4-yl)amino)benzamide **34** as a white solid. Yield: 0.68 g, 22.7%. ^{1}H NMR (400 MHz, DMSO-d_6) δ 10.09 (s, 1H) 8.55 (s, 1H) 7.85−7.88 (m, 3H) 7.72 (d, J = 8.47 Hz, 2H) 7.24 (br s, 1H) 6.88 (s, 1H); MS (ESI) m/z 249 [M + H]$^+$.

To a stirred suspension of 4-((6-chloropyrimidin-4-yl)amino)-benzamide **34** (0.3 g, 1.21 mmol) in 1,4-dioxane/DCM/methanol (10 mL, 2:1:1) was added 10% Pd−C, and the reaction mixture was hydrogenated under 1 atm pressure at rt for 2 h. The reaction mixture was filtered through a Celite pad, and the pad was washed with methanol. The filtrate was concentrated under reduced pressure, taken up in a minimum amount of methanol, and refluxed to give a clear solution, which was cooled to rt. The obtained solid was filtered and dried to afford 4-(pyrimidin-4-ylamino)benzamide (**7**) as a white solid. Yield: 0.039 g, 15%. HPLC purity: 97.50%; ^{1}H NMR (400 MHz, DMSO-d_6) δ 11.55 (s, 1H), 8.97 (s, 1H), 8.41 (dd, J = 7.0, 1.4 Hz, 1H), 7.99−7.90 (m, 3H), 7.79 (d, J = 8.5 Hz, 2H), 7.35 (s, 1H), 7.18 (d, J = 7.0 Hz, 1H); ^{13}C NMR (125 MHz, DMSO-d_6) δ 167.0, 161.5, 152.6, 144.3, 139.8, 130.6, 128.4, 120.9, 107.6. MS (ESI) m/z 215.09 [M + H]$^+$; HRMS: measured m/z [M + H]$^+$ 215.0927 (calcd, for $C_{11}H_{11}N_4O$: 215.0926).

*5-((9H-Purin-6-yl)amino)isoindolin-1-one (**8**).* Synthesized as reported in U.S. Patent Application No. WO2017075394.[69] A mixture of 6-chloro-9*H*-purine **35** (0.15 g, 0.97 mmol), 5-aminoisoindoline-1-one **36** (0.14 g, 0.97 mmol), and (1*S*)-(+)-camphor-10-sulfonic acid (0.27 g, 1.16 mmol) in isopropanol (10 mL) was heated in a sealed tube at 100 °C for 4 h. After completion of the reaction, the mixture was concentrated, and the obtained solid was filtered and recrystallized from ethanol and isopropanol to afford 5-((9*H*-purin-6-yl)amino)-isoindolin-1-one (**8**) as off-white solid. Yield: 0.15 g, 58%. HPLC purity: 99.92%; ^{1}H NMR (400 MHz, DMSO-d_6) δ 11.01 (s, 1H), 8.66 (s, 2H), 8.44 (s, 1H), 8.31 (d, J = 1.9 Hz, 1H), 7.99 (dd, J = 8.3, 1.8 Hz, 1H), 7.67 (d, J = 8.3 Hz, 1H), 4.40 (s, 2H); ^{13}C NMR (125 MHz, DMSO-d_6) δ 169.5, 149.8, 149.7, 149.5, 141.2, 141.4, 127.9, 123.3, 120.1, 114.9, 114.3, 44.8. MS (ESI) m/z 267 [M + H]$^+$. HRMS: measured m/z [M + H]$^+$ 267.0989 (calcd. for $C_{13}H_{11}N_6O$: 267.0989).

*3-Methyl-5-(pyrimidin-4-ylamino)isoindolin-1-one (**9**).* Synthesized as reported in U.S. Patent Application No. WO2017075394.[69] To a stirred solution of ethyl 4-bromo-2-(bromomethyl)benzoate **37** (16 g, 52.1 mmol) in dimethylformamide (150 mL) at 0 °C, triethylamine (22 mL, 156.3 mmol) was added and stirred for 15 min, 4-methoxybenzylamine (8.84 mL, 67.7 mmol) was added, and the reaction mixture was stirred at rt for 30 min and then heated at 65 °C for 5 h (Scheme 4). The reaction mixture was cooled, quenched with ice, and acidified with 1 N hydrochloric acid to pH = 3. The precipitated solid was filtered, dried, and purified by silica gel column chromatography using 30% ethyl acetate in hexane to afford 5-bromo-2-(4-methoxybenzyl)isoindolin-1-one **38**. Yield: 13.04 g, 75.4%. ^{1}H NMR (400 MHz, chloroform-d_1) δ 7.74 (d, J = 8.0 Hz, 1H), 7.60 (d, J = 8.4 Hz, 1H), 7.53 (s, 1H), 7.22 (d, J = 8.4 Hz, 2H), 6.86 (d, J = 8.4 Hz, 2H), 4.72 (s, 2H), 4.22 (s, 2H), 3.79 (s, 3H); MS (ESI) m/z 332 [M + H]$^+$.

To an ice cooled suspension of sodium hydride (0.072 g, 60% dispersion in mineral oil, 1.8 mmol) in dry THF (5 mL) a solution of 5-bromo-2-(4-methoxybenzyl)isoindolin-1-one **38** (0.5 g, 1.5 mmol) in dry THF (5 mL) was added dropwise under nitrogen atmosphere. The reaction mixture was stirred for 1 h, and iodomethane (0.14 mL, 2.2 mmol) was added. The reaction mixture was stirred at rt for 2 h and then quenched with ice−water and extracted with ethyl acetate. The combined organic layer was dried over anhydrous sodium sulfate, filtered, and concentrated under reduced pressure. The residue was purified by silica gel column chromatography using 0−8% of ethyl acetate in hexane to afford 5-bromo-2-(4-methoxybenzyl)-3-methyl-isoindolin-1-one **39**. Yield: 0.29 g, 57%. ^{1}H NMR (400 MHz, DMSO-d_6) δ 7.88 (s, 1H), 7.68 (m, 2H), 7.22 (d, J = 8.4 Hz, 2H), 6.89 (d, J = 8.8 Hz, 2H), 4.94 (d, J = 15.6 Hz, 1H), 4.38 (m, 1H), 4.31 (d, J = 15.2 Hz, 1H), 3.72 (s, 3H), 1.38 (d, J = 6.8 Hz, 3H); MS (ESI) m/z 246, 248 [M + H]$^+$.

A mixture of 5-bromo-2-(4-methoxybenzyl)-3-methylisoindolin-1-one **39** (0.2 g, 0.578 mmol), 4-aminopyrimidine (0.066 g, 0.693 mmol), sodium *t*-butoxide (0.111 g, 1.15 mmol) and X-Phos (0.027 g, 0.057 mmol) in toluene (2 mL) was degassed with argon for 30 min. $Pd_2(dba)_3$ (0.053 g, 0.057 mmol) was added under argon atmosphere, and degassing was continued for another 10 min. The reaction mixture was heated at 110 °C for 4 h. After completion of the reaction (monitored by TLC), it was diluted with ethyl acetate and filtered through a Celite pad, and the filtrate was concentrated under reduced pressure. The residue was purified by silica gel column chromatography to afford 2-(4-methoxybenzyl)-3-methyl-5-(pyrimidin-4-ylamino)isoindolin-1-one. Yield: 0.12 g, 58%. ^{1}H NMR (400 MHz, chloroform-d_1) δ 8.73−8.79 (m, 1H) 8.34 (d, J = 6.10 Hz, 1H) 7.84 (d, J = 8.28 Hz, 1H) 7.70 (s, 1H) 7.35−7.43 (m, 2H) 7.22 (d, J = 8.72 Hz, 2H) 6.84 (d, J = 8.72 Hz, 2H) 6.76 (dd, J = 6.10, 1.31 Hz, 1H) 5.30 (s, 2H) 4.38 (q, J = 6.54 Hz, 1H) 3.78 (s, 3H) 1.45 (d, J = 6.54 Hz, 3H); MS (ESI) m/z 361 [M + H]$^+$.

A solution of 2-(4-methoxybenzyl)-3-methyl-5-(pyrimidin-4-ylamino)isoindolin-1-one (0.12 g, 0.332 mmol) in trifluoroacetic acid (2 mL) was heated at 100 °C for 18 h. After completion of reaction (monitored by TLC), the mixture was concentrated under reduced pressure. The residue was dissolved in methanol, and carbonate-supported polymer was added and stirred for 1 h. The

DOI: 10.1021/acs.jmedchem.7b01795
J. Med. Chem. 2018, 61, 3516−3540

mixture was filtered, and the filtrate was concentrated under reduced pressure. The crude material was purified by prep. HPLC to afford compound **9** as an off-white solid; Yield: 0.015 g, 19%. HPLC purity: 96.68%; ^{1}H NMR (400 MHz, methanol-d_4) δ 8.67 (s, 1H), 8.27 (d, J = 6.1 Hz, 1H), 8.13 (s, 1H), 7.74−7.61 (m, 2H), 6.86 (d, J = 6.0 Hz, 1H), 4.69 (q, J = 6.8 Hz, 1H), 1.48 (d, J = 6.7 Hz, 3H), 1.15 (d, J = 6.2 Hz, 1H); ^{13}C NMR (125 MHz, DMSO-d_6) δ 168.7, 159.6, 157.9, 155.5, 150.4, 142.9, 125.6, 123.3, 119.0, 112.6, 107.8, 51.4, 20.4. MS (ESI) m/z 241[M + H]$^+$; HRMS: measured m/z [M + H]$^+$ 241.1083 (calcd. for $C_{13}H_{13}N_4O$: 241.1085).

*3,3-Dimethyl-5-(pyrimidin-4-ylamino)isoindolin-1-one (**10**).* Synthesized as reported in U.S. Patent Application No. WO2017075394.[69] To a solution of 5-bromo-2-(4-methoxybenzyl)isoindolin-1-one **38** (1 g, 3 mmol) in THF (10 mL) at 0 °C, sodium hydride (0.3 g, 7.5 mmol) was added portion-wise, and the reaction mixture was allowed to stir at rt for 30 min. Methyl iodide (0.57 mL, 9 mmol) was added, and the reaction mixture was stirred at 70 °C for 16 h. The reaction mixture was quenched with water and extracted with ethyl acetate. The organic layer was separated, dried over sodium sulfate, and concentrated under reduced pressure. The residue was purified by silica gel column chromatography using 30% ethyl acetate in hexane to afford 5-bromo-2-(4-methoxybenzyl)-3,3-dimethylisoindolin-1-one. Yield: 0.4 g, 36.9%. ^{1}H NMR (400 MHz, DMSO-d_6) δ 8.05 (s, 1H) 7.64−7.67 (m, 2H) 7.36 (d, J = 8.72 Hz, 2H) 6.84 (d, J = 8.72 Hz, 2H) 4.62 (s, 2H) 3.78 (s, 3H) 1.38 (s, 6H); MS (ESI) m/z 360 [M + H]$^+$.

To a solution of 2-(4-methoxybenzyl)-3,3-dimethyl-5-(pyrimidin-4-ylamino)isoindolin-1-one (0.3 g, 0.8 mmol) in toluene (6 mL), 4-aminopyrimidine (0.095 g, 0.99 mmol) and then sodium t-butoxide (0.16 g, 1.66 mmol) were added, and the reaction mixture was degassed with argon for 15 min. $Pd_2(dba)_3$ (0.076 g, 0.08 mmol) and X-phos (0.039 g, 0.08 mmol) were added, and the reaction mixture was heated at 110 °C for 16 h. The reaction mixture was diluted with water and extracted with ethyl acetate. The organic layer was separated, dried over sodium sulfate, and concentrated under reduced pressure. The residue was purified by silica gel chromatography using 5% methanol in DCM to afford 2-(4-methoxybenzyl)-3,3-dimethyl-5-(pyrimidin-4-ylamino)isoindolin-1-one. Yield: 0.2 g, 65%. ^{1}H NMR (400 MHz, DMSO-d_6) δ 9.98 (brs, 1H) 8.72 (s, 1H) 8.32−8.38 (m, 1H) 7.98 (s, 1H) 7.64−7.76 (m, 2H) 7.36 (d, J = 8.72 Hz, 2H) 6.83−6.87 (m, 3H) 4.62 (s, 2H) 3.78 (s, 3H) 1.38 (s, 6H); MS (ESI) m/z 375 [M + H]$^+$.

A solution of 2-(4-methoxybenzyl)-3,3-dimethyl-5-(pyrimidin-4-ylamino)isoindolin-1-one (0.26 g, 0.69 mmol) in trifluoroacetic acid (8 mL) was heated at 95 °C for 16 h. The reaction mixture was concentrated under reduced pressure, and the residue was basified with a saturated solution of sodium bicarbonate. The compound was extracted with 10% methanol in DCM. The organic layer was separated, dried over sodium sulfate, concentrated under reduced pressure, and the residue purified by silica gel column chromatography with 5% methanol in DCM to afford compound **10**. Yield: 0.038 g, 22%. HPLC purity: 97.84%; ^{1}H NMR (400 MHz, DMSO-d_6) δ 9.89 (s, 1H), 8.66 (s, 1H), 8.42 (s, 1H), 8.30 (d, J = 5.9 Hz, 1H), 7.87 (d, J = 1.9 Hz, 1H), 7.69 (dd, J = 8.3, 1.9 Hz, 1H), 7.52 (d, J = 8.3 Hz, 1H), 6.83 (dd, J = 5.9, 1.3 Hz, 1H), 1.40 (s, 6H); ^{13}C NMR (125 MHz, DMSO-d_6) δ 167.5, 159.6, 157.9, 155.5, 154.4, 143.0, 124.8, 123.5, 119.0, 111.3, 107.9, 57.8, 27.6; MS (ESI) m/z 255 [M + H]$^+$. HRMS: measured m/z [M + H]$^+$ 255.1240 (calcd. for $C_{14}H_{15}N_4O$: 255.1240).

*6-Oxo-5-(pyrimidin-4-ylamino)-1,6-dihydropyridine-2-carboxamide. (**11**).* To a solution of 5-chloro-2-pyridinecarboxylic acid **40** (5 g, 31.74 mmol) in ethanol (50 mL), conc. H_2SO_4 (0.5 mL) was added, and the mixture was heated at 80 °C for 12 h. The reaction mixture was cooled to rt and concentrated under reduced pressure. The residue was dissolved in ethyl acetate and washed with saturated aqueous $NaHCO_3$ solution and brine, dried over anhydrous Na_2SO_4, filtered, and concentrated under reduced pressure to afford ethyl 5-chloropicolinate as white crystalline solid. Yield: 5 g, 86%. ^{1}H NMR (400 MHz, DMSO-d_6) δ 8.69 (m, 1H), 8.08 (m, 1H), 7.81 (m, 1H), 4.47 (m,2H), 1.43 (t, J = 7.2 Hz, 3H); MS (ESI) m/z 186 [M + H]$^+$.

To a solution of ethyl 5-chloropicolinate (5 g, 27 mmol) in chloroform (60 mL), urea hydrogen peroxide (5.08 g, 54.05 mmol) was added under ice cooling. Trifluoroacetic anhydride (7.5 mL, 54.0 mmol in $CHCl_3$ (60 mL)) was added dropwise over 30 min, and the mixture was stirred for 2 h at rt. A saturated aqueous sodium thiosulfate solution was added dropwise to the reaction mixture followed by extraction with chloroform, and the organic layer was dried over anhydrous Na_2SO_4, filtered, and concentrated under reduced pressure. The residue was purified by silica gel column chromatography using 0−50% ethyl acetate in hexanes to afford 5-chloro-2-(ethoxycarbonyl)pyridine 1-oxide **41**. Yield: 3.5 g, 64.8%. ^{1}H NMR (400 MHz, DMSO-d_6) δ 8.65 (s, 1H),7.76 (m, 1H), 7.58 (m, 1H), 4.33 (m, 2H), 1.29 (m, 3H); MS (ESI) m/z 202 [M + H]$^+$.

Trifluoroacetic anhydride (8 mL, 57.71 mmol) was added dropwise to a solution of 5-chloro-2-(ethoxycarbonyl)pyridine 1-oxide **41** (2 g, 9.95 mmol) in DMF (12 mL) under ice cooling over 20 min, and the mixture was stirred at 50 °C for 1.5 h. The reaction mixture was cooled to 0 °C, water was added, and the mixture was neutralized with $NaHCO_3$ and extracted with DCM. The organic layer was dried over anhydrous Na_2SO_4, filtered, and concentrated under reduced pressure. The residue was triturated with ethyl acetate and n-pentane to afford ethyl 5-chloro-6-oxo-1,6-dihydropyridine-2-carboxylate. Yield: 1.3 g, 60%. ^{1}H NMR (400 MHz, DMSO-d_6) δ 7.65(m,1H), 6.15 (m,1H), 4.43 (m, 2H), 1.43 (m, 3H); MS (ESI) m/z 202 [M + H]$^+$.

To a stirred suspension of ethyl 5-chloro-6-oxo-1,6-dihydropyridine-2-carboxylate (0.5 g, 2.48 mmol), K_2CO_3 (0.684 g, 4.96 mmol), LiBr (0.43 g, 4.96 mmol), and tetrabutylammonium bromide (0.08g, 0.248 mmol) in toluene (13 mL) and water (0.13 mL), benzyl bromide (0.44 mL, 3.72 mmol) was added, and the resulting suspension was heated at 80 °C for 1 h. The mixture was allowed to reach rt, diluted with DCM, and filtered. The filtrate was concentrated *in vacuo*, and the residue was purified by silica gel column chromatography using 30% ethyl acetate in hexanes to afford ethyl 1-benzyl-5-chloro-6-oxo-1,6-dihydropyridine-2-carboxylate **42**. Yield: 0.47 g, 65.2%. ^{1}H NMR (400 MHz, DMSO-d_6) δ 7.90 (d, J = 7.29 Hz, 1H) 7.29−7.35 (m, 2H) 7.26 (d, J = 7.29 Hz, 1H) 7.08 (d, J = 6.86 Hz, 2H) 6.84 (d, J = 7.72 Hz, 1H) 5.49 (s, 2H) 4.18 (q, J = 6.86 Hz, 2H) 1.12 (t, J = 7.29 Hz, 3H); MS (ESI) m/z 292 [M + H]$^+$.

A solution of ethyl 1-benzyl-5-chloro-6-oxo-1,6-dihydropyridine-2-carboxylate **42** (0.3 g, 1.028 mmol), 4-aminopyrimidine (0.117 g, 1.234 mmol), and Cs_2CO_3 (0.67 g, 2.05 mmol) in 1,4-dioxane (10 mL) was degassed with argon for 30 min. $Pd_2(dba)_3$ (0.066 g, 0.071 mmol) and Xantphos (0.059 g, 0.102 mmol) were added under argon atmosphere, and the reaction mixture was heated at 90 °C for 15 h. The reaction mixture was cooled and filtered through a Celite pad. The filtrate was concentrated under reduced pressure and purified by silica gel column chromatography using 1−2% methanol in DCM to afford ethyl 1-benzyl-6-oxo-5-(pyrimidin-4-ylamino)-1,6-dihydropyridine-2-carboxylate **43**. Yield: 0.22 g, 61%. ^{1}H NMR (400 MHz, DMSO-d_6) δ 9.58 (s, 1H) 8.79 (s, 1H) 8.64 (d, J = 8.14 Hz, 1H) 8.41 (d, J = 5.57 Hz, 1H) 7.41 (d, J = 5.57 Hz, 1H) 7.28−7.34 (m, 2H) 7.21−7.26 (m, 1H) 7.09−7.15 (m, 3H) 5.67 (s, 2H) 4.19 (q, J = 6.86 Hz, 2H) 1.16 (t, J = 7.07 Hz, 3H); MS (ESI) m/z 351 [M + H]$^+$.

To a mixture of ethyl 1-benzyl-6-oxo-5-(pyrimidin-4-ylamino)-1,6-dihydropyridine-2-carboxylate **43** (0.1 g, 0.285 mmol) in toluene (5 mL), trifluoromethanesulfonic acid (0.171 g, 1.14 mmol) was added, and the reaction mixture was heated at 140 °C in a microwave for 20 min. The reaction was concentrated under reduced pressure and partitioned between ethyl acetate and water. The aqueous layer was neutralized with sodium bicarbonate and extracted with ethyl acetate. The combined organic layer was dried over anhydrous Na_2SO_4, filtered, and concentrated under reduced pressure. The residue was purified by silica gel column chromatography using 1% methanol in DCM to afford ethyl 6-oxo-5-(pyrimidin-4-ylamino)-1,6-dihydropyridine-2-carboxylate. Yield: 0.045 g, 60.8%. MS (ESI) m/z 261 [M + H]$^+$.

A mixture of ethyl 6-oxo-5-(pyrimidin-4-ylamino)-1,6-dihydropyridine-2-carboxylate (0.035 g, 0.1 mmol) and 25% ammonia in water (5 mL) was stirred at rt for 16 h. The mixture was concentrated under reduced pressure and triturated with DCM−pentane to afford 6-oxo-5-

DOI: 10.1021/acs.jmedchem.7b01795
J. Med. Chem. 2018, 61, 3516−3540

(pyrimidin-4-ylamino)-1,6-dihydropyridine-2-carboxamide **11** as light green solid. Yield: 0.012 g, 52.2%. HPLC purity: 99.09%; ^{1}H NMR (400 MHz, DMSO-d_6) δ 11.27 (s, 1H), 9.35 (s, 1H), 8.75 (s, 1H), 8.61 (d, J = 7.7 Hz, 1H), 8.36 (d, J = 5.9 Hz, 1H), 8.06 (s, 1H), 7.67 (s, 1H), 7.38 (d, J = 5.9 Hz, 1H), 7.03 (d, J = 7.6 Hz, 1H); ^{13}C NMR (125 MHz, DMSO-d_6) δ 161.9, 159.5, 157.6, 156.6, 153.3, 133.0, 128.6, 119.3, 109.5, 107.1. MS (ESI) m/z 232[M + H] $^+$. HRMS: measured m/z [M + H]$^+$ 232.0829 (calcd. for $C_{10}H_{10}N_5O_2$: 232.0830).

*3,3-Dimethyl-6-(pyrimidin-4-ylamino)-2,3-dihydroimidazo[1,5-a]pyridine-1,5-dione (**12**).* Prepared as in U.S. Patent 9,382,248 (Scheme 5).[30] Aqueous ammonia (15 mL, 30% solution) was added to ethyl 5-chloro-6-oxo-1,6-dihydropyridine-2-carboxylate (0.65 g, 3.2 mmol) at 0 °C, and the reaction mixture was allowed to stir at rt for 16 h. The reaction mixture was concentrated under reduced pressure, and the residue was triturated with diethyl ether, filtered, and dried to afford 5-chloro-6-oxo-1,6-dihydropyridine-2-carboxamide. Yield: 0.43 g, 75%. ^{1}H NMR (400 MHz, DMSO-d_6) δ 7.90 (s,1H), 7.53 (m, 1H, 7.38 (s, 1H), 6.81 (m, 1H), 5.9−6.2 (brs, 1H); MS (ESI) m/z 173 [M + H]$^+$.

Procedure A: To a solution of 5-chloro-6-oxo-1,6-dihydropyridine-2-carboxamide (1.4 g, 7.9 mmol) in 1,4-dioxane (20 mL), acetone (4.6 g, 79 mmol) and concentrated sulfuric acid (0.038 g, 0.39 mmol) were added at rt and the reaction mixture was heated at 100 °C for 8 h. The reaction mixture was concentrated under reduced pressure, and the residue was triturated with diethyl ether and hexane, filtered, and dried to afford 6-chloro-3,3-dimethyl-2,3-dihydroimidazo[1,5-a]pyridine-1,5-dione. Yield: 1.4 g, 83%. ^{1}H NMR (400 MHz, DMSO-d_6) δ 9.99 (s, 1H), 7.93 (m, 1H), 6.71 (m, 1H), 1.76 (s, 6H); MS (ESI) m/z 213 [M + H]$^+$.

Procedure B: To a solution of 6-chloro-3,3-dimethyl-2,3-dihydroimidazo[1,5-a]pyridine-1,5-dione (0.25 g, 1.18 mmol) in 1,4-dioxane (8 mL), 4-aminopyrimidine (0.14 g, 1.41 mmol), Brettphos (0.19 g, 0.23 mmol), and cesium carbonate (0.76 g, 2.36 mmol) were added, and the reaction mixture was degassed with argon for 5 min. Tris dibenzylideneacetone dipalladium (0) (0.11 g, 0.12 mmol) was then added, and the reaction was degassed with argon for another 5 min and then stirred at 100 °C for 10 h. The reaction mixture was cooled to rt, filtered through Celite, and the filtrate concentrated under reduced pressure. The residue was purified by silica gel column chromatography using 5% methanol in DCM to afford 3,3-dimethyl-6-(pyrimidin-4-ylamino)-2,3-dihydroimidazo[1,5-a]pyridine-1,5-dione **12** as a light yellow solid. Yield: 0.036 g, 11%. HPLC purity: 97.48%; ^{1}H NMR (400 MHz, DMSO-d_6) δ 9.70 (s, 1H), 9.42 (s, 1H), 8.81−8.73 (m, 2H), 8.37 (d, J = 5.9 Hz, 1H), 7.40−7.34 (m, 1H), 6.87 (d, J = 7.7 Hz, 1H), 1.82 (s, 6H); ^{13}C NMR (125 MHz, DMSO-d_6) δ 1659.6, 159.5, 157.6, 155.4, 154.1, 133.0, 128..2, 120.9, 109.6, 102.8, 77.0, 24.8. MS (ESI) m/z 272 [M + H]$^+$. HRMS: measured m/z [M + H]$^+$ 272.1142 (calcd. for $C_{13}H_{14}N_5O_2$: 272.1139).

*8-Fluoro-3,3-dimethyl-6-(pyrimidin-4-ylamino)-2H-imidazo[1,5-a]pyridine-1,5-dione (**13**).* Prepared as in U.S. Patent 9,382,248.[30] To a stirred solution of 5-bromo-3-fluoro-pyridine-2-carboxylic acid (1.0 g, 4.55 mmol) in ethanol (20 mL) was added sulfuric acid (0.67 g, 6.82 mmol) at rt, and the reaction mixture was stirred at reflux overnight. The reaction mixture was cooled to rt, and the solvent was removed under vacuum. The residue was neutralized with a saturated aqueous sodium bicarbonate solution and extracted with ethyl acetate (2 × 100 mL). The organic layers were separated and dried with magnesium sulfate, filtered, and concentrated to afford ethyl 5-bromo-3-fluoro-pyridine-2-carboxylate as an off-white solid. Yield: 1.0 g, 89%. ^{1}H NMR (400 MHz, DMSO-d_6) δ 8.61 (s, 1H), 7.77−7.75 (m, 1H), 4.51 (q, J = 7.16 Hz, 2H), 1.43 (t, J = 7.16 Hz, 3H).; MS (ESI) m/z 250 [M + H]$^+$.

To a stirred solution of ethyl 5-bromo-3-fluoro-pyridine-2-carboxylate (0.9 g, 3.63 mmol) in DCM (50 mL) at 0 °C was added trifluoroacetic anhydride (1.52 g, 7.26 mmol) and urea hydrogen peroxide (0.72 g, 7.62 mmol). The reaction mixture was stirred at rt overnight, and the reaction mixture was neutralized with a dipotassium hydrogen phosphate solution and then with a sodium bisulfite solution. The product was extracted with DCM (2 × 100 mL). The organic layers were separated, dried with magnesium sulfate, filtered, and concentrated to afford ethyl 5-bromo-3-fluoro-1-oxido-pyridin-1-ium-2-carboxylate as an off-white solid. Yield: 0.9 g, 89%. ^{1}H NMR (400 MHz, DMSO-d_6) δ: 8.22 (s, 1H), 7.30−7.26 (m, 1H), 4.50 (q, J = 7.2 Hz, 2H), 1.42 (t, J = 7.2 Hz, 3H). MS (ESI) m/z 266 [M + H]$^+$.

To a stirred solution of ethyl 5-bromo-3-fluoro-1-oxido-pyridin-1-ium-2-carboxylate (0.85 g, 3.21 mmol) in dimethylformamide (15 mL) was added trifluoroacetic anhydride (1.35 g, 6.42 mmol) at 0 °C. The reaction mixture was warmed to 50 °C and stirred for 1 h, quenched with saturated aqueous sodium bicarbonate solution, and extracted with DCM (2 × 100 mL). The organic layers were separated, dried with magnesium sulfate, filtered, and concentrated to afford ethyl 5-bromo-3-fluoro-6-oxo-1H-pyridine-2-carboxylate as a yellow solid. Yield: 0.8 g, 94%. ^{1}H NMR (400 MHz, DMSO-d_6) δ 7.83 (d, J = 8.0 Hz,1H), 4.47 (q, J = 7.2 Hz, 2H), 1.43 (t, J = 7.2 Hz, 3H). MS (ESI) m/z 264 [M + H]$^+$.

In a flask charged with ethyl 5-bromo-3-fluoro-6-oxo-1H-pyridine-2-carboxylate (0.8 g, 3.03 mmol) at 0 °C was added liquid ammonia (15 mL, 3.03 mmol) in ethanol (5 mL). The stirred mixture was warmed to 45 °C for 2 h. The ammonia and ethanol were evaporated under reduced pressure, methanol was added, and the mixture was refluxed for 2 h and filtered while hot. The volume of the filtrate was reduced by 2/3 and to the remaining methanol was added diethyl ether until a solid precipitated. The solid was filtered and dried under vacuum to afford 5-bromo-3-fluoro-6-oxo-1H-pyridine-2-carboxamide as a light brown solid. Yield: 0.6 g, 85%. ^{1}H NMR (400 MHz, DMSO-d_6) δ 7.88−7.86 (m, 1H), 7.67 (s, 1H), 7.50 (s, 1H).

The synthesis of intermediate 6-bromo-8-fluoro-3,3-dimethyl-2H-imidazo[1,5-a]pyridine-1,5-dione was carried out as described above using Procedure A. Off-white solid; Yield: 0.24 g, 34%. ^{1}H NMR (400 MHz, DMSO-d_6) δ 7.87 (d, J = 7.44 Hz, 1H), 7.06 (s, 1H), 1.96 (s, 6H); MS (ESI) m/z 275 [M + H]$^+$.

The synthesis of compound **13** was carried out as described above using the general protocol of Procedure B. Off-white solid; Yield: 0.032 g, 13%. HPLC purity: 97.22%; ^{1}H NMR (400 MHz, DMSO-d_6) δ 9.72 (s, 1H), 9.61 (s, 1H), 8.83 (d, J = 5.1 Hz, 1H), 8.79 (s, 1H), 8.45 (d, J = 5.7 Hz, 1H), 7.46 (d, J = 5.6 Hz, 1H), 1.82 (s, 6H); ^{13}C NMR (125 MHz, DMSO-d_6) δ 159.3, 157.5, 156.6 (d, J = 221 Hz), 152.2, 145.3, 143.5, 133.9 (d, J = 17.4 Hz), 113.1 (d, J = 27.5 Hz) 111.4 (d, J = 30 Hz) 110.0, 77.5, 24.7. HRMS: measured m/z [M + H]$^+$ 290.1053 (calcd. for $C_{13}H_{13}FN_5O_2$: 290.1048).

*3,3,8-Trimethyl-6-(pyrimidin-4-ylamino)-2H-imidazo[1,5-a]pyridine-1,5-dione (**14**).* Prepared as in U.S. Patent 9,382,248.[30] A vial was charged with 8-chloro-3,3-dimethyl-6-(pyrimidin-4-ylamino)-2H-imidazo[1,5-a]pyridine-1,5-dione (0.20 g, 0.65 mmol), trimethylboroxine (0.16 g, 1.31 mmol), and potassium phosphate (0.28 g, 1.31 mmol) in 1,4-dioxane (10 mL) at rt under argon. Then reaction mixture was purged with argon for 10 min followed by addition of tris(dibenzylideneacetone)dipalladium(0) (60 mg, 0.07 mmol) and tricyclohexylphosphine (18 mg, 0.07 mmol). The vial was sealed and heated at 140 °C in a microwave reactor for 1 h. The reaction mixture was concentrated to dryness, and the crude residue was subjected to flash column chromatography using silica gel with a solvent gradient of 0.2−0.5% methanol in DCM. The solid obtained was stirred in n-pentane and filtered. The resulting product 3,3,8-trimethyl-6-(pyrimidin-4-ylamino)-2H-imidazo[1,5-a]pyridine-1,5-dione **14** was obtained as an off-white solid. Yield: 0.035 g, 18%. HPLC purity: 97.73; ^{1}H NMR (400 MHz, DMSO-d_6) δ 9.57 (s, 1H), 9.39 (s, 1H), 8.77 (s, 1H), 8.60 (s, 1H), 8.37 (d, J = 5.76 Hz, 1H), 7.77 (d, J = 5.64 Hz, 1H), 2.44 (s, 3H), 1.79 (s, 6H); ^{13}C NMR (125 MHz, DMSO-d_6) δ 160.8, 159.3, 157.6, 155.4, 153.4, 132.4, 123.6, 122.8, 116.2, 109.6, 75.2, 24.9, 13.6. HRMS: measured m/z [M + H]$^+$ 286.1302 (calcd. for $C_{14}H_{16}N_5O_2$: 286.1299).

*8-Chloro-3,3-dimethyl-6-(pyrimidin-4-ylamino)-2,3-dihydroimidazo[1,5-a]pyridine-1,5-dione (**15**).* Prepared as in U.S. Patent 9,382,248.[30] To a stirred solution of 5-bromo-3-chloro-pyridine-2-carboxylic acid (150.0 g, 634.38 mmol) in ethanol (1.5 L) was added sulfuric acid (93.26 g, 951.58 mmol) at rt. The reaction was stirred at 80 °C overnight. The reaction mixture was cooled to rt,

DOI: 10.1021/acs.jmedchem.7b01795
J. Med. Chem. 2018, 61, 3516−3540

and solvent was removed under reduced pressure. The resulting residue was neutralized with saturated aqueous sodium bicarbonate solution and extracted with ethyl acetate (2 × 1 L). The organic layers were then separated, combined, dried with magnesium sulfate, and concentrated to dryness to afford ethyl 5-bromo-3-chloro-pyridine-2-carboxylate as an off white solid. Yield: 163 g, 97%. ^{1}H NMR (400 MHz, chloroform-d_1) δ 8.26 (d, J = 0.8 Hz, 1H), 7.47 (d, J = 0.8 Hz, 1H), 4.49 (q, J = 7.2 Hz, 2H), 1.40 (t, J = 7.2 Hz, 3H).

To a stirred solution of ethyl 5-bromo-3-chloro-pyridine-2-carboxylate (151.0 g, 570.89 mmol) in DCM (1.73 L) was added trifluoroacetic anhydride (30.0 mL, 1.14 mol) and urea hydrogen peroxide (112.69 g, 1.20 mol) at 0 °C. The reaction was stirred overnight at rt, and the reaction mixture was neutralized with a potassium phosphate dibasic solution. A sodium bisulfite solution was added followed by extraction with DCM (2 × 100 mL). The organic layers were separated, combined, dried with magnesium sulfate, filtered, and concentrated to afford ethyl 5-bromo-3-chloro-1-oxido-pyridin-1-ium-2-carboxylate as an off white solid. Yield: 150.5 g, 94%. ^{1}H NMR (400 MHz, DMSO-d_6) δ 8.26 (d, J = 1.2 Hz, 1H), 7.48 (d, J = 1.2 Hz, 1H), 4.50 (q, J = 7.12 Hz, 2H), 1.42 (t, J = 12.12 Hz, 3H). MS (ESI) m/z 282 [M + H]$^+$.

To a stirred solution of ethyl 5-bromo-3-chloro-1-oxido-pyridin-1-ium-2-carboxylate (150 g, 534.8 mmol) in dimethylformamide (900 mL) at 0 °C was added trifluoroacetic anhydride (224.63 g, 1.07 mmol). The temperature of the reaction mixture was raised to 50 °C and stirring was continued for 1 h. After the oxidation was complete, the reaction was quenched with a saturated aqueous sodium bicarbonate solution and extracted with DCM (2 × 100 mL). The organic layers were separated, combined, dried with magnesium sulfate, and concentrated to afford ethyl 5-bromo-3-chloro-6-oxo-1*H*-pyridine-2-carboxylate as a yellow solid. Yield: 75 g, 50%. ^{1}H NMR (400 MHz, DMSO-d_6) δ 10.44−10.02 (m, 1H), 7.86 (s, 1H), 4.47 (q, J = 7.2 Hz, 2H), 1.43 (t, J = 5.6 Hz, 3H). MS (ESI) m/z 282 [M + H]$^+$.

In a flask containing ethyl 5-bromo-3-chloro-6-oxo-1*H*-pyridine-2-carboxylate (75.0 g, 267.38 mmol) was added liquid ammonia (150.0 mL, 267.38 mmol) in ethanol (100 mL) at 0 °C. The reaction mixture was stirred at 45 °C for 2 h. At this time the mixture was concentrated to remove the ethanolic ammonia. The crude solids were washed with diethyl ether (500 mL) and dissolved in refluxing methanol (1 L) and filtered hot. The filtrate was concentrated under reduced pressure until 1/3 of solvent volume remained. Diethyl ether was added until all solids precipitated. The solid was filtered and dried under vacuum to afford 5-bromo-3-chloro-6-oxo-1*H*-pyridine-2-carboxamide as a light brown solid. Yield: 45 g, 69%. ^{1}H NMR (400 MHz, DMSO-d_6) δ 7.92−7.82 (m, 1H), 7.61−7.59 (m, 1H), 7.36 (s, 1H). MS (ESI) m/z 249 [M − 1]$^-$.

The synthesis of intermediate 6-bromo-8-chloro-3,3-dimethyl-2*H*-imidazo[1,5-*a*]pyridine-1,5-dione was carried out as described above using the general protocol of Procedure A. White solid; Yield: 390 mg, 48%. ^{1}H NMR (400 MHz, DMSO-d_6) δ 10.03 (s, 1H), 8.24 (s, 1H), 1.75 (s, 6H). MS (ESI) m/z 289 [M − 1]$^-$.

The synthesis of compound **15** was carried out as described above using the general protocol of Procedure B. Off white solid; Yield: 0.020 g, 10%. HPLC purity: 99.24%; ^{1}H NMR (400 MHz, DMSO-d_6) δ 9.78 (s, 1H), 9.64 (s, 1H), 8.84 (s, 1H), 8.79 (s, 1H), 8.43 (d, J = 5.6 Hz, 1H), 7.44 (d, J = 5.2 Hz, 1H), 1.81 (s, 6H); ^{13}C NMR (125 MHz, DMSO-d_6) δ 159.3, 158.1, 157.6, 155.7, 153.1, 133.4, 122.5, 121.0, 110.5, 109.9, 76.6, 24.7. HRMS: measured m/z [M + H]$^+$ 306.0755 (calcd. for $C_{13}H_{13}ClN_5O_2$: 306.0752).

*N-(6-((1-Oxoisoindolin-5-yl)amino)pyrimidin-4-yl)-cyclopropanecarboxamide (**16**).* Synthesized as reported in U.S. Patent Application No. WO2017075394 (Scheme 6).[69] To a stirred solution of 6-chloro-4-aminopyrimidine **47** (1 g, 7.75 mmol) in THF (20 mL), 4-(dimethylamino)pyridine (0.047 g, 0.387 mmol) and di-*t*-butyl dicarbonate (3.55 g, 16.27 mmol) were added dropwise, and the reaction mixture was stirred at rt for 16 h. The reaction mixture was diluted with water and extracted with ethyl acetate. The combined organic layer was washed with brine, dried over anhydrous sodium sulfate, filtered, and concentrated under reduced pressure to afford *t*-butyl *N*-*t*-butoxycarbonyl-*N*-(6-chloropyrimidin-4-yl)carbamate, which was used for the next step without further purification. Yield: 1.3 g, 51%; ^{1}H NMR (400 MHz, DMSO-d_6): δ 8.668 (s, 1H), 7.857 (s, 1H), 1.68 (s, 18H); MS (ESI) m/z 330 [M + H]$^+$.

A mixture of *t*-butyl *N*-*t*-butoxycarbonyl-*N*-(6-chloropyrimidin-4-yl)carbamate (0.5 g, 1.51 mmol), cyclopropanecarboxamide (0.19 g, 2.27 mmol), cesium carbonate (0.69 g, 2.12 mmol), and Xantphos (0.13 g, 0.22 mmol) in 1,4-dioxane (8 mL) was degassed with argon for 15 min. $Pd_2(dba)_3$ (0.069 g, 0.075 mmol) was added under an argon atmosphere, and the reaction mixture was stirred at 90 °C for 18 h. The reaction mixture was diluted with water and extracted with ethyl acetate, and the organic layer was washed with brine, dried over anhydrous sodium sulfate, filtered, and concentrated under reduced pressure. The residue was purified by silica gel column chromatography using 0−40% ethyl acetate in hexane to afford *t*-butyl *N*-*t*-butoxycarbonyl-*N*-(6-(cyclopropanecarboxamido)pyrimidin-4-yl)-carbamate **48** as a yellow solid; Yield: 0.55 g, 96%. ^{1}H NMR (400 MHz, DMSO-d_6) δ 11.30 (s, 1H), 8.67 (m, 1H), 8.25 (m, 1H), 2.03 (m, 1H), 1.46 (s, 18H), 0.87 (m, 4H); MS (ESI) m/z 379 [M + H]$^+$.

Procedure C: A stirred solution of *t*-butyl *N*-*t*-butoxycarbonyl-*N*-(6-(cyclopropanecarboxamido)pyrimidin-4-yl)carbamate **48** (0.55 g, 1.45 mmol) and 4 M HCl in 1,4-dioxane (4 mL) was stirred at rt for 1 h. The reaction mixture was concentrated under reduced pressure, and the residue was triturated with diethyl ether and hexane to afford *N*-(6-aminopyrimidin-4-yl)cyclopropanecarboxamide as white solid, which was used for the next step without further purification. Yield: 0.3 g, crude. ^{1}H NMR (400 MHz, DMSO-d_6) δ 10.54 (s,1H), 8.10 (s,1H), 7.10 (m,1H), 6.73 (s,2H), 1.97 (m,1H), 0.78 (m, 4H); MS (ESI) m/z 179 [M + H]$^+$.

A mixture of *N*-(6-aminopyrimidin-4-yl)cyclopropanecarboxamide (0.3 g, 1.68 mmol), 5-bromo-2-(4-methoxybenzyl)isoindolin-1-one (0.61 g, 1.85 mmol), cesium carbonate (1.64 g, 5.05 mmol), and X-Phos (0.16 g, 0.33 mmol) in 1,4-dioxane (10 mL) was degassed with argon for 30 min. $Pd_2(dba)_3$ (0.15 g, 0.16 mmol) was added under argon atmosphere. The reaction mixture was stirred at 90 °C for 18 h and was then diluted with water and extracted with ethyl acetate. The organic layer was washed with brine, dried over anhydrous sodium sulfate, filtered, and concentrated under reduced pressure, and the residue was purified by silica gel column chromatography using 0−5% methanol in DCM to afford *N*-(6-((2-(4-methoxybenzyl)-1-oxoisoindolin-5-yl)amino)pyrimidin-4-yl)cyclopropanecarboxamide **49**. Yield: 0.3 g, 42%. ^{1}H NMR (400 MHz, DMSO-d_6) δ 10.88 (s, 1H) 9.92 (s, 1H) 8.45 (s, 1H) 7.97 (s, 1H) 7.72 (dd, J = 8.28, 1.41 Hz, 1H) 7.59−7.65 (m, 2H) 7.20 (d, J = 8.48 Hz, 2H) 6.90 (d, J = 8.48 Hz, 2H) 4.62 (s, 2H) 4.30 (s, 2H) 3.72 (s, 3H) 2.00−2.07 (m, 1H) 0.81−0.86 (m, 4H); MS (ESI) m/z 430 [M + H]$^+$.

A solution of *N*-(6-((2-(4-methoxybenzyl)-1-oxoisoindolin-5-yl)-amino)pyrimidin-4-yl)cyclopropanecarboxamide **49** (0.2 g, 0.466 mmol) in trifluoroacetic acid (3 mL) was heated at reflux overnight. The mixture was cooled to 0 °C and neutralized with aqueous 1 N sodium bicarbonate solution. The precipitated solid was filtered and washed with hexane-diethyl ether (1:1) to afford compound **16** as an off-white solid; Yield: 0.066 g, 46%. HPLC purity: 98.34%; ^{1}H NMR (400 MHz, DMSO-d_6) δ 10.88 (s, 1H), 9.91 (s, 1H), 8.47 (d, J = 1.1 Hz, 1H), 8.32 (s, 1H), 8.10−8.05 (m, 1H), 7.69−7.53 (m, 3H), 4.34 (s, 2H), 2.03 (p, J = 6.2 Hz, 1H), 0.84 (d, J = 6.3 Hz, 4H); ^{13}C NMR (125 MHz, DMSO-d_6) δ 173.6, 169.9, 161.2, 157.5, 156.7, 145.3, 143.3, 125.9, 123.2, 118.7, 113.2, 93.7, 44.8, 14.3, 8.1. MS (ESI) m/z 310 [M + H]$^+$. HRMS: measured m/z [M + H]$^+$ 310.1299 (calcd. for $C_{16}H_{16}N_5O_2$: 310.1300).

*N-(6-((3,3-Dimethyl-1,5-dioxo-1,2,3,5-tetrahydroimidazo[1,5-a]-pyridin-6-yl)amino)pyrimidin-4-yl)cyclopropanecarboxamide (**17**).* Prepared as in U.S. Patent 9,382,248.[30] The synthesis of compound **17** was carried out as described above using the general protocol of Procedure B. Beige solid; Yield: 0.075 g, 15%. HPLC purity: 99.59%; ^{1}H NMR (400 MHz, DMSO-d_6) δ 10.87 (s, 1H), 9.68 (s, 1H), 9.20 (s, 1H), 8.64 (d, J = 7.7 Hz, 1H), 8.51 (s, 1H), 7.88 (d, J = 1.0 Hz, 1H), 6.85 (d, J = 7.6 Hz, 1H), 2.04−2.01 (m, J = 6.2 Hz, 1H), 1.80 (s, 6H), 0.84 (d, J = 6.1 Hz, 4H); ^{13}C NMR (125 MHz, DMSO-d_6) δ 160.9, 159.6, 157.2, 156.8, 154.1, 133.3, 128.1, 120.1, 102.7, 954., 77.0, 24.8,

DOI: 10.1021/acs.jmedchem.7b01795
J. Med. Chem. 2018, 61, 3516−3540

14.2, 8.0. HRMS: measured m/z [M + H]$^+$ 355.1519 (calcd. for $C_{17}H_{19}N_6O_3$: 355.1513).

*N-[6-[[8-Chloro-3-(3-chlorophenyl)-3-methyl-1,5-dioxo-2H-imidazo[1,5-a]pyridin-6-yl]amino]pyrimidin-4-yl]-cyclopropanecarboxamide (**18**).* Prepared as in U.S. Patent 9,382,248.[30] The synthesis of intermediate 6-bromo-8-chloro-3-(3-chlorophenyl)-3-methyl-2*H*-imidazo[1,5-*a*]pyridine-1,5-dione was carried out as described above using the general protocol of Procedure A. White solid; Yield: 0.13 g, 17%. ^{1}H NMR (400 MHz, DMSO-d_6) δ 10.38 (s, 1H), 8.32 (s, 1H), 7.52 (s, 1H), 7.47−7.38 (m, 2H), 7.34 (d, J = 7.6 Hz, 1H), 2.18 (s, 3H); MS (ESI) m/z 386.83 [M + H]$^+$. The synthesis of compound **18** was carried out as described above using the general protocol of Procedure B. Light yellow solid; Yield: 0.04 g, 25%. HPLC purity: 97.80%; ^{1}H NMR (400 MHz, DMSO-d_6) δ 10.90 (s, 1H), 10.09 (s, 1H), 9.44 (s, 1H), 8.75 (s, 1H), 8.59 (s, 1H), 7.90 (s, 1H), 7.52 (s, 1H), 7.45−7.39 (m, 2H), 7.34 (d, J = 7.2 Hz, 1H), 2.23 (s, 3H), 2.02−1.97 (m, 1H), 0.82−0.81 (m, 4H); ^{13}C NMR (125 MHz, DMSO-d_6) δ 173.2, 160.7, 158.5, 157.2, 157.0, 152.4, 140.9, 134.1, 133.0, 130.9, 128.6, 126.4, 124.7, 121.8, 121.0, 111.2, 96.1, 77.0, 22.3, 14.7, 8.0. HRMS: measured m/z [M + H]$^+$ 485.0891 (calcd. for $C_{22}H_{19}Cl_2N_6O_3$: 485.0890).

*3-[3-(6-Isoquinolyl)imidazo[1,2-b]pyridazin-6-yl]-oxycyclobutanamine. (**19**).* To a 40 mL vial was added 3-bromo-6-chloro-imidazo[1,2-*b*]pyridazine (100 mg, 0.43 mmol), potassium carbonate (176 mg, 1.27 mmol), and isoquinolin-6-ylboronic acid (119 mg, 0.69 mmol). Monoglyme (2 mL) and water (1 mL) were added, and the heterogeneous yellow reaction mixture was stirred at rt. Tetrakis(triphenylphosphine)palladium(0) (35 mg, 0.03 mmol) was added, the vial was purged with argon (×2), and the vial was heated at 85 °C overnight. After cooling to rt, the reaction was diluted with EtOAc and water (∼3:1 EtOAc/water) and extracted with EtOAc. The combined organics were then dried over Na_2SO_4 and concentrated to provide a yellow residue, which was purified on silica gel eluting with EtOAc affording 6-(6-chloroimidazo[1,2-*b*]pyridazin-3-yl)isoquinoline as a yellow solid (75 mg, 62% yield). ^{1}H NMR (400 MHz, DMSO-d_6) δ 9.35 (s, 1H), 8.78 (s, 1H), 8.56−8.55 (m, 2H), 8.38−8.35 (m, 2H), 8.27 (d, J = 21.7 Hz, 1H), 7.90 (d, J = 14.2 Hz, 1H), 7.52 (d, J = 23.6 Hz, 1H); MS (ESI) m/z 282.96 [M + H]$^+$.

To a 10 mL flask was added sodium hydride (14 mg, 0.36 mmol), followed by THF (3.5 mL), and the flask was placed in a bath at 0 °C. *t*-Butyl *N*-(3-hydroxycyclobutyl)carbamate (67 mg, 0.36 mmol) was added slowly, the mixture was stirred for 15 min at 0 °C, then 6-(6-chloroimidazo[1,2-*b*]pyridazin-3-yl)isoquinoline (50 mg, 0.18 mmol) was added, and the reaction was stirred for 10 min at 0 °C and stirred at rt overnight. The reaction was quenched with water, diluted with half saturated brine, and extracted with DCM (3×). The organic layer was dried over sodium sulfate and concentrated and purified via column chromatography eluting with 0−10% MeOH/DCM affording *t*-butyl *N*-[3-[3-(6-isoquinolyl)imidazo[1,2-*b*]pyridazin-6-yl]-oxycyclobutyl]carbamate as a pale yellow powder (45 mg, 29% yield). ^{1}H NMR (400 MHz, DMSO-d_6) δ 9.32 (s, 1H), 8.93 (s, 1H), 8.53 (d, J = 14.2 Hz, 1H), 8.39 (s, 1H), 8.34 (d, J = 20.9 Hz, 1H), 8.21 (d, J = 21.6 Hz, 1H), 8.17 (d, J = 24.1 Hz, 1H), 7.87 (d, J = 13.3 Hz, 1H), 7.05 (d, J = 24.2 Hz, 1H), 5.39−5.38 (m, 1H), 4.20−4.18 (m, 1H), 2.60−2.57 (m, 4H), 1.41 (s, 9H); ^{13}C NMR (125 MHz, DMSO-d_6) δ 160.6, 146.9, 139.4, 144.0, 138.1, 134.8, 132.9, 131.9, 129.6, 129.4, 127.1, 126.9, 126.8, 126.5, 123.8, 118.2, 71.2, 42.5, 34.4. MS (ESI) m/z 432.17 [M + H]$^+$.

To a 20 mL vial was added *t*-butyl *N*-[3-[3-(6-isoquinolyl)imidazo-[1,2-*b*]pyridazin-6-yl]oxycyclobutyl]carbamate (43 mg, 0.10 mmol) and 1.5 mL of MeOH. To the stirring suspension was added 4 N HCl (0.12 mL, 0.50 mmol) in 1,4-dioxane, and the solution became homogeneous. The reaction was stirred at 23 °C overnight and concentrated and triturated with DCM. The resultant powder was then dried *in vacuo* to provide 3-[3-(6-isoquinolyl)imidazo[1,2-*b*]pyridazin-6-yl]oxycyclobutanamine **19**. Yield: 20 mg, 58%. ^{1}H NMR (500 MHz, DMSO-d_6) δ 9.82 (s, 1H), 9.22 (s, 1H), 8.85 (d, J = 14.9 Hz, 1H), 8.68−8.60 (m, 6H), 8.28 (d, J = 23.9 Hz, 1H), 7.19 (d, J = 23.8 Hz, 1H), 5.80 (br s, 1H), 3.91 (br s, 1H), 2.86−2.81 (m, 2H), 2.70−2.66 (m, 2H). MS (ESI) m/z 332 [M + H]$^+$; Anal. Calcd for $C_{19}H_{17}N_5O$ + 2.5HCl + 3.5H_2O: C, 47.00; H, 5.50; N, 14.42. Found: C, 46.91; H, 5.49; N, 14.46. HRMS: measured m/z [M + H]$^+$ 332.1506 (calcd. for $C_{19}H_{18}N_5O$: 332.1504)

*N-(6-((8′-Chloro-1′,5′-dioxo-1′,5′-dihydro-2′H-spiro-[cyclohexane-1,3′-imidazo[1,5-a]pyridin]-6′-yl)amino)pyrimidin-4-yl)cyclopropanecarboxamide (**20**).* Prepared as in U.S. Patent 9,382,248.[30] The synthesis of intermediate 6′-bromo-8′-chloro-2′*H*-spiro[cyclohexane-1,3′-imidazo[1,5-*a*]pyridine]-1′,5′-dione was carried out as described above using the general protocol of Procedure A. Off white solid; Yield: 1.93 g, 64%. ^{1}H NMR (400 MHz, DMSO-d_6) δ 10.59 (s, 1H), 8.24 (s, 1H), 2.84 (t, J = 10.7 Hz, 2H), 1.78−1.70 (m, 2H), 1.69−1.55 (m, 3H), 1.54−1.49 (m, 2H), 1.25−1.15 (m, 1H). MS (ESI) m/z 331 [M + H].

The synthesis of compound **20** was carried out as described above using the general protocol of Procedure B. Yellow solid; Yield: 0.051 g, 2.1%. HPLC purity: 98.19%; ^{1}H NMR (400 MHz, DMSO-d_6) δ 10.93 (s, 1H), 10.29 (s, 1H), 9.43 (s, 1H), 8.70 (s, 1H), 8.58 (s,1H),7.97(s, 1H), 2.93 (t, J = 11.2 Hz, 2H), 2.02−1.92 (m, 1H), 1.76−1.73 (m, 2H), 1.68−1.58 (m, 3H), 1.58−1.46 (m, 2H), 1.21−1.19 (m, 1H), 0.85−0.83 (m, 4H); ^{13}C NMR (125 MHz, DMSO-d_6) δ 173.9, 162.9, 159.4, 157.8, 157.5, 153.7, 134.4, 122.8, 121.2, 111.1, 96.7, 80.3, 32.9, 24.7, 22.4, 14.8, 8.6. HRMS: measured m/z [M + H]$^+$ 429.1433 (calcd. for $C_{20}H_{22}ClN_6O_3$: 429.1436).

*6′-((6-Aminopyrimidin-4-yl)amino)-8′-chloro-2′H-spiro-[cyclohexane-1,3′-imidazo[1,5-a]pyridine]-1′,5′-dione (**21**).* Prepared as in U.S. Patent 9,382,248.[30] The synthesis of compound **21** was carried out as described above using the general protocol of Procedure B. Yield: 22 mg. HPLC purity: 99.31%; ^{1}H NMR (400 MHz, DMSO-d_6) δ 10.22 (s, 1H), 8.90 (s, 1H), 8.63 (s, 1H), 8.20 (s, 1H), 6.61 (s, 2H), 6.24 (s, 1H), 2.94 (t, J = 11.36 Hz, 2H), 1.78−1.60 (m, 5H), 1.56−1.52 (d, J = 12.1 Hz, 2H), 1.27−1.18 (m, 1H); ^{13}C NMR (125 MHz, DMSO-d_6) δ 159.3, 158.7, 153.3, 152.6, 133.2, 123.3, 122.4, 110.3, 87.9, 79.9, 32.3, 24.1, 21.9. HRMS: measured m/z [M + H]$^+$ 361.1185 (calcd. for $C_{16}H_{18}ClN_6O_2$: 361.1174).

*6-[(6-Amino-5-chloro-pyrimidin-4-yl)amino]-8-chloro-spiro[2H-imidazo[1,5-a]pyridine-3,1′-cyclohexane]-1,5-dione Hydrochloride (**22**).* Prepared as in U.S. Patent 9,382,248.[30] To a stirred solution of 4-amino-5,6-dichloropyrimidine (3.0 g, 18.29 mmol) in THF (30 mL), 4-dimethylaminopyridine (0.16 g, 1.31 mmol) and di-*t*-butyl dicarbonate (8.77 g, 40.2 mmol) were added at rt. The reaction was stirred at rt overnight and concentrated, and the residue was diluted with water and extracted with ethyl acetate (2 × 50 mL), dried (magnesium sulfate), and concentrated to afford ethyl *t*-butyl *N*-*t*-butoxycarbonyl-*N*-(5,6-dichloropyrimidin-4-yl)carbamate as a white solid. Yield: 3.1 g, 47%. ^{1}H NMR (400 MHz, DMSO-d_6) δ 9.06 (s, 1H), 1.40 (s, 18H). MS (ESI) m/z 364.3 [M + H]$^+$.

The synthesis of intermediate *t*-butyl *N*-*t*-butoxycarbonyl-*N*-[5-chloro-6-[(8-chloro-1,5-dioxo-spiro[2*H*-imidazo[1,5-*a*]pyridine-3,1′-cyclohexane]-6-yl)amino]pyrimidin-4-yl]carbamate was carried out as described above using the general protocol of Procedure B. Yellow solid; Yield: 0.10 g, 26%. ^{1}H NMR (400 MHz, DMSO-d_6) δ 10.46 (s, 1H), 8.99 (s, 1H), 8.95 (s, 1H), 8.66 (s, 1H), 2.90 (t, J = 10.74, 2H), 1.65 (m, 7H), 1.46 (m, 18H), 1.20 (m, 1H); MS (ESI) m/z 595.45 [M + H]$^+$.

The synthesis of compound **22** was carried out as described above using the general protocol of Procedure C. Yellow solid; Yield: 0.059 g, 81%. HPLC purity: 97.48%; ^{1}H NMR: (400 MHz, DMSO-d_6) δ 10.35 (s, 1H), 8.62 (s, 1H), 8.55 (s, 1H), 8.23 (s, 2H), 7.27 (s, 1H), 2.91 (t, J = 2.28, 2H), 1.77−1.68 (m, 2H), 1.65−1.54 (m, 3H), 1.55−1.52 (m, 2H), 1.28−1.22 (m, 1H); ^{13}C NMR (125 MHz, DMSO-d_6) δ 158.7, 158.2, 153.9, 153.6, 153.2, 132.6, 122.8, 120.1, 111.0, 93.8, 80.0, 32.4, 24.1, 21.9. HRMS: measured m/z [M + H]$^+$ 395.0790 (calcd. for $C_{16}H_{17}Cl_2N_6O_2$: 395.0712).

*6′-((6-Aminopyrimidin-4-yl)amino)-8′-methyl-2′H-spiro-[cyclohexane-1,3′-imidazo[1,5-a]pyridine]-1′,5′-dione Hydrochloride (**23**).* Prepared as in U.S. Patent 9,382,248.[30] To a stirred solution of 4-amino-6-chloropyrimidine (4900 g, 1 equiv, 37.08 mol) in THF (10 V, 50 L), at 0 °C was added *N*,*N*-dimethylaminopyridine (463 g, 0.1 equiv, 3.70 mol). Di-*t*-butyl dicarbonate (24.8 L, 3 equiv, 113.9 mol) was then added slowly over 1 h (gas evolution was observed) to

DOI: 10.1021/acs.jmedchem.7b01795
J. Med. Chem. 2018, 61, 3516−3540

the resultant reaction. The reaction mixture became dark brown with stirring at rt over a period of 16 h. The reaction mixture was poured into an ice/water mixture (30 L) and further stirred for 30 min prior to solvent extraction of the aqueous phase with ethyl acetate (10 L). The organic and aqueous phases were separated, and the resultant aqueous layer was extracted twice with ethyl acetate (2 × 10 L), the combined organic layer was washed twice with water (2 × 10 L), then brine (1 × 10 L), and dried over anhydrous sodium sulfate. The organic layer was concentrated under reduced pressure at 50 °C to obtain crude product, which was slurried with hexane (10 L) for 1 h, filtered, and dried under reduced pressure at 50 °C to obtain a brick red solid. Yield: 1030 g (82.6%). ^{1}H NMR (400 MHz, DMSO-d_6) δ: 8.86 (s, 1H), 7.85 (s, 1H), 1.48 (s, 18H). MS (ESI) m/z 330 [M + H]$^+$.

To a stirring solution of di-*t*-butyl (6-chloropyrimidin-4-yl) carbamate (5000 g, 1 equiv, 15.20 mol) in 1,4-dioxane (5 V, 25 L) at rt was added cyclopropanecarboxamide (1291 g, 1 equiv, 15.20 mol) followed by the addition of cesium carbonate (3950 g, 0.8 equiv, 12.15 mol). After purging the reaction mixture (dark brown solution) with argon for 30 min, Xantphos (120 g, 0.015 equiv, 0.23 mol) and palladium(II) acetate (51 g, 0.015 equiv, 0.23 mol) were added. Purging of the reaction with argon was continued for another 15 min, and the reaction mixture was then heated to 90 °C for 4 h, during which time the color of the reaction changed to orange. The reaction mixture was cooled to 50 °C and was filtered through a Celite bed and washed with EtOAc (3 × 10 L), and the combined organic layers were washed with water (2 × 10 L), dried over anhydrous sodium sulfate, and concentrated under reduced pressure to provide crude product (6200 g). Diethyl ether (6.0 L) was added, the mixture was stirred for 30 min, and the solid was filtered, washed with ether (2 × 1 L), and then dried to afford di-*t*-butyl (6-(cyclopropanecarboxamido) pyrimidin-4-yl) carbamate as an orange solid. This compound was used in the next step without further purification. Yield: 4500 g, (78.2%). ^{1}H NMR (400 MHz, DMSO-d_6) δ: 11.30 (s, 1H), 8.66 (s, 1H), 8.25 (s, 1H), 2.16−2.02 (m, 1H), 1.48−1.39 (m, 18H), 0.80−0.60 (m, 4H). MS (ESI) m/z 378.43 [M + H]$^+$.

Trifluoroacetic acid (16 L, 10 equiv, 212 mol) was slowly added over 1 h to a stirring solution of di-*t*-butyl (6-(cyclopropanecarboxamido) pyrimidin-4-yl) (8050 g, 1 equiv, 21.20 mol) in DCM (5 V, 40 L). Evolution of gas was observed during the addition of trifluoroacetic acid, and the reaction became dark brown when stirred continuously for 4 h at rt. The reaction was concentrated to dryness under reduced pressure, and DCM (25 L) was added to the residue. The mixture was cooled to 0 °C, and NH_4OH (25% aq. solution, 6 L) was added slowly (pH = 10) over 30 min while stirring the reaction mixture continuously. The resulting mixture was stirred at 0 °C for an additional 30 min, and the solid formed was filtered and washed with water (2 × 10 L) followed by washing with methanol (2 × 2 L) and DCM (15 L). The washed solid was dried under high vacuum overnight to afford *N*-(6-aminopyrimidin-4-yl) cyclopropanecarboxamide as light yellow solid. Yield: 2320 g (61.0%). ^{1}H NMR (400 MHz, DMSO-d_6) δ: 10.54 (s, 1H), 8.10 (s, 1H), 7.10 (s, 1H), 6.72 (br, 2H), 2.00−1.94 (m, 1H), 0.81−0.78 (m, 4H). MS (ESI) m/z 178.19 [M + H]$^+$. The title compound was prepared according to Procedure A using 5-bromo-3-methyl-6-oxo-1,6-dihydropyridine-2-carboxamide (prepared from 5-bromo-3-methylpicolinic acid in a similar fashion to that used for the preparation of ethyl 5-chloro-6-oxo-1,6-dihydropyridine-2-carboxylate). Off-white solid; Yield: 1280 g, 82%. ^{1}H NMR (500 MHz, DMSO-d_6) δ 10.37 (s, 1H), 8.01 (s, 1H), 2.92−2.82 (m, 2H), 2.38 (s, 3H), 1.75−1.65 (m, 5H), 1.43 (d, J = 24 Hz, 2H), 1.25−1.15 (m, 1H). MS (ESI) m/z 311 [M + H]$^+$.

The title compound was prepared according to Procedure B using 6′-bromo-8′-methyl-2′*H*-spiro[cyclohexane-1,3′-imidazo[1,5-*a*]-pyridine]-1′,5′-dione (1230 g) and *N*-(6-aminopyrimidin-4-yl)-cyclopropanecarboxamide (650 g); 1420 g (98% yield). ^{1}H NMR (500 MHz, DMSO-d_6) δ 10.85 (br, 1H), 10.07 (br, 1H), 9.09 (s, 1H), 8.53 (s, 1H), 8.46 (s, 1H), 7.85 (s, 1H), 3.95−3.05 (m, 2H), 2.45 (s, 3H), 2.05−1.95 (m, 1H), 1.80−1.60 (m, 5H), 1.44 (d, J = 24 Hz, 2H), 1.25−1.15 (m, 1H), 0.89−0.80 (m, 4H).

Procedure D: *N*-(6-((8′-methyl-1′,5′-dioxo-1′,5′-dihydro-2′*H*-spiro-[cyclohexane-1,3′-imidazo[1,5-*a*]pyridin]-6′-yl)amino)pyrimidin-4-yl)cyclopropanecarboxamide (1420 g), THF (5.7 L), and EtOH (5.7 L) were added to a 50 L reactor and agitated at 100 rpm. The temperature was adjusted to 20 °C. To a 45 L carboy was added water (5.7 L, deionized (DI)) and KOH (1170 g), and the contents of the carboy were agitated until a solution formed. The KOH solution was then added to the 50 L reactor followed by addition of ethylenediamine (2.83 L). After stirring for 16 h the pH was adjusted to 2 by the addition of concentrated HCl (1180 g), and the temperature was adjusted to 20 °C, the mixture was agitated, and the solid material was filtered through a Nutsche filter (18″). The reactor was then rinsed with water (14 L, DI), and the aqueous rinse was transferred to the filter while manually suspending the solid in the wash. A second rinse was performed using water (14 L, DI), and the rinse was transferred again to the filter while manually suspending the solid in the wash. Sodium bicarbonate (1300 g) and water (26.0 L, DI) were then added to the rinsed 50 L reactor, and the filter cake was slowly introduced into the reactor over a time period of about 30 min to avoid excess gas liberation. The resulting suspension was agitated for 2 h followed by filtration through a Nutsche filter (18″). The filter cake was washed with water (15.0 L) and allowed to condition overnight. The filter cake was once again suspended in an aqueous solution of sodium bicarbonate, agitated for 2 h, and filtered through a Nutsche filter (18″). Following washing with water, the filter cake was allowed to condition overnight and then transferred to drying trays and dried under vacuum at 45 °C. Yield: 1050 g, 80%. HPLC purity: 99.74%; ^{1}H NMR (500 MHz, DMSO-d_6) δ 10.20 (s, 1H), 9.68 (s, 1H), 8.47 (s, 1H), 8.09 (s, 1H), 7.97 (br, 2H), 6.42 (s, 1H), 3.00−2.90 (m, 2H), 2.43 (s, 3H), 1.80−1.60 (m, 5H), 1.5 (d, J = 24 Hz, 2H), 1.25−1.12 (m, 1H); ^{13}C NMR (125 MHz, DMSO-d_6) δ 163.8, 161.6, 159.2, 157.8, 153.4, 133.5, 121.5, 121.2, 116.6, 87.6, 78.8, 32.5, 24.2, 21.9, 13.8. HRMS: measured m/z [M + H]$^+$ 341.1729 (calcd. for $C_{17}H_{21}N_6O_2$: 341.1721).

*6-[(6-Aminopyrimidin-4-yl)amino]-8-chloro-3,3-dimethyl-2H-imidazo[1,5-a]pyridine-1,5-dione (**24**).* The synthesis of intermediate 6-bromo-8-chloro-3,3-dimethyl-2*H*-imidazo[1,5-*a*]pyridine-1,5-dione was carried out as described above using the general protocol of Procedure A. White solid; Yield: 390 mg, 48%. ^{1}H NMR (400 MHz, DMSO-d_6) δ 10.03 (s, 1H), 8.24 (s, 1H), 1.75 (s, 6H); MS (ESI) m/z 289 [M-1]$^-$.

The synthesis of intermediate *N*-[6-[(8-chloro-3,3-dimethyl-1,5-dioxo-2*H*-imidazo[1,5-*a*]pyridin-6-yl)-amino]pyrimidin-4-yl]-cyclopropanecarboxamide was carried out as described above using the general protocol of Procedure B. Light yellow solid; Yield: 42 mg, 17%. ^{1}H NMR (400 MHz, DMSO-d_6) δ 10.92 (s, 1H), 9.74 (s, 1H), 9.49 (s, 1H), 8.70 (s, 1H), 8.59 (s, 1H), 7.98 (s, 1H), 2.16−2.02 (m, 1H), 1.79 (s, 6H), 0.84 (d, J = 6.0 Hz, 4H); MS (ESI) m/z 389.28 [M + H]$^+$.

The synthesis of **24** was carried out as described in Procedure D above using *N*-[6-[(8-chloro-3,3-dimethyl-1,5-dioxo-2*H*-imidazo[1,5-*a*]pyridin-6-yl)amino]pyrimidin-4-yl]cyclopropanecarboxamide (0.25g, 0.64 mmol). Light yellow solid; Yield: 0.14 g, 68%. HPLC purity: 97.83%; ^{1}H NMR (400 MHz, DMSO-d_6) δ 9.64 (s, 1H), 8.92 (s, 1H), 8.64 (s, 1H), 8.20 (s, 1H), 6.60 (s, 2H), 6.25 (s, 1H), 1.79 (s, 6H); ^{13}C NMR (125 MHz, DMSO-d_6) δ 159.4, 157.8, 156.1, 153.3, 150.6, 132.6, 142.1, 123.9, 109.8, 87.7, 76.7, 24.7. HRMS: measured m/z [M + H]$^+$ 321.0869 (calcd. for $C_{13}H_{14}ClN_6O_2$: 321.0861).

*6-[(6-Aminopyrimidin-4-yl)amino]-8-chloro-spiro[2H-imidazo-[1,5-a]pyridine-3,1′-cyclopentane]-1,5-dione (**25**).* The synthesis of intermediate 6-bromo-8-chloro-spiro[2*H*-imidazo[1,5-*a*]pyridine-3,1′-cyclopentane]-1,5-dione was carried out as described above using the general protocol of Procedure A. Off-white solid; Yield: 380 mg; 60%. ^{1}H NMR (400 MHz, DMSO-d_6): δ 10.39 (s, 1H), 8.25 (s, 1H), 2.73 (m, 4H), 2.21 (m, 2H), 1.93 (m, 2H); MS (ESI) m/z 315.06 [M − 1]$^-$.

The title compound was prepared according to the Procedure B using 6-bromo-8-chloro-spiro[2*H*-imidazo[1,5-*a*]pyridine-3,1′-cyclopentane]-1,5-dione (0.3 g, 0.94 mmol) and *t*-butyl *N*-(6-aminopyrimidin-4-yl)carbamate (178 mg, 0.85 mmol) to provide *t*-butyl *N*-[6-[(8-chloro-1,5-dioxo-spiro[2*H*-imidazo[1,5-*a*]pyridine-3,1′-cyclopentane]-6-yl)amino]pyrimidin-4-yl]carbamate. Light yellow solid;

DOI: 10.1021/acs.jmedchem.7b01795
J. Med. Chem. 2018, 61, 3516−3540

Yield: 0.30 g, 71%. ^{1}H NMR (400 MHz, DMSO-d_6) δ 10.1−9.50 (bs, 2H), 8.67 (s, 1H), 8.50 (s, 1H), 7.79 (s, 1H), 3.56 (s, 1H), 2.86−2.70 (m, 2H), 2.05−1.90 (m, 2H), 1.85−1.75 (m, 2H), 1.73−1.60 (m, 2H), 1.48 (s, 9H); MS (ESI) m/z 447.10 [M + H]$^+$.

The synthesis of compound **25** was carried out as described above using the general protocol of Procedure C. Light yellow solid; Yield: 0.07 g, 45%. HPLC purity: 98.50%; ^{1}H NMR (400 MHz, DMSO-d_6) δ 10.04 (s, 1H), 9.15 (s, 1H), 8.60 (s, 1H), 8.26 (s, 1H), 6.85 (s, 2H), 6.30 (s, 1H), 2.77 (s, 2H), 1.97 (s, 2H), 1.90−1.70 (m, 4H); ^{13}C NMR (125 MHz, DMSO-d_6) δ 159.3, 158.1, 153.0, 133.5, 122.8, 121.4, 110.4, 88.0, 85.2, 70.0, 35.4, 26.3, 24.8. HRMS: measured m/z [M + H]$^+$ 347.1018 (calcd. for $C_{15}H_{16}ClN_6O_2$: 347.1023).

*6-[(6-Aminopyrimidin-4-yl)amino]-8-chloro-4′,4′-difluoro-spiro-[2H-imidazo[1,5-a]pyridine-3,1′-cyclohexane]-1,5-dione (**26**).* The synthesis of intermediate 6-bromo-8-chloro-4′,4′-difluoro-spiro[2*H*-imidazo[1,5-*a*]pyridine-3,1′-cyclohexane]-1,5-dione was carried out as described above using the general protocol of Procedure A. Off-white solid; Yield: 5.9 g. 80%. ^{1}H NMR (400 MHz, DMSO-d_6) δ 9.79 (s, 1H), 7.89 (s, 1H), 2.12 (m, 6H), 1.66 (m, 2H); MS (ESI) m/z 364.92 [M − 1]$^-$.

The synthesis of intermediate *N*-[6-[(8-chloro-4′,4′-difluoro-1,5-dioxo-spiro[2*H*-imidazo[1,5-*a*]pyridine-3,1′-cyclohexane]-6-yl)-amino]pyrimidin-4-yl]cyclopropanecarboxamide was carried out as described above using the general protocol of Procedure B. Off-white solid; Yield: 4.71g, 63%. ^{1}H NMR (400 MHz, DMSO-d_6) δ 10.92 (s, 1H), 10.47 (s, 1H), 9.51 (s, 1H), 8.71 (s, 1H), 8.59 (s, 1H), 7.98 (s, 1H), 3.32−3.25 (m, 2H), 2.28−2.17 (m, 4H), 2.16−2.02 (m, 1H), 1.79−1.70 (m, 2H), 0.84−0.81 (m,4H); MS (ESI) m/z 465.38 [M + H]$^+$.

The synthesis of **26** was carried out as described above using the general protocol of Procedure D. Light yellow solid; Yield: 0.35g, 41%. HPLC purity: 97.85%; ^{1}H NMR (400 MHz, DMSO-d_6) δ 10.56 (s, 1H), 9.87 (s, 1H), 8.51 (s, 1H), 8.43 (s, 1H), 7.89(s, 2H), 6.52 (s, 1H), 3.45−3.22 (m, 2H), 2.36−2.15 (m, 4H), 1.74 (d, J = 12.12 Hz, 2H); ^{13}C NMR (125 MHz, DMSO-d_6) δ 163.8, 161.8, 159.3, 157.5, 153.5, 133.7, 124.8, 122.9, 121.3, 121.2, 121.0, 117.3, 87.4, 76.9, 29.6 (t, J = 23 Hz), 28.8 (d, J = 10 Hz), 13.8. HRMS: measured m/z [M + H]$^+$ 377.1533 (calcd. for $C_{17}H_{19}F_2N_6O_2$: 377.1538).

■ ASSOCIATED CONTENT

Supporting Information

The Supporting Information is available free of charge on the ACS Publications website at DOI: 10.1021/acs.jmedchem.7b01795.

Molecular formula strings (CSV)

Additional data regarding *in vitro* assays, *in vivo* efficacy, pharmacokinetic data, MNK2 protein expression, purification, crystallization, data collection, structure solution and refinement, characterization data, ^{13}C NMR, and HPLC for compounds **2**−**26** (PDF)

Accession Codes

New protein−ligand coordinates have been deposited in the PDB with codes 6CJ5, 6CJE, 6CJH, 6CJW, 6CJY, 6CK3, 6CK6, and 6CKI.

■ AUTHOR INFORMATION

Corresponding Author

*Phone 619-729-9526. E-mail: sreich@effector.com.

ORCID

Siegfried H. Reich: 0000-0002-6840-2618

Gary G. Chiang: 0000-0003-3004-7400

Notes

The authors declare the following competing financial interest(s): S.H.R., P.A.S., G.G.C., J.R.A., J.C., J.C., B.E., J.T.E., Q.H., V.K.G., E.Z.H., V.H., I.N.H., A.J., K.J., J.M., D.M., M.N., G.S.P., M.S., S.S., J.S., C.R.S., P.A.T., C.T., S.E.W., C.J.W., H.Z., and K.R.W. were employees and shareholders of eFFECTOR Therapeutics when the research was performed.

■ ACKNOWLEDGMENTS

We want to thank Kevan Shokat and Davide Ruggero for their support and helpful feedback on the manuscript. We also want to thank Theo Michels for helping with spectral analysis.

■ ABBREVIATIONS USED

ABC DLBCL, activated b-cell; DI, deionized; DLBCL, diffuse large cell B-cell lymphoma; hnRNPA1, heterogeneous nuclear ribonucleoprotein A1; HTRF, homogeneous time-resolved fluorescence; IL-6, interleukin-6; IL-8, interleukin-8; LLE, lipophilic ligand efficiency; MNK, mitogen-activated protein kinase interacting kinases; PSF, protein-associated splicing factor; PK/PD, pharmacokinetic/pharmacodynamics; TGI, tumor growth inhibition; TME, tumor microenvironment; xlogP, calculated logarithm of octanol−water partition coefficient (Dotmatics)

■ REFERENCES

(1) Sendoel, A.; Dunn, J. G.; Rodriguez, E. H.; Naik, S.; Gomez, N. C.; Hurwitz, B.; Levorse, J.; Dill, B. D.; Schramek, D.; Molina, H.; Weissman, J. S.; Fuchs, E. Translation from unconventional 5′ start sites drives tumour initiation. *Nature* **2017**, *541*, 494−499.

(2) Pelletier, J.; Graff, J.; Ruggero, D.; Sonenberg, N. Targeting the eIF4F translation initiation complex: a critical nexus for cancer development. *Cancer Res.* **2015**, *75*, 250−263.

(3) Bhat, M.; Robichaud, N.; Hulea, L.; Sonenberg, N.; Pelletier, J.; Topisirovic, I. Targeting the translation machinery in cancer. *Nat. Rev. Drug Discovery* **2015**, *14*, 261−278.

(4) Dreas, A.; Mikulski, M.; Milik, M.; Fabritius, C. H.; Brzozka, K.; Rzymski, T. Mitogen-activated protein kinase (MAPK) interacting kinases 1 and 2 (MNK1 and MNK2) as targets for cancer therapy: recent progress in the development of MNK inhibitors. *Curr. Med. Chem.* **2017**, *24*, 3025−3053.

(5) Truitt, M. L.; Ruggero, D. New frontiers in translational control of the cancer genome. *Nat. Rev. Cancer* **2016**, *16*, 288−304.

(6) Korneeva, N. L.; Song, A.; Gram, H.; Edens, M. A.; Rhoads, R. E. Inhibition of mitogen-activated protein kinase (MAPK)-interacting kinase (MNK) preferentially affects translation of mRNAs containing both a 5′-terminal cap and hairpin. *J. Biol. Chem.* **2016**, *291*, 3455−3467.

(7) Ueda, T.; Watanabe-Fukunaga, R.; Fukuyama, H.; Nagata, S.; Fukunaga, R. MNK2 and MNK1 are essential for constitutive and inducible phosphorylation of eukaryotic initiation factor 4E but not for cell growth or development. *Mol. Cell. Biol.* **2004**, *24*, 6539−6549.

(8) Wendel, H. G.; Silva, R. L.; Malina, A.; Mills, J. R.; Zhu, H.; Ueda, T.; Watanabe-Fukunaga, R.; Fukunaga, R.; Teruya-Feldstein, J.; Pelletier, J.; Lowe, S. W. Dissecting eIF4E action in tumorigenesis. *Genes Dev.* **2007**, *21*, 3232−3237.

(9) Furic, L.; Rong, L.; Larsson, O.; Koumakpayi, I. H.; Yoshida, K.; Brueschke, A.; Petroulakis, E.; Robichaud, N.; Pollak, M.; Gaboury, L. A.; Pandolfi, P. P.; Saad, F.; Sonenberg, N. eIF4E phosphorylation promotes tumorigenesis and is associated with prostate cancer progression. *Proc. Natl. Acad. Sci. U. S. A.* **2010**, *107*, 14134−14139.

(10) Diab, S.; Kumarasiri, M.; Yu, M.; Teo, T.; Proud, C.; Milne, R.; Wang, S. MAP kinase-interacting kinases-emerging targets against cancer. *Chem. Biol.* **2014**, *21*, 441−452.

(11) Piccirillo, C. A.; Bjur, E.; Topisirovic, I.; Sonenberg, N.; Larsson, O. Translational control of immune responses: from transcripts to translatomes. *Nat. Immunol.* **2014**, *15*, 503−511.

(12) Buxade, M.; Morrice, N.; Krebs, D. L.; Proud, C. G. The PSF.p54nrb complex is a novel MNK substrate that binds the mRNA for tumor necrosis factor alpha. *J. Biol. Chem.* **2008**, *283*, 57−65.

DOI: 10.1021/acs.jmedchem.7b01795
J. Med. Chem. 2018, 61, 3516−3540

(13) Buxade, M.; Parra, J. L.; Rousseau, S.; Shpiro, N.; Marquez, R.; Morrice, N.; Bain, J.; Espel, E.; Proud, C. G. The Mnks are novel components in the control of TNF alpha biosynthesis and phosphorylate and regulate hnRNP A1. *Immunity* **2005**, *23*, 177−189.
(14) Edwin, F.; Anderson, K.; Ying, C.; Patel, T. B. Intermolecular interactions of sprouty proteins and their implications in development and disease. *Mol. Pharmacol.* **2009**, *76*, 679−691.
(15) Panel, V.; Boelle, P. Y.; Ayala-Sanmartin, J.; Jouniaux, A. M.; Hamelin, R.; Masliah, J.; Trugnan, G.; Flejou, J. F.; Wendum, D. Cytoplasmic phospholipase A2 expression in human colon adenocarcinoma is correlated with cyclooxygenase-2 expression and contributes to prostaglandin E2 production. *Cancer Lett.* **2006**, *243*, 255−263.
(16) Jean-Philippe, J.; Paz, S.; Caputi, M. hnRNP A1: the Swiss army knife of gene expression. *Int. J. Mol. Sci.* **2013**, *14*, 18999−19024.
(17) Joshi, S.; Platanias, L. C. MNK kinase pathway: Cellular functions and biological outcomes. *World J. Biol. Chem.* **2014**, *5*, 321−333.
(18) Ueda, T.; Sasaki, M.; Elia, A. J.; Chio, I. I.; Hamada, K.; Fukunaga, R.; Mak, T. W. Combined deficiency for MAP kinase-interacting kinase 1 and 2 (MNK1 and MNK2) delays tumor development. *Proc. Natl. Acad. Sci. U. S. A.* **2010**, *107*, 13984−13990.
(19) Lazaris-Karatzas, A.; Montine, K. S.; Sonenberg, N. Malignant transformation by a eukaryotic initiation factor subunit that binds to mRNA 5′ cap. *Nature* **1990**, *345*, 544−547.
(20) Konicek, B. W.; Stephens, J. R.; McNulty, A. M.; Robichaud, N.; Peery, R. B.; Dumstorf, C. A.; Dowless, M. S.; Iversen, P. W.; Parsons, S.; Ellis, K. E.; McCann, D. J.; Pelletier, J.; Furic, L.; Yingling, J. M.; Stancato, L. F.; Sonenberg, N.; Graff, J. R. Therapeutic inhibition of MAP kinase interacting kinase blocks eukaryotic initiation factor 4E phosphorylation and suppresses outgrowth of experimental lung metastases. *Cancer Res.* **2011**, *71*, 1849−1857.
(21) Knauf, U.; Tschopp, C.; Gram, H. Negative regulation of protein translation by mitogen-activated protein kinase-interacting kinases 1 and 2. *Mol. Cell. Biol.* **2001**, *21*, 5500−5511.
(22) Teo, T.; Yang, Y.; Yu, M.; Basnet, S. K.; Gillam, T.; Hou, J.; Schmid, R. M.; Kumarasiri, M.; Diab, S.; Albrecht, H.; Sykes, M. J.; Wang, S. An integrated approach for discovery of highly potent and selective MNK inhibitors: screening, synthesis and SAR analysis. *Eur. J. Med. Chem.* **2015**, *103*, 539−550.
(23) Kosciuczuk, E. M.; Saleiro, D.; Kroczynska, B.; Beauchamp, E. M.; Eckerdt, F.; Blyth, G. T.; Abedin, S. M.; Giles, F. J.; Altman, J. K.; Platanias, L. C. Merestinib blocks MNK kinase activity in acute myeloid leukemia progenitors and exhibits antileukemic effects in vitro and in vivo. *Blood* **2016**, *128*, 410−414.
(24) Durante, C.; Russo, D.; Verrienti, A.; Filetti, S. XL184 (cabozantinib) for medullary thyroid carcinoma. *Expert Opin. Invest. Drugs* **2011**, *20*, 407−413.
(25) Han, W.; Ding, Y.; Xu, Y.; Pfister, K.; Zhu, S.; Warne, B.; Doyle, M.; Aikawa, M.; Amiri, P.; Appleton, B.; Stuart, D. D.; Fanidi, A.; Shafer, C. M. Discovery of a selective and potent Inhibitor of mitogen-activated protein kinase-interacting kinases 1 and 2 (MNK1/2) utilizing structure-based drug design. *J. Med. Chem.* **2016**, *59*, 3034−3045.
(26) Yu, M.; Li, P.; Basnet, S. K. C.; Kumarasiri, M.; Diab, S.; Teo, T.; Albrecht, H.; Wang, S. Discovery of 4-(dihydropyridinon-3-yl)amino-5-methylthieno[2,3-d]pyrimidine derivatives as potent MNK inhibitors: synthesis, structure-activity relationship analysis and biological evaluation. *Eur. J. Med. Chem.* **2015**, *95*, 116−126.
(27) Santag, S.; Siegel, F.; Wengner, A. M.; Lange, C.; Bomer, U.; Eis, K.; Puhler, F.; Lienau, P.; Bergemann, L.; Michels, M.; von Nussbaum, F.; Mumberg, D.; Petersen, K. BAY 1143269, a novel MNK1 inhibitor, targets oncogenic protein expression and shows potent anti-tumor activity. *Cancer Lett.* **2017**, *390*, 21−29.
(28) Oyarzabal, J.; Zarich, N.; Albarran, M. I.; Palacios, I.; Urbano-Cuadrado, M.; Mateos, G.; Reymundo, I.; Rabal, O.; Salgado, A.; Corrionero, A.; Fominaya, J.; Pastor, J.; Bischoff, J. R. Discovery of mitogen-activated protein kinase-interacting kinase 1 inhibitors by a comprehensive fragment-oriented virtual screening approach. *J. Med. Chem.* **2010**, *53*, 6618−6628.
(29) Webster, K. R.; Goel, V. K.; Hung, I. N.; Parker, G.; Staunton, J.; Neal, M.; Molter, J.; Chiang, G. G.; Jessen, K. A.; Wegerski, C. J.; Sperry, S.; Huang, V.; Chen, J.; Thompson, P. A.; Appleman, J. R.; Webber, S. E.; Sprengeler, P. A.; Reich, S. H. eFT508, a potent and selective mitogen-activated protein kinase interacting kinase (MNK) 1 and 2 inhibitor, is efficacious in preclinical models of diffuse large B-cell lymphoma (DLBCL). *Blood* **2015**, *126*, 1554.
(30) Reich, S. H.; Sprengeler, P. A.; Webber, S. E.; Xiang, A. X.; Ernst, J. MNK Inhibitors and Methods Related Thereto. U.S. Patent 9,382,248, July 5, 2016.
(31) Raheem, I. T.; Walji, A. M.; Klein, D.; Sanders, J. M.; Powell, D. A.; Abeywickrema, P.; Barbe, G.; Bennet, A.; Childers, K.; Christensen, M.; Clas, S. D.; Dubost, D.; Embrey, M.; Grobler, J.; Hafey, M. J.; Hartingh, T. J.; Hazuda, D. J.; Kuethe, J. T.; McCabe Dunn, J.; Miller, M. D.; Moore, K. P.; Nolting, A.; Pajkovic, N.; Patel, S.; Peng, Z.; Rada, V.; Rearden, P.; Schreier, J. D.; Sisko, J.; Steele, T. G.; Truchon, J. F.; Wai, J.; Xu, M.; Coleman, P. J. Discovery of 2-pyridinone aminals: a prodrug strategy to advance a second generation of HIV-1 integrase strand transfer inhibitors. *J. Med. Chem.* **2015**, *58*, 8154−8165.
(32) Jones, V. S.; Huang, R. Y.; Chen, L. P.; Chen, Z. S.; Fu, L.; Huang, R. P. Cytokines in cancer drug resistance: cues to new therapeutic strategies. *Biochim. Biophys. Acta, Rev. Cancer* **2016**, *1865*, 255−265.
(33) Lin, W. W.; Karin, M. A cytokine-mediated link between innate immunity, inflammation, and cancer. *J. Clin. Invest.* **2007**, *117*, 1175−1183.
(34) Muller, S.; Chaikuad, A.; Gray, N. S.; Knapp, S. The ins and outs of selective kinase inhibitor development. *Nat. Chem. Biol.* **2015**, *11*, 818−821.
(35) Bissantz, C.; Kuhn, B.; Stahl, M. A medicinal chemist's guide to molecular interactions. *J. Med. Chem.* **2010**, *53*, 5061−5084.
(36) Fufezan, C. The role of Buergi-Dunitz interactions in the structural stability of proteins. *Proteins: Struct., Funct., Genet.* **2010**, *78*, 2831−2838.
(37) Paulini, R.; Muller, K.; Diederich, F. Orthogonal multipolar interactions in structural chemistry and biology. *Angew. Chem., Int. Ed.* **2005**, *44*, 1788−1805.
(38) Jauch, R.; Jakel, S.; Netter, C.; Schreiter, K.; Aicher, B.; Jackle, H.; Wahl, M. C. Crystal structures of the MNK2 kinase domain reveal an inhibitory conformation and a zinc binding site. *Structure* **2005**, *13*, 1559−1568.
(39) Huang, H.; Zeqiraj, E.; Dong, B.; Jha, B. K.; Duffy, N. M.; Orlicky, S.; Thevakumaran, N.; Talukdar, M.; Pillon, M. C.; Ceccarelli, D. F.; Wan, L. C.; Juang, Y. C.; Mao, D. Y.; Gaughan, C.; Brinton, M. A.; Perelygin, A. A.; Kourinov, I.; Guarne, A.; Silverman, R. H.; Sicheri, F. Dimeric structure of pseudokinase RNase L bound to 2−5A reveals a basis for interferon-induced antiviral activity. *Mol. Cell* **2014**, *53*, 221−234.
(40) Berman, H. M.; Westbrook, J.; Feng, Z.; Gilliland, G.; Bhat, T. N.; Weissig, H.; Shindyalov, I. N.; Bourne, P. E. The Protein Data Bank. *Nucleic Acids Res.* **2000**, *28*, 235−242.
(41) Groom, C. R.; Bruno, I. J.; Lightfoot, M. P.; Ward, S. C. The Cambridge Structural Database. *Acta Crystallogr., Sect. B: Struct. Sci., Cryst. Eng. Mater.* **2016**, *72*, 171−179.
(42) Wang, R.; Gao, Y.; Lai, L. Calculating partition coefficient by atom-additive method. *Perspect. Drug Discovery Des.* **2000**, *19*, 47−66.
(43) Joshi, S.; Platanias, L. C. MNK kinases in cytokine signaling and regulation of cytokine responses. *Biomol. Concepts* **2012**, *3*, 127−139.
(44) Rowlett, R. M.; Chrestensen, C. A.; Nyce, M.; Harp, M. G.; Pelo, J. W.; Cominelli, F.; Ernst, P. B.; Pizarro, T. T.; Sturgill, T. W.; Worthington, M. T. MNK kinases regulate multiple TLR pathways and innate proinflammatory cytokines in macrophages. *Am. J. Physiol. Gastrointest. Liver Physiol.* **2008**, *294*, G452−459.
(45) Landon, A. L.; Muniandy, P. A.; Shetty, A. C.; Lehrmann, E.; Volpon, L.; Houng, S.; Zhang, Y.; Dai, B.; Peroutka, R.; Mazan-Mamczarz, K.; Steinhardt, J.; Mahurkar, A.; Becker, K. G.; Borden, K.

DOI: 10.1021/acs.jmedchem.7b01795
J. Med. Chem. 2018, 61, 3516−3540

L.; Gartenhaus, R. B. MNKs act as a regulatory switch for eIF4E1 and eIF4E3 driven mRNA translation in DLBCL. *Nat. Commun.* **2014**, *5*, 5413.

(46) Wheater, M. J.; Johnson, P. W.; Blaydes, J. P. The role of MNK proteins and eIF4E phosphorylation in breast cancer cell proliferation and survival. *Cancer Biol. Ther.* **2010**, *10*, 728−735.

(47) Duffy, A. G.; Makarova-Rusher, O. V.; Ulahannan, S. V.; Rahma, O. E.; Fioravanti, S.; Walker, M.; Abdullah, S.; Raffeld, M.; Anderson, V.; Abi-Jaoudeh, N.; Levy, E.; Wood, B. J.; Lee, S.; Tomita, Y.; Trepel, J. B.; Steinberg, S. M.; Revenko, A. S.; MacLeod, A. R.; Peer, C. J.; Figg, W. D.; Greten, T. F. Modulation of tumor eIF4E by antisense inhibition: A phase I/II translational clinical trial of ISIS 183750-an antisense oligonucleotide against eIF4E-in combination with irinotecan in solid tumors and irinotecan-refractory colorectal cancer. *Int. J. Cancer* **2016**, *139*, 1648−1657.

(48) Chen, L.; Aktas, B. H.; Wang, Y.; He, X.; Sahoo, R.; Zhang, N.; Denoyelle, S.; Kabha, E.; Yang, H.; Freedman, R. Y.; Supko, J. G.; Chorev, M.; Wagner, G.; Halperin, J. A. Tumor suppression by small molecule inhibitors of translation initiation. *Oncotarget* **2012**, *3*, 869−881.

(49) Cencic, R.; Hall, D. R.; Robert, F.; Du, Y.; Min, J.; Li, L.; Qui, M.; Lewis, I.; Kurtkaya, S.; Dingledine, R.; Fu, H.; Kozakov, D.; Vajda, S.; Pelletier, J. Reversing chemoresistance by small molecule inhibition of the translation initiation complex eIF4F. *Proc. Natl. Acad. Sci. U. S. A.* **2011**, *108*, 1046−1051.

(50) Reddy, M. V.; Mallireddigari, M. R.; Cosenza, S. C.; Pallela, V. R.; Iqbal, N. M.; Robell, K. A.; Kang, A. D.; Reddy, E. P. Design, synthesis, and biological evaluation of (E)-styrylbenzylsulfones as novel anticancer agents. *J. Med. Chem.* **2008**, *51*, 86−100.

(51) Sekiyama, N.; Arthanari, H.; Papadopoulos, E.; Rodriguez-Mias, R. A.; Wagner, G.; Leger-Abraham, M. Molecular mechanism of the dual activity of 4EGI-1: Dissociating eIF4G from eIF4E but stabilizing the binding of unphosphorylated 4E-BP1. *Proc. Natl. Acad. Sci. U. S. A.* **2015**, *112*, E4036−4045.

(52) Lock, R.; Ingraham, R.; Maertens, O.; Miller, A. L.; Weledji, N.; Legius, E.; Konicek, B. M.; Yan, S. C.; Graff, J. R.; Cichowski, K. Cotargeting MNK and MEK kinases induces the regression of NF1-mutant cancers. *J. Clin. Invest.* **2016**, *126*, 2181−2190.

(53) Cherian, J.; Nacro, K.; Poh, Z. Y.; Guo, S.; Jeyaraj, D. A.; Wong, Y. X.; Ho, M.; Yang, H. Y.; Joy, J. K.; Kwek, Z. P.; Liu, B.; Wee, J. L. K.; Ong, E. H. Q.; Choong, M. L.; Poulsen, A.; Lee, M. A.; Pendharkar, V.; Ding, L. J.; Manoharan, V.; Chew, Y. S.; Sangthongpitag, K.; Lim, S.; Ong, S. T.; Hill, J.; Keller, T. H. Structure−activity relationship studies of mitogen activated protein kinase interacting kinase (MNK) 1 and 2 and BCR-ABL1 inhibitors targeting chronic myeloid leukemic cells. *J. Med. Chem.* **2016**, *59*, 3063−3078.

(54) Sanjo, H.; Kawai, T.; Akira, S. DRAKs, novel serine/threonine kinases related to death-associated protein kinase that trigger apoptosis. *J. Biol. Chem.* **1998**, *273*, 29066−29071.

(55) Mao, P.; Hever, M. P.; Niemaszyk, L. M.; Haghkerdar, J. M.; Yanco, E. G.; Desai, D.; Beyrouthy, M. J.; Kerley-Hamilton, J. S.; Freemantle, S. J.; Spinella, M. J. Serine/threonine kinase 17A is a novel p53 target gene and modulator of cisplatin toxicity and reactive oxygen species in testicular cancer cells. *J. Biol. Chem.* **2011**, *286*, 19381−19391.

(56) Mao, P.; Hever-Jardine, M. P.; Rahme, G. J.; Yang, E.; Tam, J.; Kodali, A.; Biswal, B.; Fadul, C. E.; Gaur, A.; Israel, M. A.; Spinella, M. J. Serine/threonine kinase 17A is a novel candidate for therapeutic targeting in glioblastoma. *PLoS One* **2013**, *8*, e81803.

(57) Park, Y.; Kim, W.; Lee, J. M.; Park, J.; Cho, J. K.; Pang, K.; Lee, J.; Kim, D.; Park, S. W.; Yang, K. M.; Kim, S. J. Cytoplasmic DRAK1 overexpressed in head and neck cancers inhibits TGF-beta1 tumor suppressor activity by binding to SMAD3 to interrupt its complex formation with SMAD4. *Oncogene* **2015**, *34*, 5037−5045.

(58) Hagiwara, M. Alternative splicing: a new drug target of the post-genome era. *Biochim. Biophys. Acta, Proteins Proteomics* **2005**, *1754*, 324−331.

(59) Petsalaki, E.; Zachos, G. Clks 1, 2 and 4 prevent chromatin breakage by regulating the aurora b-dependent abscission checkpoint. *Nat. Commun.* **2016**, *7*, 11451.

(60) Lenz, G.; Wright, G. W.; Emre, N. C.; Kohlhammer, H.; Dave, S. S.; Davis, R. E.; Carty, S.; Lam, L. T.; Shaffer, A. L.; Xiao, W.; Powell, J.; Rosenwald, A.; Ott, G.; Muller-Hermelink, H. K.; Gascoyne, R. D.; Connors, J. M.; Campo, E.; Jaffe, E. S.; Delabie, J.; Smeland, E. B.; Rimsza, L. M.; Fisher, R. I.; Weisenburger, D. D.; Chan, W. C.; Staudt, L. M. Molecular subtypes of diffuse large B-cell lymphoma arise by distinct genetic pathways. *Proc. Natl. Acad. Sci. U. S. A.* **2008**, *105*, 13520−13525.

(61) Young, R. M.; Staudt, L. M. Targeting pathological B cell receptor signalling in lymphoid malignancies. *Nat. Rev. Drug Discovery* **2013**, *12*, 229−243.

(62) Anderson, P. Post-transcriptional regulons coordinate the initiation and resolution of inflammation. *Nat. Rev. Immunol.* **2010**, *10*, 24−35.

(63) Palucka, A. K.; Coussens, L. M. The basis of oncoimmunology. *Cell* **2016**, *164*, 1233−1247.

(64) Robichaud, N.; Del Rincon, S. V.; Huor, B.; Alain, T.; Petruccelli, L. A.; Hearnden, J.; Goncalves, C.; Grotegut, S.; Spruck, C. H.; Furic, L. Phosphorylation of eIF4E promotes EMT and metastasis via translational control of SNAIL and MMP-3. *Oncogene* **2015**, *34*, 2032−2042.

(65) Topisirovic, I.; Ruiz-Gutierrez, M.; Borden, K. L. Phosphorylation of the eukaryotic translation initiation factor eIF4E contributes to its transformation and mRNA transport activities. *Cancer Res.* **2004**, *64*, 8639−8642.

(66) Reich, S. H.; Bleckman, T. M.; Kephart, S. E.; Romines, W. H.; Wallace, M. B. Synthesis of Disubstituted Indazole Compounds as Cyclin Dependent Kinase Inhibitors and Methods of Inhibiting Cell Proliferation. WO2001053268, 2001.

(67) Yang, X.; Li, F.; Konze, K. D.; Meslamani, J.; Ma, A.; Brown, P. J.; Zhou, M. M.; Arrowsmith, C. H.; Kaniskan, H. U.; Vedadi, M.; Jin, J. Structure-activity relationship studies for enhancer of zeste homologue 2 (EZH2) and enhancer of zeste homologue 1 (EZH1) inhibitors. *J. Med. Chem.* **2016**, *59*, 7617−7633.

(68) Bilodeau, M. T.; Duggan, M. E.; Hartnett, J. C.; Lindsley, C. W.; Wu, Z.; Zhao, Z. Inhibitors of Akt Activity. U.S. Patent 7,579,355, August 5, 2009.

(69) Sprengeler, P. A.; Reich, S. H.; Ernst, J. T.; Webber, S. E.; Shaghafi, M.; Murphy, D.; Tran, C. Preparation of Isoindoline, Azaisoindoline, Dihydroindenone and Dihydroazaindenone Inhibitors of MNK1 and MNK2. WO 2017075394, 2017.

DOI: 10.1021/acs.jmedchem.7b01795
J. Med. Chem. 2018, 61, 3516−3540